An Operator Splitting Approach for the Interaction Between a Fluid and a Multilayered Poroelastic Structure

Martina Bukač,[1] **Ivan Yotov,**[1] **Paolo Zunino**[2]
[1] *Department of Mathematics, University of Pittsburgh, Pittsburgh, Pennsylvania 15260*

[2] *Department of Mechanical Engineering & Materials Science, University of Pittsburgh, Pittsburgh, Pennsylvania 15261*

Received 14 February 2014; accepted 18 September 2014
Published online 28 November 2014 in Wiley Online Library (wileyonlinelibrary.com).
DOI 10.1002/num.21936

We develop a loosely coupled fluid-structure interaction finite element solver based on the Lie operator splitting scheme. The scheme is applied to the interaction between an incompressible, viscous, Newtonian fluid, and a multilayered structure, which consists of a thin elastic layer and a thick poroelastic material. The thin layer is modeled using the linearly elastic Koiter membrane model, while the thick poroelastic layer is modeled as a Biot system. We prove a conditional stability of the scheme and derive error estimates. Theoretical results are supported with numerical examples. Numer Methods Partial Differential Eq 31: 1054–1100, 2015

Keywords: fluid-structure interaction; loosely coupled scheme; poroelasticity

I. INTRODUCTION

Many natural materials—including soil, wood, and some biological tissues—have a multilayered structure consisting of two or more constituent materials. Multilayered structures can have distinct properties from their constituent materials. This characteristic is often used in engineering to produce a new material which is stiffer or lighter when compared to traditional materials. In many cases, such structures are surrounded by a fluid. In this setting, we are interested in permeable structures. Examples of multilayered permeable structure that are in contact with a fluid can be found in groundwater flow modeling, reservoir engineering, and modeling of blood flow through

Correspondence to: M. Bukač, Department of Applied and Computational Mathematics and Statistics, University of Notre Dame, Notre Dame, IN 46556 (e-mail: mbukac@nd.edu)
Contract grant sponsor: NSF (to M.B.); contract grant number: DMS 1216465
Contract grant sponsor: Mathematics Research Center, University of Pittsburgh (to M.B.)
Contract grant sponsor: NSF (to I.Y.); contract grant number: DMS 1115856
Contract grant sponsor: DOE (to I.Y.); contract grant number: DE-FG02-04ER25618
Contract grant sponsor: DOE (to P.Z.); contract grant number: DE-FG02-04ER25618
Contract grant sponsor: NSF (to P.Z.); contract grant number: DMS 1311983

the major blood vessels. Thus, in order to detect the damage in a reservoir or certain pathologies of blood vessels, it is important to understand the interaction between a fluid and a multilayered permeable structure.

We study the interaction between an incompressible viscous, Newtonian fluid and a multilayered poroelastic structure. This model features two different kinds of coupling, each widely studied in the literature: the flow-porous media coupling [1–10] and the fluid-structure coupling [11–20]. Main challenges in the flow-porous media interaction problems arise from the coupling of two domains, a fluid region and a porous media region, along with the two physical processes occurring in each region. Introducing the poroelastic media, our domain becomes time dependent, and thus we must resolve difficulties related to a moving domain. Furthermore, classical partitioned solvers for the fluid-structure interaction (FSI) problems are known to have stability issues when the density of the structure is comparable to the density of the fluid [21]. This difficulty will be taken into account here, since in this work we are interested on applications in hemodynamics, among others, and the density of blood is almost equal to the density of blood vessels.

The material properties of arteries have been widely studied [22–28]. Pseudoelastic [25, 29], viscoelastic [22–24], and nonlinear material models represent well known examples. To our knowledge, only a few of them have been deeply analyzed in the time dependent domain, namely when coupled with the pulsation induced by heartbeat. These considerations also apply to poroelasticity, which is addressed here. Poroelasticity becomes particularly interesting when looking at the coupling of flow with mass transport. This is a significant potential application of our model, as mass transport provides nourishment, removes wastes, affects pathologies, and allows to deliver drugs to arteries [30]. Poroelastic phenomena are interesting in different applications where soft biological tissues are involved. We mention for example cerebro-spinal flow [31], which also involves FSI, the study of hysteresis effects observed in the myocardial tissue [32, 33], as well as the modeling of lungs as a continuum material [34]. Besides biological applications, this model can also be used in numerous other applications: geomechanics, ground-surface water flow, reservoir compaction and surface subsidence, seabed-wave interaction problem, and so forth.

Although there exist many complex and detailed models for mutilayered structures in different applications, the interaction between the fluid and a multilayered structure remains an area of active research. To our knowledge, the only theoretical result was presented in [18], where the authors proved existence of a solution to a fluid-two-layered-structure interaction problem, in which one layer is modeled as a thin (visco)elastic shell and the other layer as a linearly elastic structure. Several studies focused on numerical simulations. An interaction between the fluid and a two-layer anisotropic elastic structure was used in [35] to model the human right and left ventricles. Slightly different models were used in [36] to model fully coupled fluid-structure-soil interaction for cylindrical liquid-contained structures subjected to horizontal ground excitation. The work in [37] focused on studying velocity of acoustic waves excited in multilayered structures in contact with fluids. A fluid-multilayered structure interaction problem coupled with transport was studied in [38], with the purpose of investigating low-density lipoprotein transport within a multilayered arterial wall. However, none of these studies present a numerical scheme supported with stability and error analysis.

In this work, we propose a model that captures interaction between a fluid and a multilayered structure, which consists of a thin elastic layer and a thick poroelastic layer. In the context of cardiovascular applications, we assume that the thin layer represents a homogenized combination of the endothelium, tunica intima, and internal elastic lamina, and that the thick layer represents tunica media. The thin elastic layer is modeled using the linearly elastic Koiter membrane model, while the poroelastic medium is modeled using the Biot equations. The Biot system consists of

an elastic skeleton and connecting pores filled with fluid. We assume that the elastic skeleton is homogeneous and isotropic, while the fluid in the pores is modeled using the Darcy equations. The Biot system is coupled to the fluid and the elastic membrane via the kinematic (no-slip and conservation of mass) and dynamic (conservation of momentum) interface conditions. More precisely, we assume that the elastic membrane cannot store fluid, but allows the flow through it in the normal direction. In the tangential direction, we prescribe the no-slip boundary condition. This assumption is reasonable in blood flow modeling, as it has been shown in [39] that predominant direction of intimal transport is the radial direction normal to the endothelial surface, for all ranges of relative intimal thickness.

The coupling between a fluid and a single layer poroelastic structure has been previously studied in [12, 40–44]. In [40], the authors analyze the problem form the physical standpoint, with the aim to identify the differences between a poroelastic model and a purely elastic one on the propagation of pressure waves and the deformation of the arterial walls using a simplified FSI benchmark for blood flow in arteries. Since those numerical tests are not computationally expensive, the numerical solver is based on a monolithic approach, where the interface conditions are enforced using Nitsche's method. Other authors have already analyzed the problem from the numerical perspective. In particular, the work in [45] is based on the modeling and a numerical solution of the interaction between an incompressible, Newtonian fluid, described using the Navier–Stokes equations, and a poroelastic structure modeled as a Biot system. The problem was solved using both a monolithic and a partitioned approach. The partitioned approach was based on the domain decomposition procedure, with the purpose of solving the Navier–Stokes equations separately from the Biot system. However, subiterations were needed between the two problems due to the instabilities associated with the "added mass effect." Namely, in FSI problems, the "classical" loosely coupled methods have been shown to be unconditionally unstable if the density of the structure is comparable to the density of the fluid [21, 46], which is the case in hemodynamics applications. To resolve this problem, several different splitting strategies have been proposed [11, 13, 15, 19, 20, 47–57]. More precisely, in [11], the authors present a strongly coupled partitioned scheme based on Robin-type coupling conditions. In addition to the classical Dirichlet–Neumann and Neumann–Dirichlet schemes, they also propose a Robin–Neumann and a Robin–Robin scheme, that converge without relaxation, and need a smaller number of subiteration between the fluid and the structure in each time step than classical strongly coupled schemes, provided that the interface parameters are suitably chosen, see [45, 58].

In [50, 59], Burman and Fernández propose an explicit scheme where the coupling between the fluid and a thick structure is enforced in a weak sense using Nitsche's approach [16]. The formulation in [50] still suffers from stability issues, which were corrected by adding a weakly consistent stabilization term that includes pressure variations at the interface. The splitting error, however, lowers the temporal accuracy of the scheme, which was then corrected by proposing a few defect-correction subiterations to achieve an optimal convergence rate.

A novel loosely coupled partitioned scheme, called the kinematically coupled scheme, was introduced by Guidoboni et al. in [56], and applied to FSI problems with thin structures. The scheme is based on embedding the no-slip kinematic condition into the thin structure equations. Using the Lie operator splitting approach [60], the structure equations are split so that the structure inertia is treated together with the fluid as a Robin boundary condition, while the structure elastodynamics is treated separately. This method has been shown to be unconditionally stable, and therefore, independent of the fluid and structure densities. Stability is achieved by combining the structure inertia with the fluid subproblem to mimic the energy balance of the continuous problem. Additionally, Muha and Čanić showed that the scheme converges to a weak solution of the fully nonlinear FSI problem [61].

The main features of the kinematically coupled scheme are simple implementation, modularity, no need for subiterations between the fluid and structure subproblems, and very good performance in terms of stability, accuracy, and computational cost. Hence, modifications of this scheme have been used by several authors to study different multiphysics problems involving FSI. A modification of the scheme was proposed by Lukáčová-Medvid'ová et al. to study FSI involving non-Newtonian fluids [17, 62]. An extension of the kinematically coupled scheme was proposed in [13] where a parameter β was introduced to increase the accuracy. It was shown in [13] that the accuracy of the kinematically coupled β-scheme with $\beta = 1$ is comparable to that of monolithic scheme by Badia et al., in [49] when applied to a nonlinear benchmark FSI problem in hemodynamics. A modified kinematically coupled scheme, called "the incremental displacement-correction scheme," that treats the structure displacement explicitly in the fluid substep and then corrects it in the structure substep was recently proposed by Fernández et al. [15, 53, 55].

Inspired by the kinematically coupled scheme, in this manuscript we propose a loosely coupled finite element scheme for the fluid-membrane-poroelastic structure interaction problem based on the Lie operator splitting method. We use the operator splitting to separate the fluid problem (Navier–Stokes equations) from the Biot problem. The no-slip kinematic condition in the tangential direction is embedded into the membrane equations. We recall that this coupled problem is particularly challenging, because it combines the free fluid-porous media flow and the fluid-structure coupling mechanisms. This work shows that the kinematically coupled Lie splitting method can be successfully applied also in this case. In particular, the operator splitting is performed so that the tangential component of the structure inertia is treated together with the fluid as a Robin boundary condition. Assuming the pressure formulation for the Darcy equations, the continuity of the normal flux and the balance of normal components of stress between the Navier–Stokes fluid and the fluid in the pores is treated in a similar way as in the partitioned algorithms for the Stokes–Darcy coupled problems [6, 63]. The membrane elastodynamics is embedded into the Biot system as a Robin boundary condition. In contrast with domain decomposition methods proposed in [12], the operator splitting approach does not require subiterations between the fluid and the Biot problem, making our scheme more computationally efficient.

We prove a conditional stability of the proposed scheme, where the stability condition does not depend on the fluid and structure densities, but it is related to the decoupling of the Stokes–Darcy interaction problem. Furthermore, we derive error estimates and prove the convergence of the scheme. The rates of convergence and the stability condition are validated numerically on a classical benchmark problem typically used to test the results of FSI algorithms. In a second numerical example, we investigate the effects of porosity on the structure displacement. Namely, we consider a high storativity and a high permeability case in the Darcy equations, and compare them to the results obtained using a purely elastic model. Depending on the regime, we observe a significantly different behavior of the coupled system. This conclusion is also supported by the sensitivity analysis, based on both theoretical and numerical approach, addressed by the authors in [40].

At the level of numerical approximation, we adopt rather standard techniques, based on low order finite differences and Lagrangian finite elements for the discretization of the equations in time and space, respectively. Indeed, the main contributions of this work arise in the design of the splitting scheme. In particular, we propose a novel model to study interaction between a fluid and a composite poroelastic structure, and a novel, loosely coupled numerical scheme. The scheme is based on existing works [5, 56], which were combined and modified to resolve both issues due the fluid-structure coupling, and the fluid-porous medium coupling. We present the stability and convergence analysis of the proposed scheme, completed with the numerical examples.

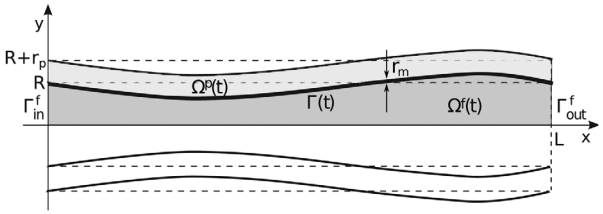

FIG. 1. Deformed domains $\Omega^f(t) \cup \Omega^p(t)$.

The rest of the article is organized as follows. In the following section, we introduce the model equations and the coupling conditions. In Section III, we propose a loosely coupled scheme based on the operator-splitting approach. The weak formulation and stability of the scheme is presented in Section IV. In Section V, we derive the error analysis of the scheme. Finally, the numerical results are presented in Section VI.

II. DESCRIPTION OF THE PROBLEM

Consider a bounded, deformable, two-dimensional domain $\Omega(t) = \Omega^f(t) \cup \Omega^p(t)$ of reference length L, which consists of two regions, $\Omega^f(t)$ and $\Omega^p(t)$, see Fig. 1. We assume that the region $\Omega^f(t)$ has reference width $2R$, and is filled by an incompressible, viscous fluid. We denote the width of the second region $\Omega^p(t)$ by r_p, and assume that $\Omega^p(t)$ is occupied by a fully saturated poroelastic matrix. The two regions are separated by a common interface $\Gamma(t)$. We assume that $\Gamma(t)$ has a mass, and represents a thin, elastic structure. Namely, we assume that the thickness of the interface r_m is "small" with respect to the radius of the fluid domain, $r_m \ll R$. Thus, the volume of the interface is negligible, so it acts as a membrane that cannot store fluid, but allows the flow through it in the normal direction.

We are interested in simulating a pressure-driven flow through the deformable channel with a two-way coupling between the fluid, thin elastic interface, and poroleastic structure. Without loss of generality, we restrict the model to a two-dimensional (2D) geometrical model representing a deformable channel. We consider only the upper half of the fluid domain supplemented by a symmetry condition at the axis of symmetry. Thus, the reference fluid and structure domains in our problem (showed by dashed lines in Fig. 1) are given, respectively, by

$$\hat{\Omega}^f := \{(x, y) | 0 < x < L, 0 < y < R\},$$
$$\hat{\Omega}^p := \{(x, y) | 0 < x < L, R < y < R + r_p\},$$

and the reference lateral boundary by $\hat{\Gamma} = \{(x, R) | 0 < x < L\}$. The inlet and outlet fluid boundaries are defined, respectively, as $\Gamma^f_{\text{in}} = \{(0, y) | 0 < y < R\}$ and $\Gamma^f_{\text{out}} = \{(L, y) | 0 < y < R\}$.

We model the flow using the Navier–Stokes equations for a viscous, incompressible, Newtonian fluid:

$$\rho_f \left(\frac{\partial \boldsymbol{v}}{\partial t} + \boldsymbol{v} \cdot \nabla \boldsymbol{v} \right) = \nabla \cdot \sigma^f + \boldsymbol{g} \quad \text{in } \Omega^f(t) \times (0, T), \tag{2.1}$$

$$\nabla \cdot \boldsymbol{v} = 0 \quad \text{in } \Omega^f(t) \times (0, T), \tag{2.2}$$

where $\boldsymbol{v} = (v_x, v_y)$ is the fluid velocity, $\sigma_f = -p_f \boldsymbol{I} + 2\mu_f \boldsymbol{D}(\boldsymbol{v})$ is the fluid stress tensor, $\boldsymbol{g}$ is a body force, p_f is the fluid pressure, ρ_f is the fluid density, μ_f is the fluid viscosity, and $\boldsymbol{D}(\boldsymbol{v}) = (\nabla \boldsymbol{v} + (\nabla \boldsymbol{v})^T)/2$ is the rate-of-strain tensor. Denote the inlet and outlet fluid boundaries by Γ^f_{in} and Γ^f_{out}, respectively. At the inlet and outlet boundary, we prescribe the normal stress:

$$\sigma^f \boldsymbol{n}_{\text{in}} = -p_{\text{in}}(t)\boldsymbol{n}_{\text{in}} \quad \text{on } \Gamma^f_{\text{in}} \times (0,T), \tag{2.3}$$

$$\sigma^f \boldsymbol{n}_{\text{out}} = 0 \qquad\qquad \text{on } \Gamma^f_{\text{out}} \times (0,T), \tag{2.4}$$

where $\boldsymbol{n}_{\text{in}}/\boldsymbol{n}_{\text{out}}$ are the outward normals to the inlet/outlet fluid boundaries, respectively. These boundary conditions are common in blood flow modeling [45, 64, 65] even though they are not physiologically optimal as the flow distribution and pressure field in the modeled domain are often unknown [66]. More physiological boundary conditions could be considered, for example, boundary conditions including effects of peripheral resistance, see [66, 67]. Along the middle line of the channel $\Gamma^f_0 = \{(x,0)|0 < x < L\}$, we impose the symmetry conditions:

$$\frac{\partial v_x}{\partial y} = 0, v_y = 0 \quad \text{on } \Gamma^f_0 \times (0,T). \tag{2.5}$$

The lateral boundary represents a deformable, thin elastic wall, whose dynamics is modeled by the linearly elastic Koiter membrane model, given in the first-order Lagrangian formulation by:

$$\rho_m r_m \frac{\partial \hat{\xi}_x}{\partial t} - C_2 \frac{\partial \hat{\eta}_y}{\partial \hat{x}} - C_1 \frac{\partial^2 \hat{\eta}_x}{\partial \hat{x}^2} = \hat{f}_x \quad \text{on } \hat{\Gamma} \times (0,T), \tag{2.6}$$

$$\rho_m r_m \frac{\partial \hat{\xi}_y}{\partial t} + C_0 \hat{\eta}_y + C_2 \frac{\partial \hat{\eta}_x}{\partial \hat{x}} = \hat{f}_y \quad \text{on } \hat{\Gamma} \times (0,T), \tag{2.7}$$

$$\frac{\partial \hat{\boldsymbol{\eta}}}{\partial t} = \hat{\boldsymbol{\xi}} \quad \text{on } \hat{\Gamma} \times (0,T), \tag{2.8}$$

where $\hat{\boldsymbol{\eta}}(\hat{x},t) = (\hat{\eta}_x(\hat{x},t), \hat{\eta}_y(\hat{x},t))$ denotes the axial and radial displacement, $\hat{\boldsymbol{\xi}}(\hat{x},t) = (\hat{\xi}_x(\hat{x},t), \hat{\xi}_y(\hat{x},t))$ denotes the axial and radial structure velocity, $\hat{\boldsymbol{f}} = (\hat{f}_x, \hat{f}_y)$ is a vector of surface density of the force applied to the membrane, ρ_m denotes the membrane density and

$$C_0 = \frac{r_m}{R^2}\left(\frac{2\mu_m\lambda_m}{\lambda_m + 2\mu_m} + 2\mu_m\right), \quad C_1 = r_m\left(\frac{2\mu_m\lambda_m}{\lambda_m + 2\mu_m} + 2\mu_m\right), \quad C_2 = \frac{r_m}{R}\frac{2\mu_m\lambda_m}{\lambda_m + 2\mu_m}. \tag{2.9}$$

The coefficients μ_m and λ_m are the Lamé coefficients for the membrane. Note that we can write the system (2.6)–(2.7) more compactly as

$$\rho_m r_m \frac{\partial \hat{\boldsymbol{\xi}}}{\partial t} + \hat{\mathcal{L}}\hat{\boldsymbol{\eta}} = \hat{\boldsymbol{f}}, \quad \hat{\mathcal{L}} := \begin{pmatrix} -C_1\partial_{\hat{x}\hat{x}} & -C_2\partial_{\hat{x}} \\ C_2\partial_{\hat{x}} & C_0 \end{pmatrix}. \tag{2.10}$$

The fluid domain is bounded by a deformable porous matrix consisting of a skeleton and connecting pores filled with fluid, whose dynamics is described by the Biot model, which in the first-order, primal, Eulerian formulation reads as follows:

$$\rho_p \frac{D\boldsymbol{V}}{Dt} - \nabla \cdot \boldsymbol{\sigma}^p = \boldsymbol{h} \quad \text{in } \Omega^p(t) \times (0,T), \tag{2.11}$$

$$\frac{D\boldsymbol{U}}{Dt} = \boldsymbol{V} \quad \text{in } \Omega^p(t) \times (0,T), \tag{2.12}$$

$$\frac{D}{Dt}(s_0 p_p + \alpha \nabla \cdot \boldsymbol{U}) - \nabla \cdot (\kappa \nabla p_p) = s \quad \text{in } \Omega^p(t) \times (0,T), \tag{2.13}$$

where $\frac{D}{Dt}$ denotes the classical concept of material derivative. The stress tensor of the poroelastic medium is given by $\boldsymbol{\sigma}^p = \boldsymbol{\sigma}^E - \alpha p_p \boldsymbol{I}$, where $\boldsymbol{\sigma}^E$ denotes the elasticity stress tensor. With the assumption that the displacement $\boldsymbol{U} = (U_x, U_y)$ of the skeleton is connected to stress tensor $\boldsymbol{\sigma}^E$ via the Saint Venant-Kirchhoff elastic model, we have $\boldsymbol{\sigma}^E(\boldsymbol{U}) = 2\mu_p \boldsymbol{D}(\boldsymbol{U}) + \lambda_p \text{tr}(\boldsymbol{D}(\boldsymbol{U}))\boldsymbol{I}$, where λ_p and μ_p denote the Lamé coefficients for the skeleton, and, with the hypothesis of "small" deformations, $\boldsymbol{D}(\boldsymbol{U}) = (\nabla \boldsymbol{U} + (\nabla \boldsymbol{U})^T)/2$. The displacement velocity is denoted by $\boldsymbol{V} = (V_x, V_y)$, $\boldsymbol{h}$ is a body force, and s is a source or sink.

System (2.11)–(2.13) consists of the momentum equation for the balance of total forces (2.11), and the storage equation (2.13) for the fluid mass conservation in the pores of the matrix, where p_p is the fluid pressure. The density of saturated porous medium is denoted by ρ_p, and κ denotes the uniformly positive definite hydraulic conductivity tensor. For simplicity of the presentation, we assume that κ is a scalar constant. The coefficient $c_0 > 0$ is the storage coefficient, and the Biot–Willis constant α is the pressure-storage coupling coefficient. The relative velocity of the fluid within the porous structure $\boldsymbol{q}$ can be reconstructed via Darcy's law

$$\boldsymbol{q} = -\kappa \nabla p_p \quad \text{in } \Omega^p(t) \times (0,T).$$

Denote the inlet and outlet poroelastic structure boundaries, respectively, by $\Gamma^p_{\text{in}} = \{(0,y) | R < y < R + r_p\}$ and $\Gamma^p_{\text{out}} = \{(L,y) | R < y < R + r_p\}$, and the reference exterior boundary by $\hat{\Gamma}^p_{\text{ext}} = \{(x, R + r_p) | 0 < x < L\}$. We assume that the poroelastic structure is fixed at the inlet and outlet boundaries:

$$\boldsymbol{U} = 0 \quad \text{on } \Gamma^p_{\text{in}} \cup \Gamma^p_{\text{out}} \times (0,T), \tag{2.14}$$

that the external structure boundary $\Gamma^p_{\text{ext}}(t)$ is exposed to external ambient pressure

$$\boldsymbol{n}_{\text{ext}} \cdot \boldsymbol{\sigma}^E \boldsymbol{n}_{\text{ext}} = -p_e \quad \text{on } \Gamma^p_{\text{ext}}(t) \times (0,T), \tag{2.15}$$

where $\boldsymbol{n}_{\text{ext}}$ is the outward unit normal vector on $\Gamma^p_{\text{ext}}(t)$, and that the tangential displacement of the exterior boundary is zero:

$$U_x = 0 \quad \text{on } \Gamma^p_{\text{ext}}(t) \times (0,T). \tag{2.16}$$

On the external surface of the arterial wall, physiologically more relevant boundary conditions could be considered (e.g., Robin boundary conditions that take into account the effects of the mechanical interaction of the artery with the surrounding connective tissue), see [68, 69]. On the fluid pressure in the porous medium, we impose drained boundary conditions [70]:

$$p_p = 0 \quad \text{on } \Gamma^p_{\text{ext}}(t) \cup \Gamma^p_{\text{in}} \cup \Gamma^p_{\text{out}} \times (0,T). \tag{2.17}$$

Initially, the fluid, elastic membrane and the poroelastic structure are assumed to be at rest, with zero displacement from the reference configuration

$$\boldsymbol{v} = 0, \quad \boldsymbol{U} = 0, \quad \frac{D\boldsymbol{U}}{Dt} = 0, \quad \hat{\boldsymbol{\eta}} = 0, \quad \frac{\partial \hat{\boldsymbol{\eta}}}{\partial t} = 0, \quad \boldsymbol{q} = 0. \tag{2.18}$$

A. The Coupling Conditions

To prescribe the coupling conditions on the physical fluid-structure interface $\Gamma(t)$, let $\boldsymbol{\eta}$ be the membrane displacement in the physical configuration and $\boldsymbol{\xi} = \frac{D\boldsymbol{\eta}}{Dt}$. While the lumen and the poroelastic medium contain fluid, we assume that the elastic membrane does not contain fluid, but allows the flow through it in the normal direction. This is a reasonable assumption because the elastic membrane represents tunica intima. It has been shown by experimental studies that the normal transport in tunica intima is significantly greater than tangential transport [39]. Denote by $\boldsymbol{n}$ the outward normal to the fluid domain and by $\boldsymbol{\tau}$ the tangential unit vector. Thus, the fluid, elastic membrane and poroelastic structure are coupled via the following boundary conditions:

- Mass conservation: since the thin lamina allows the flow through it, the continuity of normal flux is

$$\boldsymbol{v} \cdot \boldsymbol{n} = \left(\frac{D\boldsymbol{U}}{Dt} - \kappa \nabla p_p \right) \cdot \boldsymbol{n} \quad \text{on } \Gamma(t). \tag{2.19}$$

- As the permeability of the blood vessels is rather small and we do not allow filtration in the tangential direction, we prescribe no-slip boundary conditions between the fluid in the lumen and the elastic membrane, and between the elastic membrane and poroelastic medium:

$$\boldsymbol{v} \cdot \boldsymbol{\tau} = \boldsymbol{\xi} \cdot \boldsymbol{\tau}, \quad \boldsymbol{\eta} = \boldsymbol{U} \quad \text{on } \Gamma(t). \tag{2.20}$$

- Balance of normal components of the stress in the fluid phase:

$$\boldsymbol{n} \cdot \boldsymbol{\sigma}^f \boldsymbol{n} = -p_p \quad \text{on } \Gamma(t). \tag{2.21}$$

- The conservation of momentum describes balance of contact forces. Precisely, it says that the sum of contact forces at the fluid-porous medium interface is equal to zero:

$$\boldsymbol{\sigma}^f \boldsymbol{n} - \sigma^p \boldsymbol{n} + J^{-1} \boldsymbol{f} = 0 \quad \text{on } \Gamma(t), \tag{2.22}$$

where $\boldsymbol{f} := \hat{\boldsymbol{f}} \circ (\mathcal{A}_t^{-1}|_{\Gamma(t)})$, and J denotes the Jacobian of the transformation from $\Gamma(t)$ to $\hat{\Gamma}$ given by

$$J = \sqrt{\left(1 + \frac{\partial \hat{\eta}_x}{\partial \hat{x}}\right)^2 + \left(\frac{\partial \hat{\eta}_y}{\partial \hat{x}}\right)^2}. \tag{2.23}$$

B. The Problem Formulation in the Arbitrary Lagrangian–Eulerian Framework

To deal with the motion of the fluid domain, we adopt the Arbitrary Lagrangian–Eulerian (ALE) approach [65, 71, 72]. In the context of finite element method approximation of moving-boundary problems, ALE method deals efficiently with the deformation of the mesh, especially at the boundary and near the interface between the fluid and the structure, and with the issues related to the approximation of the time-derivatives $\partial \boldsymbol{v}/\partial t \approx (\boldsymbol{v}(t^{n+1}) - \boldsymbol{v}(t^n))/\Delta t$ which, due to the fact that $\Omega^f(t)$ depends on time, is not well defined as the values $\boldsymbol{v}(t^{n+1})$ and $\boldsymbol{v}(t^n)$ correspond to the values of $\boldsymbol{v}$ defined at two different domains. Following the ALE approach, we introduce two families of (arbitrary, invertible, smooth) mappings $\mathcal{A}_t$ and $\mathcal{S}_t$, defined on reference domains $\hat{\Omega}^f$ and $\hat{\Omega}^p$, respectively, which track the domain in time:

$$\mathcal{A}_t : \hat{\Omega}^f \to \Omega^f(t) \subset \mathbb{R}^2, \quad \boldsymbol{x} = \mathcal{A}_t(\hat{\boldsymbol{x}}) \in \Omega^f(t), \quad \text{for } \hat{\boldsymbol{x}} \in \hat{\Omega}^f, \tag{2.24}$$

$$\mathcal{S}_t : \hat{\Omega}^p \to \Omega^p(t) \subset \mathbb{R}^2, \quad \boldsymbol{x} = \mathcal{S}_t(\hat{\boldsymbol{x}}) \in \Omega^p(t), \quad \text{for } \hat{\boldsymbol{x}} \in \hat{\Omega}^p. \tag{2.25}$$

Note that the fluid domain is determined by the displacement of the membrane $\hat{\boldsymbol{\eta}}$, while the porous medium domain is determined by its displacement $\hat{\boldsymbol{U}}$, where $\hat{\boldsymbol{U}}$ is the displacement of the porous medium evaluated at the reference configuration. However, we can define a homeomorphism over $\Omega^f(t) \cup \Omega^p(t)$ by setting mappings $\mathcal{A}_t$ and $\mathcal{S}_t$ equal on $\Gamma(t)$. For the structure, we adopt the material mapping

$$\mathcal{S}_t(\hat{\boldsymbol{x}}) = \hat{\boldsymbol{x}} + \hat{\boldsymbol{U}}(\hat{\boldsymbol{x}}, t), \quad \forall \hat{\boldsymbol{x}} \in \hat{\Omega}^p. \tag{2.26}$$

Since the mapping $\mathcal{A}_t$ is arbitrary, with the only requirement that it matches $\mathcal{S}_t$ on $\Gamma(t)$, we can define $\mathcal{A}_t$ as

$$\mathcal{A}_t(\hat{\boldsymbol{x}}) = \hat{\boldsymbol{x}} + \mathrm{Ext}(\hat{\boldsymbol{\eta}}(\hat{x}, t)) = \hat{\boldsymbol{x}} + \mathrm{Ext}(\hat{\boldsymbol{U}}(\hat{\boldsymbol{x}}, t)|_{\hat{\Gamma}}), \quad \forall \hat{\boldsymbol{x}} \in \hat{\Omega}^f. \tag{2.27}$$

We do not have to transfer the time-derivatives in the Biot system and in Koiter membrane equations to the reference domain as the material time-derivative is suitable for the time discretization, and the membrane equations are given on the reference configuration. Our problem in the ALE formulation reads as follows: given $t \in (0, T)$, find $\boldsymbol{v} = (v_x, v_y)$, p_f, $\hat{\boldsymbol{\eta}} = (\hat{\eta}_x, \hat{\eta}_y)$, $\hat{\boldsymbol{\xi}} = (\hat{\xi}_x, \hat{\xi}_y)$, $\boldsymbol{U} = (U_x, U_y)$, $\boldsymbol{V} = (V_x, V_y)$ and p_p, with $\boldsymbol{\eta}(\boldsymbol{x}, t) = \hat{\boldsymbol{\eta}}(\mathcal{A}_t^{-1}(\boldsymbol{x}), t)$, for $\boldsymbol{x} \in \Gamma(t)$, such that

$$\rho_f \left(\left. \frac{\partial \boldsymbol{v}}{\partial t} \right|_{\hat{\boldsymbol{x}}} + (\boldsymbol{v} - \boldsymbol{w}) \cdot \nabla \boldsymbol{v} \right) = \nabla \cdot \sigma^f + \boldsymbol{g} \quad \text{in } \Omega^f(t) \times (0, T), \tag{2.28a}$$

$$\nabla \cdot \boldsymbol{v} = 0 \quad \text{in } \Omega^f(t) \times (0, T), \tag{2.28b}$$

$$\rho_m r_m \frac{\partial \hat{\boldsymbol{\xi}}}{\partial t} + \hat{\mathcal{L}} \hat{\boldsymbol{\eta}} = \hat{\boldsymbol{f}} \quad \text{on } \hat{\Gamma} \times (0, T), \tag{2.28c}$$

$$\rho_m r_m \left(\hat{\boldsymbol{\xi}} - \frac{\partial \hat{\boldsymbol{\eta}}}{\partial t} \right) = 0 \quad \text{on } \hat{\Gamma} \times (0, T), \tag{2.28d}$$

$$\rho_p \frac{D\boldsymbol{V}}{Dt} = \nabla \cdot \boldsymbol{\sigma}^p + \boldsymbol{h} \quad \text{in } \Omega^p(t) \times (0, T), \tag{2.28e}$$

$$s_0 \frac{D}{Dt} p_p + \alpha \nabla \cdot \frac{D\boldsymbol{U}}{Dt} - \nabla \cdot (\kappa \nabla p_p) = s \quad \text{in } \Omega^p(t) \times (0, T), \tag{2.28f}$$

$$\rho_p \left(\boldsymbol{V} - \frac{D\boldsymbol{U}}{Dt} \right) = 0 \quad \text{in } \Omega^p(t) \times (0, T), \tag{2.28g}$$

with the kinematic coupling conditions on $\Gamma(t)$:

$$\boldsymbol{\xi} \cdot \boldsymbol{\tau} = \boldsymbol{v} \cdot \boldsymbol{\tau}, \quad \boldsymbol{\eta} = \boldsymbol{U}, \tag{2.29}$$

dynamic coupling conditions on $\Gamma(t)$:

$$\boldsymbol{\sigma}^f \boldsymbol{n} - \sigma^p \boldsymbol{n} + J^{-1} \boldsymbol{f} = 0, \tag{2.30}$$

$$\boldsymbol{n} \cdot \boldsymbol{\sigma}^f \boldsymbol{n} = -p_p, \tag{2.31}$$

and the continuity of normal flux on $\Gamma(t)$:

$$\boldsymbol{v} \cdot \boldsymbol{n} = \left(\frac{D\boldsymbol{U}}{Dt} - \kappa \nabla p_p \right) \cdot \boldsymbol{n}, \tag{2.32}$$

with the boundary and initial conditions given in Section I, where $\boldsymbol{w}$ in (2.28a) denotes the domain velocity given by

$$\boldsymbol{w}(\boldsymbol{x},t) = \frac{\partial \mathcal{A}_t(\hat{\boldsymbol{x}})}{\partial t}, \tag{2.33}$$

Denote by $\mathcal{L}$ the inverse Piola transformation of $\hat{\mathcal{L}}$, namely $\mathcal{L} = J^{-1}\hat{\mathcal{L}}F^{-T}$, where $F = \nabla_{\boldsymbol{x}}\mathcal{A}_t$. Then, composing the Koiter membrane equations (2.10) with $\mathcal{A}_t^{-1}$, using the first condition in (2.29) and condition (2.31), we can write the tangential and normal component of condition (2.30) as follows:

$$\rho_m r_m \frac{\partial \boldsymbol{v}}{\partial t}\cdot\boldsymbol{\tau} + \boldsymbol{\tau}\cdot\mathcal{L}\boldsymbol{\eta} + J\boldsymbol{\tau}\cdot\boldsymbol{\sigma}^f\boldsymbol{n} - J\boldsymbol{\tau}\cdot\sigma^p\boldsymbol{n} = 0, \quad \text{on } \Gamma(t) \tag{2.34a}$$

$$\rho_m r_m \frac{D\boldsymbol{\xi}}{Dt}\cdot\boldsymbol{n} + \boldsymbol{n}\cdot\mathcal{L}\boldsymbol{\eta} - Jp_p - J\boldsymbol{n}\cdot\sigma^p\boldsymbol{n} = 0, \quad \text{on } \Gamma(t). \tag{2.34b}$$

We will use condition (2.30) written the form (2.34a)–(2.34b) when performing the operator splitting.

III. WEAK FORMULATION OF THE MONOLITHIC PROBLEM

For a domain Ω, we denote by $||\cdot||_{H^k(\Omega)}$ the norm in the Sobolev space $H^k(\Omega)$. The norm in $L^2(\Omega)$ is denoted by $||\cdot||_{L^2(\Omega)}$, and the $L^2(\Omega)-$ inner product by $(\cdot,\cdot)_\Omega$. We introduce the following bilinear forms

$$a_f(\boldsymbol{v},\boldsymbol{\varphi}^f) = 2\mu_f\int_{\Omega^f(t)}\boldsymbol{D}(\boldsymbol{v}):\boldsymbol{D}(\boldsymbol{\varphi}^f)d\boldsymbol{x},$$

$$b_f(p_f,\boldsymbol{\varphi}^f) = \int_{\Omega^f(t)} p_f\nabla\cdot\boldsymbol{\varphi}^f d\boldsymbol{x},$$

$$a_e(\boldsymbol{U},\boldsymbol{\varphi}^p) = 2\mu_p\int_{\Omega^p(t)}\boldsymbol{D}(\boldsymbol{U}):\boldsymbol{D}(\boldsymbol{\varphi}^p)d\boldsymbol{x} + \lambda_p\int_{\Omega^p(t)}(\nabla\cdot\boldsymbol{U})(\nabla\cdot\boldsymbol{\varphi}^p)d\boldsymbol{x},$$

$$a_p(p_p,\psi^p) = \int_{\Omega^p(t)}\kappa\nabla p_p\cdot\nabla\psi^p d\boldsymbol{x},$$

$$b_{ep}(p_p,\boldsymbol{\varphi}^p) = \alpha\int_{\Omega^p(t)} p_p\nabla\cdot\boldsymbol{\varphi}^p d\boldsymbol{x},$$

$$a_m(\hat{\boldsymbol{\eta}},\hat{\boldsymbol{\zeta}}) = r_m\int_0^L 4\mu_m\left(\left(\frac{\partial\hat{\eta}_x}{\partial\hat{x}}\frac{\partial\hat{\zeta}_x}{\partial\hat{x}} + \frac{1}{R^2}\hat{\eta}_y\hat{\zeta}_y\right) + \frac{\lambda_m}{\lambda_m+2\mu_m}\left(\frac{\partial\hat{\eta}_x}{\partial\hat{x}} + \frac{1}{R}\hat{\eta}_y\right)\left(\frac{\partial\hat{\zeta}_x}{\partial\hat{x}} + \frac{1}{R}\hat{\zeta}_y\right)\right)d\hat{x}$$

$$c_{fp}(p_p,\boldsymbol{\varphi}^f) = \int_{\Gamma(t)} p_p\boldsymbol{\varphi}^f\cdot\boldsymbol{n}dx,$$

$$c_{ep}(p_p,\boldsymbol{\varphi}^p) = \int_{\Gamma(t)} p_p\boldsymbol{\varphi}^p\cdot\boldsymbol{n}dx,$$

and the trilinear form

$$d_f(\boldsymbol{v},\boldsymbol{u},\boldsymbol{\varphi}) = \rho_f\int_{\Omega^f(t)}(\boldsymbol{v}\cdot\nabla)\boldsymbol{u}\cdot\boldsymbol{\varphi}d\boldsymbol{x}.$$

For more details on the derivation of the bilinear form $a_m(\cdot,\cdot)$ for the elastic part of the Koiter membrane (2.6)–(2.8), see [24].

To find a weak form of the Navier–Stokes equation, introduce the following test function spaces:

$$V^f(t) = \{\varphi : \Omega^f(t) \to \mathbb{R}^2 | \boldsymbol{\varphi} = \hat{\boldsymbol{\varphi}} \circ (\mathcal{A}_t)^{-1}, \hat{\boldsymbol{\varphi}} \in (H^1(\hat{\Omega}^f))^2,\ \varphi_y = 0 \text{ on } \Gamma_0^f\}, \tag{3.1}$$

$$Q^f(t) = \{\psi : \Omega^f(t) \to \mathbb{R} | \psi = \hat{\psi} \circ (\mathcal{A}_t)^{-1}, \hat{\psi} \in L^2(\hat{\Omega}^f)\}, \tag{3.2}$$

for all $t \in [0,T)$. The variational formulation of the Navier–Stokes equations now reads: given $t \in (0,T)$ find $(\boldsymbol{v}, p_f) \in V^f(t) \times Q^f(t)$ such that for all $(\boldsymbol{\varphi}^f, \psi^f) \in V^f(t) \times Q^f(t)$

$$\begin{aligned}\rho_f \int_{\Omega^f(t)} \frac{\partial \boldsymbol{v}}{\partial t} \cdot \boldsymbol{\varphi}^f d\boldsymbol{x} + d_f(\boldsymbol{v}, \boldsymbol{v}, \boldsymbol{\varphi}^f) + a_f(\boldsymbol{v}, \boldsymbol{\varphi}^f) - b_f(p_f, \boldsymbol{\varphi}^f) + b_f(\psi^f, \boldsymbol{v}) \\ = \int_{\Gamma(t)} \boldsymbol{\sigma}^f \boldsymbol{n} \cdot \boldsymbol{\varphi}^f dx + \int_{\Omega^f(t)} \boldsymbol{g} \cdot \boldsymbol{\varphi}^f d\boldsymbol{x} + \int_{\Gamma_{\text{in}}} p_{\text{in}}(t) \varphi_x^f dy.\end{aligned} \tag{3.3}$$

To write the weak form of the linearly elastic Koiter membrane, let $\hat{V}^m = (H_0^1(0,L))^2$. Then, the weak formulation reads as follows: given $t \in (0,T)$ find $(\hat{\boldsymbol{\eta}}, \hat{\boldsymbol{\xi}}) \in \hat{V}^m \times \hat{V}^m$ such that for all $(\hat{\boldsymbol{\zeta}}, \hat{\boldsymbol{\chi}}) \in \hat{V}^m \times \hat{V}^m$

$$\rho_m r_m \int_0^L \left(\hat{\boldsymbol{\xi}} - \frac{\partial \hat{\boldsymbol{\eta}}}{\partial t}\right) \cdot \hat{\boldsymbol{\chi}} d\hat{x} + \rho_m r_m \int_0^L \frac{\partial \hat{\boldsymbol{\xi}}}{\partial t} \cdot \hat{\boldsymbol{\zeta}} d\hat{x} + a_m(\hat{\boldsymbol{\eta}}, \hat{\boldsymbol{\zeta}}) = \int_0^L \hat{\boldsymbol{f}} \cdot \hat{\boldsymbol{\zeta}} d\hat{x}. \tag{3.4}$$

Finally, let us introduce

$$\begin{aligned} V^p(t) = \{&\varphi : \Omega^p(t) \to \mathbb{R}^2 | \boldsymbol{\varphi} = \hat{\boldsymbol{\varphi}} \circ (\mathcal{S}_t)^{-1}, \hat{\boldsymbol{\varphi}} \in (H^1(\hat{\Omega}^p))^2, \boldsymbol{\varphi} = 0 \\ &\text{on } \Gamma_{\text{in}}^p \cup \Gamma_{\text{out}}^p, \varphi_x = 0 \quad \text{on } \Gamma_{\text{ext}}^p(t)\}, \\ Q^p(t) = \{&\psi : \Omega^p(t) \to \mathbb{R} | \psi = \hat{\psi} \circ (\mathcal{S}_t)^{-1}, \hat{\psi} \in H^1(\hat{\Omega}^p), \psi|_{\partial\Omega^p(t)\setminus\Gamma(t)} = 0\} \end{aligned}$$

Now the weak form of the Biot system reads as follows: given $t \in (0,T)$ find $(\boldsymbol{U}, \boldsymbol{V}, p_p) \in V^p(t) \times V^p(t) \times Q^p(t)$ such that for all $(\boldsymbol{\varphi}^p, \boldsymbol{\phi}^p, \psi^p) \in V^p(t) \times V^p(t) \times Q^p(t)$

$$\begin{aligned}&\rho_p \int_{\Omega^p(t)} \left(\boldsymbol{V} - \frac{D\boldsymbol{U}}{Dt}\right) \cdot \boldsymbol{\phi}^p d\boldsymbol{x} + \rho_p \int_{\Omega^p(t)} \frac{D\boldsymbol{V}}{Dt} \cdot \boldsymbol{\varphi}^p d\boldsymbol{x} \\ &+ a_e(\boldsymbol{U}, \boldsymbol{\varphi}^p) - b_{ep}(p_p, \boldsymbol{\varphi}^p) + \int_{\Omega^p(t)} s_0 \frac{Dp_p}{Dt} \psi^p d\boldsymbol{x} \\ &+ b_{ep}(\psi^p, \frac{D\boldsymbol{U}}{Dt}) + a_p(p_p, \psi^p) = -\int_{\Gamma(t)} \boldsymbol{\sigma}^p \boldsymbol{n} \cdot \boldsymbol{\varphi}^p dx \\ &- \int_{\Gamma(t)} \kappa \nabla p_p - \int_{\Gamma_{\text{ext}}^p} p_e \boldsymbol{\varphi}_y^p dx + \int_{\Omega^p(t)} \boldsymbol{h} \cdot \boldsymbol{\varphi}^p d\boldsymbol{x} + \int_{\Omega^p(t)} s\psi^p d\boldsymbol{x}.\end{aligned} \tag{3.5}$$

To write a weak formulation of the coupled Navier–Stokes/Koiter/Biot system, define a space of admissible solutions

$$\begin{aligned} W(t) = \{&(\varphi^f, \hat{\boldsymbol{\zeta}}, \hat{\boldsymbol{\chi}}, \boldsymbol{\varphi}^p, \boldsymbol{\phi}^p) \in V^f(t) \times \hat{V}^m \times \hat{V}^m \times V^p(t) \times V^p(t) | \boldsymbol{\zeta} = \boldsymbol{\varphi}^p|_{\Gamma(t)}, \\ &\boldsymbol{\varphi}^f|_{\Gamma(t)} \cdot \boldsymbol{\tau} = \boldsymbol{\zeta} \cdot \boldsymbol{\tau}\}, \end{aligned} \tag{3.6}$$

where $\boldsymbol{\zeta} := \hat{\boldsymbol{\zeta}} \circ (\mathcal{A}_t^{-1}|_{\Gamma(t)})$, $\boldsymbol{\chi} := \hat{\boldsymbol{\chi}} \circ (\mathcal{A}_t^{-1}|_{\Gamma(t)})$, and add together Eqs. (3.3)–(3.5):

$$\begin{aligned}
&\rho_f \int_{\Omega^f(t)} \frac{\partial \boldsymbol{v}}{\partial t} \cdot \boldsymbol{\varphi}^f d\boldsymbol{x} + d_f(\boldsymbol{v}, \boldsymbol{v}, \boldsymbol{\varphi}^f) + a_f(\boldsymbol{v}, \boldsymbol{\varphi}^f) - b_f(p_f, \boldsymbol{\varphi}^f) + b_f(\psi^f, \boldsymbol{v}) \\
&\quad + \rho_m r_m \int_0^L \left(\hat{\boldsymbol{\xi}} - \frac{\partial \hat{\boldsymbol{\eta}}}{\partial t} \right) \cdot \hat{\boldsymbol{\chi}} d\hat{x} \\
&\quad + \rho_m r_m \int_0^L \frac{\partial \hat{\boldsymbol{\xi}}}{\partial t} \cdot \hat{\boldsymbol{\zeta}} d\hat{x} + a_m(\hat{\boldsymbol{\eta}}, \hat{\boldsymbol{\zeta}}) + \rho_p \int_{\Omega^p(t)} \left(\boldsymbol{V} - \frac{D\boldsymbol{U}}{Dt} \right) \cdot \boldsymbol{\phi}^p d\boldsymbol{x} \\
&\quad + \rho_p \int_{\Omega^p(t)} \frac{D\boldsymbol{V}}{Dt} \cdot \boldsymbol{\varphi}^p d\boldsymbol{x} + a_e(\boldsymbol{U}, \boldsymbol{\varphi}^p) - b_{ep}(p_p, \boldsymbol{\varphi}^p) + \int_{\Omega^p(t)} s_0 \frac{Dp_p}{Dt} \psi^p d\boldsymbol{x} \\
&\quad + b_{ep}\left(\psi^p, \frac{D\boldsymbol{U}}{Dt} \right) + a_p(p_p, \psi^p) \\
&= \int_{\Gamma(t)} \boldsymbol{\sigma}^f \boldsymbol{n} \cdot \boldsymbol{\varphi}^f dx - \int_{\Gamma(t)} \boldsymbol{\sigma}^p \boldsymbol{n} \cdot \boldsymbol{\varphi}^p dx - \int_{\Gamma(t)} \kappa \nabla p_p \cdot \boldsymbol{n} \psi^p dx + \int_0^L \hat{\boldsymbol{f}} \cdot \hat{\boldsymbol{\zeta}} dx \\
&\quad + \int_{\Omega^f(t)} \boldsymbol{g} \cdot \boldsymbol{\varphi}^f d\boldsymbol{x} + \int_{\Gamma_{\text{in}}} p_{\text{in}}(t) \varphi_x^f dy - \int_{\Gamma_{\text{ext}}^p} p_e \boldsymbol{\varphi}_y^p dx + \int_{\Omega^p(t)} \boldsymbol{h} \cdot \boldsymbol{\varphi}^p d\boldsymbol{x} + \int_{\Omega^p(t)} s \psi^p d\boldsymbol{x}.
\end{aligned} \tag{3.7}$$

Denote by $I_{\Gamma(t)}$ the interface integral

$$I_{\Gamma(t)} = \int_{\Gamma(t)} (\boldsymbol{\sigma}^f \boldsymbol{n} \cdot \boldsymbol{\varphi}^f - \boldsymbol{\sigma}^p \boldsymbol{n} \cdot \boldsymbol{\varphi}^p - \kappa \nabla p_p \cdot \boldsymbol{n} \psi^p + J^{-1} \boldsymbol{f} \cdot \boldsymbol{\zeta}) dx.$$

Decomposing the stress terms and thin shell forcing term into their normal and tangential components and using conditions (2.19) and (2.21), we have

$$\begin{aligned}
I_{\Gamma(t)} = \int_{\Gamma(t)} \Big(&- p_p \boldsymbol{\varphi}^f \cdot \boldsymbol{n} - (\boldsymbol{n} \cdot \boldsymbol{\sigma}^p \boldsymbol{n})(\boldsymbol{\varphi}^p \cdot \boldsymbol{n}) + J^{-1} (\boldsymbol{f} \cdot \boldsymbol{n})(\boldsymbol{\zeta} \cdot \boldsymbol{n}) + \boldsymbol{v} \cdot \boldsymbol{n} \psi^p - \frac{D\boldsymbol{U}}{Dt} \cdot \boldsymbol{n} \psi^p \\
&+ (\boldsymbol{\tau} \cdot \boldsymbol{\sigma}^f \boldsymbol{n})(\boldsymbol{\varphi}^f \cdot \boldsymbol{\tau}) - (\boldsymbol{\tau} \cdot \boldsymbol{\sigma}^p \boldsymbol{n})(\boldsymbol{\varphi}^p \cdot \boldsymbol{\tau}) + J^{-1} (\boldsymbol{f} \cdot \boldsymbol{\tau})(\boldsymbol{\zeta} \cdot \boldsymbol{\tau}) \Big) dx.
\end{aligned} \tag{3.8}$$

For each triple of test functions $(\boldsymbol{\varphi}^f, \hat{\boldsymbol{\zeta}}, \boldsymbol{\varphi}^p) \in W(t)$, due to the condition (2.22), we have

$$I_{\Gamma(t)} = \int_{\Gamma(t)} \left(-p_p \boldsymbol{\varphi}^f \cdot \boldsymbol{n} - (\boldsymbol{n} \cdot \boldsymbol{\sigma}^p \boldsymbol{n})(\varphi^p \cdot \boldsymbol{n}) + J^{-1} (\boldsymbol{f} \cdot \boldsymbol{n})(\boldsymbol{\varphi}^p \cdot \boldsymbol{n}) + \boldsymbol{v} \cdot \boldsymbol{n} \psi^p - \frac{D\boldsymbol{U}}{Dt} \cdot \boldsymbol{n} \psi^p \right) dx.$$

Finally, using conditions (2.21) and (2.22), we have

$$I_{\Gamma(t)} = \int_{\Gamma(t)} \left(-p_p \boldsymbol{\varphi}^f \cdot \boldsymbol{n} + p_p \boldsymbol{\varphi}^p \cdot \boldsymbol{n} + \boldsymbol{v} \cdot \boldsymbol{n} \psi^p - \frac{D\boldsymbol{U}}{Dt} \cdot \boldsymbol{n} \psi^p \right) dx.$$

Thus, the weak formulation of the coupled Navier–Stokes/Koiter/Biot system reads as follows: given $t \in (0, T)$ find $\boldsymbol{X} = (\boldsymbol{v}, \hat{\boldsymbol{\eta}}, \hat{\boldsymbol{\xi}}, \boldsymbol{U}, \boldsymbol{V}, p_f, p_p) \in V^f(t) \times \hat{V}^m \times \hat{V}^m \times V^p(t) \times$

$V^p(t) \times Q^f(t) \times Q^p(t)$, with $\boldsymbol{\eta} = \boldsymbol{U}|_{\Gamma(t)}, \boldsymbol{\xi} = \boldsymbol{V}|_{\Gamma(t)}$, and $\boldsymbol{v} \cdot \boldsymbol{\tau}|_{\Gamma(t)} = \boldsymbol{\xi} \cdot \boldsymbol{\tau}$, such that for all $\boldsymbol{Y} = (\boldsymbol{\varphi}^f, \hat{\boldsymbol{\xi}}, \hat{\boldsymbol{\chi}}, \boldsymbol{\varphi}^p, \boldsymbol{\phi}^p, \psi^f, \psi^p) \in W(t) \times Q^f(t) \times Q^p(t)$

$$\mathcal{P}(\boldsymbol{X}, \boldsymbol{Y}) + d_f(\boldsymbol{v}, \boldsymbol{v}, \boldsymbol{\varphi}^f) = \mathcal{F}(\boldsymbol{Y}), \tag{3.9}$$

where

$$\begin{aligned}
\mathcal{P}(\boldsymbol{X}, \boldsymbol{Y}) = {} & \rho_f \int_{\Omega^f(t)} \frac{\partial \boldsymbol{v}}{\partial t} \cdot \boldsymbol{\varphi}^f d\boldsymbol{x} + a_f(\boldsymbol{v}, \boldsymbol{\varphi}^f) - b_f(p_f, \boldsymbol{\varphi}^f) + b_f(\psi^f, \boldsymbol{v}) \\
& + \rho_m r_m \int_0^L \left(\hat{\boldsymbol{\xi}} - \frac{\partial \hat{\boldsymbol{\eta}}}{\partial t} \right) \cdot \hat{\boldsymbol{\chi}} d\hat{x} + \rho_m r_m \int_0^L \frac{\partial \hat{\boldsymbol{\xi}}}{\partial t} \cdot \hat{\boldsymbol{\zeta}} d\hat{x} + a_m(\hat{\boldsymbol{\eta}}, \hat{\boldsymbol{\zeta}}) \\
& + \rho_p \int_{\Omega^p(t)} \left(\boldsymbol{V} - \frac{D\boldsymbol{U}}{Dt} \right) \cdot \boldsymbol{\phi}^p d\boldsymbol{x} + \rho_p \int_{\Omega^p(t)} \frac{D\boldsymbol{V}}{Dt} \cdot \boldsymbol{\varphi}^p d\boldsymbol{x} + a_e(\boldsymbol{U}, \boldsymbol{\varphi}^p) - b_{ep}(p_p, \boldsymbol{\varphi}^p) \\
& + \int_{\Omega^p(t)} s_0 \frac{Dp_p}{Dt} \psi^p d\boldsymbol{x} + b_{ep}\left(\psi^p, \frac{D\boldsymbol{U}}{Dt} \right) + a_p(p_p, \psi^p) + c_{fp}(p_p, \boldsymbol{\varphi}^f) - c_{ep}(p_p, \boldsymbol{\varphi}^p) \\
& - c_{fp}(\psi_p, \boldsymbol{v}) + c_{ep}\left(\psi_p, \frac{D\boldsymbol{U}}{Dt} \right),
\end{aligned} \tag{3.10}$$

and

$$\mathcal{F}(\boldsymbol{Y}) = \int_{\Omega^f(t)} \boldsymbol{g} \cdot \boldsymbol{\varphi}^f d\boldsymbol{x} + \int_{\Gamma_{\text{in}}} p_{\text{in}}(t) \varphi_x^f dy - \int_{\Gamma_{\text{ext}}^p} p_e \boldsymbol{\varphi}_y^p dx + \int_{\Omega^p(t)} \boldsymbol{h} \cdot \boldsymbol{\varphi}^p d\boldsymbol{x} + \int_{\Omega^p(t)} s \psi^p d\boldsymbol{x}. \tag{3.11}$$

Note that the interface terms are contained in bilinear forms $c_{fp}(\cdot, \cdot)$ and $c_{ep}(\cdot, \cdot)$. In the error analysis, for simplicity, we will focus on the time dependent Stokes problem, in which case term $d_f(\boldsymbol{v}, \boldsymbol{v}, \boldsymbol{\varphi}^f)$ will be dropped.

IV. A LOOSELY COUPLED OPERATOR-SPLITTING APPROACH

To approximate the fluid-multilayered structure interaction problem described in Section II, we propose a loosely coupled scheme based on a time-splitting approach known as the Lie splitting [60]. The Lie splitting is applied following the same approach as in [13, 56]. Denote the vector of unknowns by $\boldsymbol{X}$. Then, system (2.28) is equivalent to

$$\frac{\partial \boldsymbol{X}}{\partial t} + A(\boldsymbol{X}) = 0, \quad \text{in } (0, T), \tag{4.1}$$

where $A = A_1 + A_2$ is an operator from a Hilbert space H into itself. The Lie scheme corresponds to solving the following subproblems

$$\begin{aligned}
&\frac{\partial \boldsymbol{X}_1}{\partial t} + A_1(\boldsymbol{X}_1) = 0 \quad \text{in } (t^n, t^{n+1}), \quad \text{with } \boldsymbol{X}_1(t^n) = \boldsymbol{X}^n, \\
&\frac{\partial \boldsymbol{X}_2}{\partial t} + A_2(\boldsymbol{X}_2) = 0 \quad \text{in } (t^n, t^{n+1}), \quad \text{with } \boldsymbol{X}_2(t^n) = \boldsymbol{X}_1(t^{n+1}).
\end{aligned}$$

Operators A_1 and A_2, where $A_i = (A_i^v, A_i^{\xi_\tau}, A_i^{\xi_n}, A_i^\eta, A_i^V, A_i^{p_p}, A_i^U)^T$, for $i = 1, 2$, are defined as follows

$$A_1 = \begin{bmatrix} \rho_f(\boldsymbol{v} - \boldsymbol{w}) \cdot \nabla \boldsymbol{v} - \nabla \cdot \sigma^f \\ J\boldsymbol{\tau} \cdot \boldsymbol{\sigma}^f \boldsymbol{n} \\ 0 \\ 0 \\ 0 \\ 0 \\ 0 \end{bmatrix}, \quad A_2 = \begin{bmatrix} 0 \\ \boldsymbol{\tau} \cdot \mathcal{L}\boldsymbol{\eta} - J\boldsymbol{\tau} \cdot \sigma^p \boldsymbol{n} \\ \boldsymbol{n} \cdot \mathcal{L}\boldsymbol{\eta} - J p_p - J\boldsymbol{n} \cdot \sigma^p \boldsymbol{n} \\ \boldsymbol{\xi} \\ -\nabla \cdot \boldsymbol{\sigma}^p \\ \alpha \nabla \cdot \boldsymbol{V} - \nabla \cdot (\kappa \nabla p_p) \\ \boldsymbol{V} \end{bmatrix}. \tag{4.2}$$

Using this approach, our system is decoupled into a fluid problem and the Biot problem. Furthermore, we not only split the coupled problem into two different domains, but we also treat different physical phenomena separately. Details of the loosely coupled scheme in the weak formulation are given below.

A. Weak Formulation of the Numerical Algorithm in the Discrete Form

In this section, we present the loosely coupled numerical algorithm in the variational formulation. For simplicity, we work out the analysis assuming that the displacement of the boundary is small enough and can be neglected. Under these assumptions, domains $\Omega^f(t)$ and $\Omega^p(t)$ are fixed:

$$\Omega^f(t) = \hat{\Omega}^f, \quad \Omega^p(t) = \hat{\Omega}^p, \quad \forall t \in (0, T).$$

Although simplified, this problem still retains the main difficulties associated with the "added-mass" effect and the difficulties that partitioned schemes encounter when modeling fluid-porous medium coupling. Since from now on all the variables are defined on the fixed domain, we will drop the "hat" notation to avoid cumbersome expressions.

Let $t^n := n\Delta t$ for $n = 1, \ldots, N$, where $T = N\Delta t$ is the final time. Let the test function spaces V^f, Q^f, V^p, and Q^p be defined as in (3.1), (3.2), (3), and (3), respectively. The discretization in time is preformed using the backward Euler scheme. We denote the discrete time derivatives by

$$d_t \boldsymbol{\varphi}^{n+1} = \frac{\boldsymbol{\varphi}^{n+1} - \boldsymbol{\varphi}^n}{\Delta t} \quad \text{and} \quad d_{tt} \boldsymbol{\varphi}^{n+1} = \frac{d_t \boldsymbol{\varphi}^{n+1} - d_t \boldsymbol{\varphi}^n}{\Delta t}.$$

To discretize the problem in space, we use the finite element method. Thus, we define the finite element spaces $V_h^f \subset V^f$, $Q_h^f \subset Q^f$, $V_h^p \subset V^p$, $Q_h^p \subset Q^p$, and $V_h^m := V_h^p|_\Gamma$. We assume that spaces V_h^f and Q_h^f are inf-sup stable. The definition of these discrete spaces will be made precise at the beginning of Section V. We assume that all the finite element initial conditions are equal to zero:

$$\boldsymbol{v}_h^0 = 0, \quad \boldsymbol{U}_h^0 = 0, \quad \boldsymbol{V}_h^0 = 0, \quad \boldsymbol{\eta}_h^0 = 0, \quad \boldsymbol{\xi}_h^0 = 0, \quad p_{p,h}^0 = 0.$$

Finally, the fully discrete numerical scheme is given as follows:

- Step 1. Given $t^{n+1} \in (0, T], n = 0, \ldots, N-1$, find $\boldsymbol{v}_h^{n+1} \in V_h^f$ and $p_{f,h}^{n+1} \in Q_h^f$, with $\boldsymbol{V}_h^n$ and $p_{p,h}^n$ obtained at the previous time step, such that for all $(\boldsymbol{\varphi}_h^f, \psi_h^f) \in V_h^f \times Q_h^f$:

$$\rho_f \int_{\Omega^f} d_t \boldsymbol{v}_h^{n+1} \cdot \boldsymbol{\varphi}_h^f d\boldsymbol{x} + d_f(\boldsymbol{v}_h^{n+1}, \boldsymbol{v}_h^{n+1}, \boldsymbol{\varphi}_h^f) + a_f(\boldsymbol{v}_h^{n+1}, \boldsymbol{\varphi}_h^f)$$
$$+ \rho_m r_m \int_\Gamma \frac{\boldsymbol{v}_h^{n+1} \cdot \boldsymbol{\tau} - \boldsymbol{V}_h^n \cdot \boldsymbol{\tau}}{\Delta t} (\boldsymbol{\varphi}_h^f \cdot \boldsymbol{\tau}) dx$$

$$- b_f(p_{f,h}^{n+1}, \boldsymbol{\varphi}_h^f) + b_f(\psi_h^f, \boldsymbol{v}_h^{n+1}) + c_{fp}(p_{p,h}^n, \boldsymbol{\varphi}_h^f)$$
$$= \int_{\Omega^f} \boldsymbol{g}(t^{n+1}) \cdot \boldsymbol{\varphi}_h^f d\boldsymbol{x} + \int_{\Gamma_{\text{in}}} p_{\text{in}}(t^{n+1}) \varphi_{x,h}^f dy. \tag{4.3}$$

- Step 2. Given $\boldsymbol{v}_h^{n+1}$ computed in Step 1, find $\boldsymbol{U}_h^{n+1} \in V_h^p$, $\boldsymbol{V}_h^{n+1} \in V_h^p$, and $p_{p,h}^{n+1} \in Q_h^p$, such that for all $(\boldsymbol{\varphi}_h^p, \boldsymbol{\phi}_h^p, \psi_h^p) \in V_h^p \times V_h^p \times Q_h^p$:

$$\rho_p \int_{\Omega^p} (\boldsymbol{V}_h^{n+1} - d_t \boldsymbol{U}_h^{n+1}) \cdot \boldsymbol{\phi}_h^p d\boldsymbol{x} + \rho_p \int_{\Omega^p} d_t \boldsymbol{V}_h^{n+1} \cdot \boldsymbol{\varphi}_h^p d\boldsymbol{x} + a_e(\boldsymbol{U}_h^{n+1}, \boldsymbol{\varphi}_h^p) + \int_{\Omega^p} s_0 d_t p_{p,h}^{n+1} \psi_h^p d\boldsymbol{x}$$
$$+ a_p(p_{p,h}^{n+1}, \psi_h^p) - b_{ep}(p_{p,h}^{n+1}, \boldsymbol{\varphi}_h^p) + b_{ep}(\psi_h^p, d_t \boldsymbol{U}_h^{n+1}) + \rho_m r_m \int_\Gamma (d_t \boldsymbol{V}_h^{n+1} \cdot \boldsymbol{n})(\boldsymbol{\varphi}_h^p \cdot \boldsymbol{n}) dx$$
$$+ \rho_m r_m \int_\Gamma \frac{\boldsymbol{V}_h^{n+1} \cdot \boldsymbol{\tau} - \boldsymbol{v}_h^{n+1} \cdot \boldsymbol{\tau}}{\Delta t} (\boldsymbol{\varphi}_h^p \cdot \boldsymbol{\tau}) dx + a_m(\boldsymbol{U}_h|_\Gamma^{n+1}, \boldsymbol{\varphi}_h^p|_\Gamma) - c_{ep}(p_{p,h}^{n+1}, \boldsymbol{\varphi}_h^p)$$
$$+ c_{ep}(\psi_h^p, d_t \boldsymbol{U}_h^{n+1}) - c_{fp}(\psi_h^p, \boldsymbol{v}_h^{n+1}) = - \int_{\Gamma_{\text{ext}}^p} p_e \boldsymbol{\varphi}_{y,h}^p dx + \int_{\Omega^p} \boldsymbol{h}(t^{n+1}) \cdot \boldsymbol{\varphi}_h^p d\boldsymbol{x}$$
$$+ \int_{\Omega^p} s(t^{n+1}) \psi_h^p d\boldsymbol{x}. \tag{4.4}$$

The proposed scheme is an explicit loosely coupled scheme where the first step consists of a fluid (Navier–Stokes) problem, and the second step consists of a poroelastic problem. Both subproblems are solved with Robin-type boundary conditions, which take into account thin-shell inertia and kinematic conditions implicitly. Moreover, the kinematic condition is taken as an initial condition in each of the subproblems. We note that the original monolithic problem becomes fully decoupled, and there are no subiterations needed between the two subproblems.

Remark 1. Once $\boldsymbol{U}_h^{n+1}$ and $\boldsymbol{V}_h^{n+1}$ are computed, we can find the membrane displacement $\boldsymbol{\eta}_h^{n+1}$ and velocity $\boldsymbol{\xi}_h^{n+1}$ via

$$\boldsymbol{\eta}_h^{n+1} = \boldsymbol{U}_h^{n+1}|_\Gamma, \quad \boldsymbol{\xi}_h^{n+1} = \boldsymbol{V}_h^{n+1}|_\Gamma.$$

Remark 2. One can apply additional splitting to Step 1 and Step 2 of the algorithm described above. Namely, the fluid problem described in Step 1 can be split into its viscous part (the Stokes equations for an incompressible fluid) and the pure advection part (incorporating the fluid and ALE advection simultaneously). The Biot system described in Step 2 can be split so the elastodynamics is treated separately from the pressure. For the details of possible Biot splitting strategies, see [73] and the references therein.

B. Stability Analysis

To present our results in a more compact manner, in the analysis we study the Stokes equations instead of the Navier–Stokes equations. Let us introduce the following seminorms

$$||\boldsymbol{\varphi}_h^p||_E := a_e(\varphi_h^p, \varphi_h^p)^{1/2} \quad \forall \boldsymbol{\varphi}_h^p \in V_h^p, \tag{4.5}$$

and

$$||\boldsymbol{\zeta}_h||_M := a_m(\boldsymbol{\zeta}_h, \boldsymbol{\zeta}_h)^{1/2} \quad \forall \boldsymbol{\zeta}_h \in V_h^m. \tag{4.6}$$

Furthermore, we define the time discrete norms:

$$||\boldsymbol{\varphi}||_{l^2(0,T;S)} = \left(\Delta t \sum_{n=0}^{N-1} ||\boldsymbol{\varphi}^{n+1}||_S^2 \right)^{1/2}, \quad ||\boldsymbol{\varphi}||_{l^\infty(0,T;S)} = \max_{0\le n\le N} ||\boldsymbol{\varphi}^n||_S,$$

where $S \in \{H^k(\Omega^f), H^k(\Omega^p), H^k(0,L), E, M\}$.

Let $\mathcal{E}_f^n$ denote the discrete energy of the fluid problem, $\mathcal{E}_p^n$ denote the discrete energy of the Biot problem, and $\mathcal{E}_m^n$ denote the discrete energy of the Koiter membrane at time level n, defined respectively by

$$\mathcal{E}_f^n = \frac{\rho_f}{2} ||\boldsymbol{v}_h^n||^2_{L^2(\Omega^f)}, \tag{4.7}$$

$$\mathcal{E}_p^n = \frac{\rho_p}{2} ||\boldsymbol{V}_h^n||^2_{L^2(\Omega^p)} + \frac{1}{2} ||\boldsymbol{U}_h^n||^2_E + \frac{s_0}{2} ||p_{p,h}^n||^2_{L^2(\Omega^p)}, \tag{4.8}$$

$$\mathcal{E}_m^n = \frac{\rho_m r_m}{2} ||\xi_h^n||^2_{L^2(0,L)} + \frac{1}{2} ||\eta_h^n||^2_M. \tag{4.9}$$

Before proceeding, let us address the following property that will serve as auxiliary result for the stability and error analysis.

Lemma 1. *Suppose* $(\boldsymbol{U}_h^{n+1}, \boldsymbol{V}_h^{n+1}, p_{p,h}^{n+1})$ *is a solution to (4.4). Then,*

$$\boldsymbol{V}_h^{n+1} = d_t \boldsymbol{U}_h^{n+1}. \tag{4.10}$$

Proof. Let $(\varphi_h^p, \boldsymbol{\phi}_h^p, \psi_h^p) = (\boldsymbol{0}, \boldsymbol{V}_h^{n+1} - d_t \boldsymbol{U}_h^{n+1}, 0)$ in (4.4). Then, we have

$$\| \boldsymbol{V}_h^{n+1} - d_t \boldsymbol{U}_h^{n+1} \|^2_{L^2(\Omega^p)} = 0,$$

and the assertion follows. ∎

The stability of the loosely coupled scheme (4.3)–(4.4) is stated in the following result. The constants that appear in (4.11) are defined in Appendix. They depend on the geometry and triangulation of the domain, and the configuration of Dirichlet conditions on the boundary.

Theorem 1. *Assume that the fluid-poroelastic system is isolated, that is,* $p_{in} = 0, p_e = 0, \boldsymbol{g} = 0, \boldsymbol{h} = 0$ *and* $s = 0$. *Let* $\{(\boldsymbol{v}_h^n, p_{p,h}^n, \boldsymbol{V}_h^n, \boldsymbol{U}_h^n, \boldsymbol{\xi}_h^n, \boldsymbol{\eta}_h^n, p_{p,h}^n)\}_{0\le n\le N}$ *be the solution of (4.3) and (4.4). Then, under the condition*

$$\left(2\mu_f - \frac{C_K^2 C_{TI} C_T^2 C_{PF} \Delta t}{s_0 h} \right) \ge \gamma > 0 \quad \textit{i.e. } \Delta t < \frac{2\mu_f s_0 h}{C_K^2 C_{TI} C_T^2 C_{PF}}, \tag{4.11}$$

the following estimate holds:

$$\begin{aligned}
&\mathcal{E}_f^N + \mathcal{E}_p^N + \mathcal{E}_m^N + \frac{\Delta t}{4} \rho_f ||d_t \boldsymbol{v}_h||^2_{l^2(0,T;L^2(\Omega^f))} + \frac{\Delta t^2}{4} \rho_m r_m \sum_{n=0}^{N-1} \left\| \frac{\boldsymbol{v}_h^{n+1} \cdot \boldsymbol{\tau} - \boldsymbol{V}_h^n \cdot \boldsymbol{\tau}}{\Delta t} \right\|^2_{L^2(\Gamma)} \\
&\quad + \frac{\gamma}{2} ||D(\boldsymbol{v}_h)||^2_{l^2(0,T;L^2(\Omega^f))} + \frac{\Delta t^2}{2} \rho_m r_m \sum_{n=0}^{N-1} \left\| \frac{\boldsymbol{V}_h^{n+1} \cdot \boldsymbol{\tau} - \boldsymbol{v}_h^{n+1} \cdot \boldsymbol{\tau}}{\Delta t} \right\|^2_{L^2(\Gamma)} \\
&\quad + \frac{\Delta t}{2} \rho_m r_m ||d_t \boldsymbol{\xi}_h \cdot \boldsymbol{n}||^2_{l^2(0,T;L^2(\Gamma))} + \frac{\Delta t}{2} \rho_p ||d_t \boldsymbol{V}_h||^2_{l^2(0,T;L^2(\Omega^p))}
\end{aligned}$$

$$+\frac{\Delta t}{2}||d_t\boldsymbol{U}_h||^2_{l^2(0,T;E)}+\frac{\Delta t}{2}||d_t\eta_h||^2_{l^2(0,T;M)}+\delta\Delta t||p_{f,h}||^2_{l^2(0,T;L^2(\Omega^f))}$$
$$+\frac{\Delta t}{4}s_0||d_t p_{p,h}||^2_{l^2(0,T;L^2(\Omega^p))}+\frac{1}{2}||\sqrt{\kappa}\nabla p_{p,h}||^2_{l^2(0,T;L^2(\Omega^p))}\leq\mathcal{E}_f^0+\mathcal{E}_p^0+\mathcal{E}_m^0, \tag{4.12}$$

where δ is given in the proof.

Proof. To prove the energy estimate, we test the problem (4.3) with $(\boldsymbol{\varphi}_h^f,\psi_h^f)=(\boldsymbol{v}_h^{n+1},p_{f,h}^{n+1})$, and problem (4.4) with $(\boldsymbol{\varphi}_h^p,\boldsymbol{\phi}_h^p,\psi_h^p)=(d_t\boldsymbol{U}_h^{n+1},d_t\boldsymbol{V}_h^{n+1},p_{p,h}^{n+1})$. Note that, due to (4.10), we have $\boldsymbol{V}_h^{n+1}=d_t\boldsymbol{U}_h^{n+1}$. Adding the equations together and multiplying by Δt, we get

$$\begin{aligned}
&\frac{\rho_f}{2}\left(||\boldsymbol{v}_h^{n+1}||^2_{L^2(\Omega^f)}-||\boldsymbol{v}_h^{n}||^2_{L^2(\Omega^f)}+||\boldsymbol{v}_h^{n+1}-\boldsymbol{v}_h^{n}||^2_{L^2(\Omega^f)}\right)+2\mu_f\Delta t||D(\boldsymbol{v}_h^{n+1})||^2_{L^2(\Omega^f)}\\
&\quad+\frac{\rho_m r_m}{2}\left(||\boldsymbol{v}_h^{n+1}\cdot\boldsymbol{\tau}||^2_{L^2(\Gamma)}-||\boldsymbol{V}_h^{n}\cdot\boldsymbol{\tau}||^2_{L^2(\Gamma)}+||\boldsymbol{v}_h^{n+1}\cdot\boldsymbol{\tau}-\boldsymbol{V}_h^{n}\cdot\boldsymbol{\tau}||^2_{L^2(\Gamma)}\right)\\
&\quad+\frac{\rho_p}{2}\left(||\boldsymbol{V}_h^{n+1}||^2_{L^2(\Omega^p)}-||\boldsymbol{V}_h^{n}||^2_{L^2(\Omega^p)}+||\boldsymbol{V}_h^{n+1}-\boldsymbol{V}_h^{n}||^2_{L^2(\Omega^p)}\right)\\
&\quad+\frac{1}{2}\left(||\boldsymbol{U}_h^{n+1}||^2_{E}-||\boldsymbol{U}_h^{n}||^2_{E}+||\boldsymbol{U}_h^{n+1}-\boldsymbol{U}_h^{n}||^2_{E}\right)\\
&\quad+\frac{s_0}{2}\left(||p_{p,h}^{n+1}||^2_{L^2(\Omega^p)}-||p_{p,h}^{n}||^2_{L^2(\Omega^p)}+||p_{p,h}^{n+1}-p_{p,h}^{n}||^2_{L^2(\Omega^p)}\right)\\
&\quad+\Delta t||\sqrt{\kappa}\nabla p_{p,h}^{n+1}||^2_{L^2(\Omega^p)}+\frac{\rho_m r_m}{2}\left(||\boldsymbol{V}_h^{n+1}\cdot\boldsymbol{n}||^2_{L^2(\Gamma)}-||\boldsymbol{V}_h^{n}\cdot\boldsymbol{n}||^2_{L^2(\Gamma)}+||\boldsymbol{V}_h^{n+1}\cdot\boldsymbol{n}-\boldsymbol{V}_h^{n}\cdot\boldsymbol{n}||^2_{L^2(\Gamma)}\right)\\
&\quad+\frac{\rho_m r_m}{2}\left(||\boldsymbol{V}_h^{n+1}\cdot\boldsymbol{\tau}||^2_{L^2(\Gamma)}-||\boldsymbol{v}_h^{n+1}\cdot\boldsymbol{\tau}||^2_{L^2(\Gamma)}+||\boldsymbol{V}_h^{n+1}\cdot\boldsymbol{\tau}-\boldsymbol{v}_h^{n+1}\cdot\boldsymbol{\tau}||^2_{L^2(\Gamma)}\right)\\
&\quad+\frac{1}{2}\left(||\boldsymbol{U}_h^{n+1}|_\Gamma||^2_{M}-||\boldsymbol{U}_h^{n}|_\Gamma||^2_{M}+||\boldsymbol{U}_h^{n+1}|_\Gamma-\boldsymbol{U}_h^{n}|_\Gamma||^2_{M}\right)\leq\Delta t c_{fp}(p_{p,h}^{n+1},\boldsymbol{v}_h^{n+1})-\Delta t c_{fp}(p_{p,h}^{n},\boldsymbol{v}_h^{n+1}).
\end{aligned}$$

Canceling $||\boldsymbol{v}_h^{n+1}\cdot\boldsymbol{\tau}||^2_{L^2(\Gamma)}$ and using the discrete energy defined by (4.7)–(4.9), we have

$$\begin{aligned}
&\mathcal{E}_f^{n+1}+\mathcal{E}_p^{n+1}+\mathcal{E}_m^{n+1}+\frac{\rho_f\Delta t^2}{2}||d_t\boldsymbol{v}_h^{n+1}||^2_{L^2(\Omega^f)}+2\mu_f\Delta t||D(\boldsymbol{v}_h^{n+1})||^2_{L^2(\Omega^f)}+\frac{\rho_m r_m}{2}||\boldsymbol{v}_h^{n+1}\cdot\boldsymbol{\tau}\\
&\quad-\boldsymbol{V}_h^{n}\cdot\boldsymbol{\tau}||^2_{L^2(\Gamma)}+\frac{\rho_m r_m}{2}||\boldsymbol{V}_h^{n+1}\cdot\boldsymbol{\tau}-\boldsymbol{v}_h^{n+1}\cdot\boldsymbol{\tau}||^2_{L^2(\Gamma)}+\frac{\rho_m r_m\Delta t^2}{2}||d_t\boldsymbol{V}_h^{n+1}\cdot\boldsymbol{n}||^2_{L^2(\Gamma)}\\
&\quad+\frac{\rho_p\Delta t^2}{2}||d_t\boldsymbol{V}_h^{n+1}||^2_{L^2(\Omega^p)}+\frac{\Delta t^2}{2}||d_t\boldsymbol{U}_h^{n+1}||^2_{E}+\frac{\Delta t^2}{2}||d_t\boldsymbol{U}_h^{n+1}|_\Gamma||_{M}+\frac{s_0\Delta t^2}{2}||d_t p_{p,h}^{n+1}||^2_{L^2(\Omega^p)}\\
&\quad+\Delta t||\sqrt{\kappa}\nabla p_{p,h}^{n+1}||^2_{L^2(\Omega^p)}\leq\Delta t c_{fp}(p_{p,h}^{n+1},\boldsymbol{v}_h^{n+1})-\Delta t c_{fp}(p_{p,h}^{n},\boldsymbol{v}_h^{n+1})+\mathcal{E}_f^n+\mathcal{E}_p^n+\mathcal{E}_m^n.
\end{aligned}\tag{4.13}$$

The term $\Delta t c_{fp}(p_{p,h}^{n+1}-p_{p,h}^{n},\boldsymbol{v}_h^{n+1})$ arises in classical partitioned schemes for Navier Stokes/Stokes–Darcy coupling, and has been previously addressed in [6]. Following the similar approach as in [6], we can estimate the interface term using Cauchy–Schwarz inequality (A5), Young's inequality (A3) (for $\epsilon_1>0$), and the local trace-inverse inequality (A4) in the following way:

$$\Delta t c_{fp}(p_{p,h}^{n+1}-p_{p,h}^{n},\boldsymbol{v}_h^{n+1})=\Delta t\int_\Gamma(p_{p,h}^{n+1}-p_{p,h}^{n})\boldsymbol{v}_h^{n+1}\cdot\boldsymbol{n}dx$$

$$\leq \frac{\epsilon_1 \Delta t}{2} ||p_{p,h}^{n+1} - p_{p,h}^{n}||^2_{L^2(\Gamma)} + \frac{\Delta t}{2\epsilon_1} ||\boldsymbol{v}_h^{n+1}||^2_{L^2(\Gamma)}$$

$$\leq \frac{\epsilon_1 \Delta t C_{TI}}{2h} ||p_{p,h}^{n+1} - p_{p,h}^{n}||^2_{L^2(\Omega)} + \frac{\Delta t}{2\epsilon_1} ||\boldsymbol{v}_h^{n+1}||^2_{L^2(\Gamma)}.$$

Finally, using trace inequality (A7), Poincaré inequality (A6), and Korn's inequality (A8), we have

$$\Delta t c_{fp}(p_{p,h}^{n+1} - p_{p,h}^{n}, \boldsymbol{v}_h^{n+1}) \leq \frac{\epsilon_1 \Delta t C_{TI}}{2h} ||p_{p,h}^{n+1} - p_{p,h}^{n}||^2_{L^2(\Omega)} + \frac{\Delta t C_T^2 C_K^2 C_{PF}}{2\epsilon_1} ||D(\boldsymbol{v}_h^{n+1})||^2_{L^2(\Omega)}. \tag{4.14}$$

Both terms are combined with the equivalent terms on the right-hand side. Setting $\epsilon_1 = \frac{s_0 h}{2\Delta t C_{TI}}$ gives rise to the stability condition in (4.11). To recover control on the pressure in the fluid domain, we exploit the inf-sup stability of the approximation spaces V_h^f and Q_h^f. Namely, spaces V_h^f and Q_h^f are inf-sup stable provided

$$\inf_{p_{f,h}^{n+1} \in Q_h^f} \sup_{\boldsymbol{\varphi}^f \in V_h^f} \frac{b_f(p_{f,h}^{n+1}, \boldsymbol{\varphi}_h^f)}{||\boldsymbol{\varphi}_h^f||_{H^1(\Omega^f)} ||p_{f,h}^{n+1}||_{L^2(\Omega^f)}} = \beta_f > 0. \tag{4.15}$$

Combining the inf-sup condition (4.15) with (4.3) tested with $\psi_h^f = 0$, we obtain

$$\beta_f ||p_{f,h}^{n+1}||_{L^2(\Omega^f)} \leq \sup_{\boldsymbol{\varphi}_h^f \in V_h^f} \frac{\sum_{k=1,2} \mathcal{T}_k(\boldsymbol{\varphi}_h^f)}{||\boldsymbol{\varphi}_h^f||_{H^1(\Omega^f)}} \tag{4.16}$$

where $\beta_f > 0$ is a constant independent of the mesh characteristic size and $\mathcal{T}_k(\boldsymbol{\varphi}_h^f)$ is a shorthand notation for the following terms

$$\mathcal{T}_1(\boldsymbol{\varphi}_h^f) := \rho_f \int_{\Omega^f} d_t \boldsymbol{v}_h^{n+1} \cdot \boldsymbol{\varphi}_h^f d\boldsymbol{x} + \rho_m r_m \int_\Gamma \frac{\boldsymbol{v}_h^{n+1} \cdot \boldsymbol{\tau} - \boldsymbol{V}_h^n \cdot \boldsymbol{\tau}}{\Delta t} (\boldsymbol{\varphi}_h^f \cdot \boldsymbol{\tau}) dx,$$

$$\mathcal{T}_2(\boldsymbol{\varphi}_h^f) := a_f(\boldsymbol{v}_h^{n+1}, \boldsymbol{\varphi}_h^f) + c_{fp}(p_{p,h}^n, \boldsymbol{\varphi}_h^f).$$

Exploiting the Cauchy–Schwarz (A5), trace (A7), and Poincaré (A6) inequalities, we obtain the following upper bounds

$$\sup_{\boldsymbol{\varphi}_h^f \in V_h^f} \frac{\mathcal{T}_1(\boldsymbol{\varphi}_h^f)}{||\boldsymbol{\varphi}_h^f||_{H^1(\Omega^f)}} \leq C_T C_{PF} \left(\rho_f ||d_t \boldsymbol{v}_h^{n+1}||_{L^2(\Omega^f)} + \rho_m r_m \left\| \frac{\boldsymbol{v}_h^{n+1} \cdot \boldsymbol{\tau} - \boldsymbol{V}_h^n \cdot \boldsymbol{\tau}}{\Delta t} \right\|_{L^2(\Gamma)} \right),$$

$$\sup_{\boldsymbol{\varphi}_h^f \in V_h^f} \frac{\mathcal{T}_2(\boldsymbol{\varphi}_h^f)}{||\boldsymbol{\varphi}_h^f||_{H^1(\Omega^f)}} \leq 2\mu_f ||D(\boldsymbol{v}_h^{n+1})||_{L^2(\Omega^f)} + C_T C_{PF} \kappa^{-1/2} ||\sqrt{\kappa} \nabla p_{p,h}^n||_{L^2(\Omega^p)}.$$

Let us now multiply the square of (4.16) as well as the bounds for $\mathcal{T}_k(\boldsymbol{\varphi}_h^f)$ by $\epsilon_2 \Delta t^2$ and combine the resulting inequality with (4.13) and (4.14) to get,

$$\mathcal{E}_f^{n+1} + \mathcal{E}_p^{n+1} + \mathcal{E}_m^{n+1} + \frac{\Delta t^2}{2} \rho_f (1 - 4\epsilon_2 C_T^2 C_{PF}^2 \rho_f) ||d_t \boldsymbol{v}_h^{n+1}||^2_{L^2(\Omega^f)}$$

$$+ 2\mu_f \Delta t \left(1 - \frac{C_T^2 C_K^2 C_{PF}}{4\mu_f \epsilon_1} - 2\epsilon_2 \Delta t \mu_f\right) ||D(\boldsymbol{v}_h^{n+1})||^2_{L^2(\Omega^f)}$$

$$+ \frac{\Delta t^2}{2} \rho_m r_m (1 - 4\epsilon_2 C_T^2 C_{PF}^2 \rho_m r_m) \left\| \frac{\boldsymbol{v}_h^{n+1} \cdot \boldsymbol{\tau} - \boldsymbol{V}_h^n \cdot \boldsymbol{\tau}}{\Delta t} \right\|^2_{L^2(\Gamma)} + \frac{\rho_m r_m \Delta t^2}{2} \left\| \frac{\boldsymbol{V}_h^{n+1} \cdot \boldsymbol{\tau} - \boldsymbol{v}_h^{n+1} \cdot \boldsymbol{\tau}}{\Delta t} \right\|^2_{L^2(\Gamma)}$$

$$+ \frac{\rho_m r_m \Delta t^2}{2} ||d_t \boldsymbol{\xi}_h^{n+1} \cdot \boldsymbol{n}||^2_{L^2(\Gamma)} + \frac{\rho_p \Delta t^2}{2} ||d_t \boldsymbol{V}_h^{n+1}||^2_{L^2(\Omega^p)} + \frac{\Delta t^2}{2} ||d_t \boldsymbol{U}_h^{n+1}||^2_E + \frac{\Delta t^2}{2} ||d_t \boldsymbol{\eta}_h^{n+1}||^2_M$$

$$+ \frac{\Delta t^2}{2} \left(s_0 - \frac{\epsilon_1 \Delta t C_{TI}}{h}\right) ||d_t p_{p,h}^{n+1}||^2_{L^2(\Omega^p)} + \epsilon_2 \beta_f^2 \Delta t^2 ||p_{f,h}^{n+1}||^2_{L^2(\Omega^f)} + \Delta t ||\sqrt{\kappa} \nabla p_{p,h}^{n+1}||^2_{L^2(\Omega^p)}$$

$$- 2\epsilon_2 \Delta t^2 \frac{C_T^2 C_{PF}^2}{\kappa} ||\sqrt{\kappa} \nabla p_{p,h}^n||^2_{L^2(\Omega^p)} \leq \mathcal{E}_f^n + \mathcal{E}_p^n + \mathcal{E}_m^n. \tag{4.17}$$

Note that here we used equalities $\boldsymbol{\eta}_h^{n+1} = \boldsymbol{U}_h^{n+1}|_\Gamma$ and $\boldsymbol{\xi}_h^{n+1} = \boldsymbol{V}_h^{n+1}|_\Gamma$. After summing up with respect to the time index n, we observe that

$$\Delta t \sum_{n=0}^{N-1} \left[||\sqrt{\kappa} \nabla p_{p,h}^{n+1}||^2_{L^2(\Omega^p)} - 2\epsilon_2 \Delta t^2 \frac{C_T^2 C_{PF}^2}{\kappa} ||\sqrt{\kappa} \nabla p_{p,h}^n||^2_{L^2(\Omega^p)} \right]$$

$$= \Delta t \sum_{n=1}^{N-1} \left(1 - 2\epsilon_2 \Delta t \frac{C_T^2 C_{PF}^2}{\kappa}\right) ||\sqrt{\kappa} \nabla p_{p,h}^n||^2_{L^2(\Omega^p)} + \Delta t ||\sqrt{\kappa} \nabla p_{p,h}^N||^2_{L^2(\Omega^p)}.$$

By setting

$$\epsilon_2 = \frac{1}{2} \min \left(\frac{1}{2\rho_f C_T^2 C_{PF}^2}, \frac{1}{2\rho_m r_m C_T^2 C_{PF}^2}, \frac{1}{2\Delta t \mu_f} - \frac{C_T^2 C_K^2 C_{PF} C_{TI}}{2\mu_f^2 s_0 h}, \frac{\kappa}{\Delta t C_T^2 C_{PF}^2} \right)$$

we prove the desired estimate with $\delta = \epsilon_2 \beta_f^2$. ∎

Remark 3. Numerical algorithm (4.3) and (4.4) can be seen as a combination of a partitioned scheme for Stokes/Darcy coupled problem presented in [6] and the kinematically coupled scheme [13, 56] for decoupling FSI problems. While the kinematically coupled scheme is proven to be unconditionally stable, the partitioned algorithm for Stokes/Darcy coupled problem gives rise to a stability condition. Indeed, we recover the same property here. The stability condition is independent of the fluid and structure densities, and therefore the scheme is not affected by the instabilities related to the added mass effect. The bilinear form responsible for the stability condition depends only on the Darcy pressure and the fluid velocity, and is equivalent to the problematic one in the Stokes/Darcy system.

V. ERROR ANALYSIS

In this section, we analyze the convergence rate of the proposed method with respect to the monolithic solution. We start by subtracting the discrete solution obtained by the proposed scheme from the continuous solution, giving rise to the consistency error terms and the operator splitting error residuals. The operator splitting error can clearly be separated into terms arising from splitting

the Stokes/Darcy system (operator $\mathcal{R}_{os1}$ below), and terms due to the relaxation of the kinematic condition (2.29) (operator $\mathcal{R}_{os2}$ below), typical when splitting FSI problems.

While we do not expect to obtain suboptimal convergence due to the Stokes/Darcy splitting, it has been shown by Fernandez [15] that the kinematically coupled scheme exhibits suboptimal convergence. We observe the same behavior here. We follow the standard approach in which we use the dissipative terms from the backward Euler scheme and the viscous dissipation to absorb the error due to the Stokes/Darcy splitting. The error due to the splitting of fluid and structure subproblems cannot be handled in the same way, and gives rise to a suboptimal term. However, as we show in the following section, we do not observe the suboptimal behavior in the numerical results.

For the spatial approximation, we apply Lagrangian finite elements of polynomial degree $k \geq 1$ for all the variables, except for the fluid pressure, for which we use elements of degree $s<k$. We assume that the regularity assumptions reported in Lemma 1 of Appendix are satisfied and that our finite element spaces satisfy the usual approximation properties, as well as the fluid velocity-pressure spaces satisfy the discrete inf-sup condition (4.15).

Let P_h be the Lagrangian interpolation operator onto V_h^p, and let $\Pi_h^{f/p}$ be the L^2-orthogonal projection onto $Q_h^{f/p}$, satisfying

$$(p_r - \Pi_h^r p_r, \psi_h) = 0, \quad \forall \psi_h \in Q_h^r, r \in \{f, p\}. \tag{5.1}$$

Then, $I_h := P_h|_\Gamma$ is a Lagrangian interpolation operator onto V_h^m. Introduce a Stokes-like projection operator $(S_h, R_h) : V^f \to V_h^f \times Q_h^f$, defined for all $\boldsymbol{v} \in V^f$ by

$$(S_h \boldsymbol{v}, R_h \boldsymbol{v}) \in V_h^f \times Q_h^f, \tag{5.2}$$

$$(S_h \boldsymbol{v})|_\Gamma = I_h(\boldsymbol{v}|_\Gamma), \tag{5.3}$$

$$a_f(S_h \boldsymbol{v}, \boldsymbol{\varphi}_h^f) - b(R_h \boldsymbol{v}, \boldsymbol{\varphi}_h^f) = a_f(\boldsymbol{v}, \boldsymbol{\varphi}_h^f), \forall \boldsymbol{\varphi}_h^f \in V_h^f \text{ such that } \boldsymbol{\varphi}_h^f|_\Gamma = 0, \tag{5.4}$$

$$b(\psi_h^f, S_h \boldsymbol{v}) = 0, \forall \psi_h^f \in Q_h^f. \tag{5.5}$$

The finite element theory for Lagrangian interpolants and L^2 projections [74] gives the classical approximation properties reported in Lemma 3. Since P_h is the Lagrangian interpolant, so is its trace on Γ. Therefore, we inherit optimal approximation properties also on this subset. We refer to Lemma 3 for a precise statement of these properties.

We recall that the discrete problem, namely (4.3) and (4.4), is based on a nonconforming discretization approach, because the discrete finite element spaces do not satisfy the interface constraints on the test functions defined in (3.6) and used in the continuous problem formulation (3.9). To account for the corresponding consistency error of the scheme, we derive below the variational formulation of the continuous problem without enforcing the constraints (3.6), see in particular Eq. (5.6), and we will then subtract the continuous and discrete variational equations set into conforming test and trial spaces. Assuming $\boldsymbol{\eta} = \boldsymbol{U}|_{\Gamma(t)}, \boldsymbol{\xi} = \boldsymbol{V}|_{\Gamma(t)}$, and $\boldsymbol{\varphi}_h^p|_\Gamma = \boldsymbol{\zeta}_h, \boldsymbol{\phi}_h^p|_\Gamma = \boldsymbol{\chi}_h$, the weak formulation is given as follows: Find $\boldsymbol{X} = (\boldsymbol{v}, \boldsymbol{U}, \boldsymbol{V}, p_f, p_p) \in V_h^f \times V_h^p \times V_h^p \times Q_h^f \times Q_h^p$ such that for all $\boldsymbol{Y}_h = (\boldsymbol{\varphi}_h^f, \boldsymbol{\varphi}_h^p, \boldsymbol{\phi}_h^p, \psi_h^f, \psi_h^p) \in V_h^f \times V_h^p \times V_h^p \times Q_h^f \times Q_h^p$ we have

$$\mathcal{P}(\boldsymbol{X}, \boldsymbol{Y}_h) = \mathcal{F}(\boldsymbol{Y}_h) + \int_\Gamma \boldsymbol{\tau} \cdot \boldsymbol{\sigma}^f \boldsymbol{n} (\boldsymbol{\varphi}_h^f \cdot \boldsymbol{\tau} - \boldsymbol{\varphi}_h^p \cdot \boldsymbol{\tau}) dx. \tag{5.6}$$

Denote the bilinear form of the coupled discrete problem by $\hat{P}(X_h, Y_h)$:

$$\begin{aligned}\hat{P}(X_h, Y_h) &= \rho_f \int_{\Omega^f} d_t \boldsymbol{v}_h^{n+1} \cdot \boldsymbol{\varphi}_h^f d\boldsymbol{x} + a_f(\boldsymbol{v}_h^{n+1}, \boldsymbol{\varphi}_h^f) + \rho_m r_m \int_\Gamma \frac{\boldsymbol{v}_h^{n+1} \cdot \boldsymbol{\tau} - \boldsymbol{V}_h^n \cdot \boldsymbol{\tau}}{\Delta t} (\boldsymbol{\varphi}_h^f \cdot \boldsymbol{\tau}) dx \\ &- b_f(p_{f,h}^{n+1}, \boldsymbol{\varphi}_h^f) + b_f(\psi_h^f, \boldsymbol{v}_h^{n+1}) + c_{fp}(p_{p,h}^n, \boldsymbol{\varphi}_h^f) + \rho_p \int_{\Omega^p} (\boldsymbol{V}_h^{n+1} - d_t \boldsymbol{U}_h^{n+1}) \cdot \boldsymbol{\phi}_h^p d\boldsymbol{x} \\ &+ \rho_p \int_{\Omega^p} d_t \boldsymbol{V}_h^{n+1} \cdot \boldsymbol{\varphi}_h^p d\boldsymbol{x} + a_e(\boldsymbol{U}_h^{n+1}, \boldsymbol{\varphi}_h^p) + \int_{\Omega^p} s_0 d_t p_{p,h}^{n+1} \psi_h^p d\boldsymbol{x} + a_p(p_{p,h}^{n+1}, \psi_h^p) \\ &- b_{ep}(p_{p,h}^{n+1}, \boldsymbol{\varphi}_h^p) + b_{ep}(\psi_h^p, d_t \boldsymbol{U}_h^{n+1}) + \rho_m r_m \int_\Gamma (d_t \boldsymbol{V}_h^{n+1} \cdot \boldsymbol{n})(\boldsymbol{\varphi}_h^p \cdot \boldsymbol{n}) dx \\ &+ \rho_m r_m \int_\Gamma \frac{\boldsymbol{V}_h^{n+1} \cdot \boldsymbol{\tau} - \boldsymbol{v}_h^{n+1} \cdot \boldsymbol{\tau}}{\Delta t} (\boldsymbol{\varphi}_h^p \cdot \boldsymbol{\tau}) dx + a_m(\boldsymbol{U}_h|_\Gamma^{n+1}, \boldsymbol{\varphi}_h^p|_\Gamma) - c_{ep}(p_{p,h}^{n+1}, \boldsymbol{\varphi}_h^p) \\ &+ c_{ep}(\psi_h^p, d_t \boldsymbol{U}_h^{n+1}) - c_{fp}(\psi_h^p, \boldsymbol{v}_h^{n+1}),\end{aligned}$$

where $\boldsymbol{X}_h = (\boldsymbol{v}_h^{n+1}, \boldsymbol{U}_h^{n+1}, \boldsymbol{V}_h^{n+1}, p_{f,h}^{n+1}, p_{p,h}^{n+1})$.

To analyze the error of our numerical scheme, denote $e_f^{n+1} = \boldsymbol{v}^{n+1} - \boldsymbol{v}_h^{n+1}, e_{fp}^{n+1} = p_f^{n+1} - p_{f,h}^{n+1}, e_u^{n+1} = \boldsymbol{U}^{n+1} - \boldsymbol{U}_h^{n+1}, e_v^{n+1} = \boldsymbol{V}^{n+1} - \boldsymbol{V}_h^{n+1}$, and $e_p^{n+1} = p_p^{n+1} - p_{p,h}^{n+1}$. We start by subtracting (4.3) and (4.4) from (5.6), giving rise to the following error equations:

$$\hat{P}(E, Y_h) = \mathcal{R}_f^{n+1}(\boldsymbol{\varphi}_h^f) + \mathcal{R}_s^{n+1}(\boldsymbol{\varphi}_h^p) + \mathcal{R}_v^{n+1}(\boldsymbol{\phi}_h^p) + \mathcal{R}_p^{n+1}(\psi_h^p) + \mathcal{R}_{\text{os}}^{n+1}(\boldsymbol{\varphi}_h^f - \boldsymbol{\varphi}_h^p),$$

for all $\boldsymbol{Y}_h \in V_h^f \times V_h^p \times V_h^p \times Q_h^f \times Q_h^p$, where $E = (e_f^{n+1}, e_u^{n+1}, e_v^{n+1}, e_{fp}^{n+1}, e_p^{n+1})$, and the consistency error terms are given by

$$\begin{aligned}\mathcal{R}_f^{n+1}(\boldsymbol{\varphi}_h^f) &= \rho_f \int_{\Omega^f} (d_t \boldsymbol{v}^{n+1} - \partial_t \boldsymbol{v}^{n+1}) \cdot \boldsymbol{\varphi}_h^f d\boldsymbol{x} \\ \mathcal{R}_s^{n+1}(\boldsymbol{\varphi}_h^p) &= \rho_p \int_{\Omega^p} (d_t \boldsymbol{V}^{n+1} - \partial_t \boldsymbol{V}^{n+1}) \cdot \boldsymbol{\varphi}_h^p d\boldsymbol{x} + \rho_m r_m \int_\Gamma (d_t \boldsymbol{V}^{n+1} - \partial_t \boldsymbol{V}^{n+1}) \cdot \boldsymbol{\varphi}_h^p dx, \\ \mathcal{R}_v^{n+1}(\boldsymbol{\phi}_h^p) &= -\rho_p \int_{\Omega^p} (d_t \boldsymbol{U}^{n+1} - \partial_t \boldsymbol{U}^{n+1}) \cdot \boldsymbol{\phi}_h^p d\boldsymbol{x}, \\ \mathcal{R}_p^{n+1}(\psi_h^p) &= \int_{\Omega^p} s_0 (d_t p_p^{n+1} - \partial_t p_p^{n+1}) \psi_h^p d\boldsymbol{x} + b_{ep}(\psi_h^p, d_t \boldsymbol{U}^{n+1} - \partial_t \boldsymbol{U}^{n+1}) \\ &\quad + c_{ep}(\psi_h^p, d_t \boldsymbol{U}^{n+1} - \partial_t \boldsymbol{U}^{n+1}), \\ \mathcal{R}_{\text{os1}}^{n+1}(\varphi_h^f) &= c_{fp}(p_p^n - p_p^{n+1}, \boldsymbol{\varphi}_h^f), \\ \mathcal{R}_{\text{os2}}^{n+1}(\varphi_h^f - \boldsymbol{\varphi}_h^p) &= \int_\Gamma \left(\boldsymbol{\tau} \cdot \boldsymbol{\sigma}^f \boldsymbol{n} + \rho_m r_m \frac{\boldsymbol{v}^{n+1} \cdot \boldsymbol{\tau} - \boldsymbol{V}^n \cdot \boldsymbol{\tau}}{\Delta t} \right) (\boldsymbol{\varphi}_h^f \cdot \boldsymbol{\tau} - \boldsymbol{\varphi}_h^p \cdot \boldsymbol{\tau}) dx.\end{aligned}$$

Let us split the error of the method into the approximation error θ_r and the truncation error δ_r, with $r = f, fp, u, v, p$, as follows:

$$\begin{aligned}e_f^{n+1} &= \boldsymbol{v}^{n+1} - \boldsymbol{v}_h^{n+1} = (\boldsymbol{v}^{n+1} - S_h \boldsymbol{v}^{n+1}) + (S_h \boldsymbol{v}^{n+1} - \boldsymbol{v}_h^{n+1}) =: \theta_f^{n+1} + \delta_f^{n+1}, \\ e_{fp}^{n+1} &= p_f^{n+1} - p_{f,h}^{n+1} = (p_f^{n+1} - \Pi_h^f p_f^{n+1}) + (\Pi_h^f p_f^{n+1} - p_{f,h}^{n+1}) =: \theta_{fp}^{n+1} + \delta_{fp}^{n+1},\end{aligned}$$

$$e_u^{n+1} = \boldsymbol{U}^{n+1} - \boldsymbol{U}_h^{n+1} = (\boldsymbol{U}^{n+1} - P_h\boldsymbol{U}^{n+1}) + (P_h\boldsymbol{U}^{n+1} - \boldsymbol{U}_h^{n+1}) =: \theta_u^{n+1} + \delta_u^{n+1},$$
$$e_v^{n+1} = \boldsymbol{V}^{n+1} - \boldsymbol{V}_h^{n+1} = (\boldsymbol{V}^{n+1} - P_h\boldsymbol{V}^{n+1}) + (P_h\boldsymbol{V}^{n+1} - \boldsymbol{V}_h^{n+1}) =: \theta_v^{n+1} + \delta_v^{n+1},$$
$$e_p^{n+1} = p_p^{n+1} - p_{p,h}^{n+1} = (p_p^{n+1} - \Pi_h^p p_p^{n+1}) + (\Pi_h^p p_p^{n+1} - p_{p,h}^{n+1}) =: \theta_p^{n+1} + \delta_p^{n+1}.$$

Our plan is to rearrange the terms in the error equations so that we have the truncation errors on the left-hand side, and the consistency and interpolation errors on the right-hand side. After that, we will choose $\boldsymbol{\varphi}_h^f = \delta_f^{n+1}, \psi_h^f = \delta_{fp}^{n+1}, \boldsymbol{\varphi}_h^p = d_t\delta_u^{n+1}, \boldsymbol{\phi}_h^p = d_t\delta_v^{n+1}$, and $\psi_h^p = \delta_p^{n+1}$, and use the stability estimate for the truncation errors. Finally, we will bound the remaining terms, and use the triangle inequality to get the error estimates for e_f, e_u, e_v, and e_p.

Rearranging the terms in the error equations, and using property (5.1) of the projection operator Π_h^p, we have

$$\begin{aligned}
\hat{P}(\delta_h, Y_h) = {} & \mathcal{R}_f^{n+1}(\boldsymbol{\varphi}_h^f) + \mathcal{R}_s^{n+1}(\boldsymbol{\varphi}_h^p) + \mathcal{R}_v^{n+1}(\boldsymbol{\phi}_h^p) + \mathcal{R}_p^{n+1}(\psi_h^p) + \mathcal{R}_{\text{os1}}^{n+1}(\boldsymbol{\varphi}_h^f) + \mathcal{R}_{\text{os2}}^{n+1}(\boldsymbol{\varphi}_h^f - \boldsymbol{\varphi}_h^p) \\
& - \rho_f \int_{\Omega^f} d_t\theta_f^{n+1} \cdot \boldsymbol{\varphi}_h^f d\boldsymbol{x} - a_f(\theta_f^{n+1}, \boldsymbol{\varphi}_h^f) + b_f(\theta_{fp}^{n+1}, \boldsymbol{\varphi}_h^f) \\
& - b_f(\psi_h^f, \theta_f^{n+1}) + \rho_p \int_{\Omega^p} d_t\theta_u^{n+1} \cdot \boldsymbol{\phi}_h^p d\boldsymbol{x} - \rho_m r_m \int_\Gamma \frac{\theta_f^{n+1} \cdot \boldsymbol{\tau} - \theta_v^n \cdot \boldsymbol{\tau}}{\Delta t} (\boldsymbol{\varphi}_h^f \cdot \boldsymbol{\tau}) dx \\
& - \rho_p \int_{\Omega^p} \theta_v^{n+1} \cdot \boldsymbol{\phi}_h^p d\boldsymbol{x} + \rho_p \int_{\Omega^p} d_t\theta_v^{n+1} \cdot \boldsymbol{\varphi}_h^p d\boldsymbol{x} - a_e(\theta_u^{n+1}, \boldsymbol{\varphi}_h^p) - a_p(\theta_p^{n+1}, \psi_h^p) \\
& + b_{ep}(\theta_p^{n+1}, \boldsymbol{\varphi}_h^p) - b_{ep}(\psi_h^p, d_t\theta_u^{n+1}) - \rho_m r_m \int_\Gamma (d_t\theta_v^{n+1} \cdot \boldsymbol{n})(\boldsymbol{\varphi}_h^p \cdot \boldsymbol{n}) dx \\
& - \rho_m r_m \int_\Gamma \frac{\theta_v^{n+1} \cdot \boldsymbol{\tau} - \theta_f^{n+1} \cdot \boldsymbol{\tau}}{\Delta t} (\boldsymbol{\varphi}_h^p \cdot \boldsymbol{\tau}) dx - a_m(\theta_u^{n+1}|_\Gamma, \boldsymbol{\varphi}_h^p|_\Gamma) + c_{ep}(\theta_p^{n+1}, \boldsymbol{\varphi}_h^p) \\
& - c_{ep}(\psi_h^p, d_t\theta_u^{n+1}) + c_{fp}(\psi_h^p, \theta_f^{n+1}) + c_{fp}(\theta_p^n, \boldsymbol{\varphi}_h^f), \qquad (5.7)
\end{aligned}$$

for all $\boldsymbol{Y}_h \in V_h^f \times V_h^p \times V_h^p \times Q_h^f \times Q_h^p$, where $\delta_h = (\delta_f^{n+1}, \delta_u^{n+1}, \delta_v^{n+1}, \delta_{fp}^{n+1}, \delta_p^{n+1})$.

Let $\mathcal{E}_\delta^n$ be defined as

$$\mathcal{E}_\delta^n = \frac{\rho_f}{2}||\delta_f^n||^2_{L^2(\Omega^f)} + \frac{\rho_p}{2}||\delta_v^n||^2_{L^2(\Omega^p)} + \frac{1}{2}||\delta_u^n||^2_E + \frac{s_0}{2}||\delta_p^n||^2_{L^2(\Omega^p)} + \frac{\rho_m r_m}{2}||\delta_v^n||^2_{L^2(\Gamma)} + \frac{1}{2}||\delta_u|_\Gamma^n||^2_M.$$

Note that $\mathcal{E}_\delta^n$ corresponds to the total discrete energy defined in Theorem 1 measured for the truncation error.

Theorem 2. *Consider the solution $(\boldsymbol{v}_h, p_{p,h}, \boldsymbol{V}_h, \boldsymbol{U}_h, \boldsymbol{\xi}_h, \boldsymbol{\eta}_h, p_{p,h})$ of (4.3) and (4.4). Assume that the time step condition (4.11) holds, and that the true solution $(\boldsymbol{v}, p_p, \boldsymbol{V}, \boldsymbol{U}, \boldsymbol{\xi}, \boldsymbol{\eta}, p_p)$ satisfies (A9). Then, the following estimate holds:*

$$\begin{aligned}
& ||\boldsymbol{v} - \boldsymbol{v}_h||^2_{l^\infty(0,T;L^2(\Omega^f))} + \frac{\gamma}{2}||\boldsymbol{v} - \boldsymbol{v}_h||^2_{l^2(0,T;H^1(\Omega^f))} + ||\boldsymbol{V} - \boldsymbol{V}_h||^2_{l^\infty(0,T;L^2(\Omega^p))} \\
& \quad + ||p_p - p_{p,h}||^2_{l^\infty(0,T;L^2(\Omega^p))} + ||p_p - p_{p,h}||^2_{l^2(0,T;H^1(\Omega^p))} + ||\boldsymbol{\xi} - \boldsymbol{\xi}_h||^2_{l^\infty(0,T;L^2(0,L))} \\
& \quad + ||\boldsymbol{U} - \boldsymbol{U}_h||^2_{l^\infty(0,T;H^1(\Omega^p))} + ||\boldsymbol{\eta} - \boldsymbol{\eta}_h||^2_{l^\infty(0,T;H^1(0,L))} + \Delta t||p_f - p_{f,h}||^2_{l^2(0,T;L^2(\Omega^f))}
\end{aligned}$$

$$\leq C(h^{2k}\mathcal{B}_1(\boldsymbol{v},\boldsymbol{U},\boldsymbol{\eta},p_p)+h^{2k+2}\mathcal{B}_2(\boldsymbol{U},\boldsymbol{V},\boldsymbol{\eta},\boldsymbol{\xi},p_p)+h^{2s+2}||p_f||^2_{l^2(0,T;H^{s+1}(\Omega^f))}$$
$$+h^{2k+4}\mathcal{B}_3(\boldsymbol{U},\boldsymbol{V},\boldsymbol{\xi})+\Delta t||\eta||^2_{l^2(0,T;H^2(0,L))}+\Delta t^2\mathcal{B}_4(\boldsymbol{v},\boldsymbol{U},\boldsymbol{V},\boldsymbol{\eta},\boldsymbol{\xi},p_p)+\Delta t^3||\partial_{tt}\boldsymbol{v}||^2_{L^2(0,T;L^2(\Gamma))}),$$

where γ is the small parameter that appears in the stability analysis, namely (4.11) of Theorem 1, and

$$\begin{aligned}
\mathcal{B}_1(\boldsymbol{v},\boldsymbol{U},\boldsymbol{\eta},p_p) &= ||\boldsymbol{v}||^2_{l^\infty(0,T;H^{k+1}(\Omega^f))}+||\boldsymbol{v}||^2_{l^2(0,T;H^{k+1}(\Omega^f))}+||p_p||^2_{l^2(0,T;H^{k+1}(\Omega^p))}\\
&\quad+||\partial_t\boldsymbol{v}||^2_{L^2(0,T;H^{k+1}(\Omega^f))}+||\partial_t\boldsymbol{U}||^2_{L^2(0,T;H^{k+1}(\Omega^p))}\\
&\quad+||\partial_t p_p||^2_{L^2(0,T;H^{k+1}(\Omega^p))}+||\partial_t\boldsymbol{\eta}||^2_{L^2(0,T;H^{k+1}(0,L))}\\
&\quad+||p_p||^2_{l^\infty(0,T;H^{k+1}(\Omega^p))}+||\boldsymbol{U}||^2_{l^\infty(0,T;H^{k+1}(\Omega^p))}+||\boldsymbol{\eta}||^2_{l^\infty(0,T;H^{k+1}(0,L))},\\
\mathcal{B}_2(\boldsymbol{U},\boldsymbol{V},\boldsymbol{\eta},\boldsymbol{\xi},p_p) &= ||\partial_t p_p||^2_{L^2(0,T;H^{k+1}(\Omega^p))}+||\partial_{tt}\boldsymbol{U}||^2_{L^2(0,T;H^{k+1}(\Omega^p))}+||\partial_{tt}\boldsymbol{V}||^2_{L^2(0,T;H^{k+1}(\Omega^p))}\\
&\quad+||\partial_{tt}\boldsymbol{\xi}||^2_{L^2(0,T;H^{k+1}(0,L))}+||\partial_t\boldsymbol{V}||^2_{L^2(0,T;H^{k+1}(\Omega^p))}+||\partial_t\boldsymbol{\xi}||^2_{L^2(0,T;H^{k+1}(0,L))}\\
&\quad+||p_p||^2_{l^\infty(0,T;H^{k+1}(\Omega^p))}+||\boldsymbol{V}||^2_{l^\infty(0,T;H^{k+1}(\Omega^p)}\\
&\quad+||\partial_t\boldsymbol{U}||^2_{l^\infty(0,T;H^{k+1}(\Omega^p))}+||\partial_t\boldsymbol{V}||^2_{l^\infty(0,T;H^{k+1}(\Omega^p))}+||\partial_t\boldsymbol{\xi}||^2_{l^\infty(0,T;H^{k+1}(0,L))},\\
\mathcal{B}_3(\boldsymbol{U},\boldsymbol{V},\boldsymbol{\xi}) &= ||\partial_{tt}\boldsymbol{U}||^2_{l^\infty(0,T;H^{k+1}(\Omega^p))}+||\partial_{tt}\boldsymbol{V}||^2_{l^\infty(0,T;H^{k+1}(\Omega^p))}+||\partial_{tt}\boldsymbol{\xi}||^2_{l^\infty(0,T;H^{k+1}(0,L))},\\
\mathcal{B}_4(\boldsymbol{v},\boldsymbol{U},\boldsymbol{V},\boldsymbol{\eta},\boldsymbol{\xi},p_p) &= ||\partial_{tt}\boldsymbol{v}||^2_{L^2(0,T;L^2(\Omega^f))}+||\partial_t p_p||^2_{L^2(0,T;H^1(\Omega^p))}+||\partial_{tt}p_p||^2_{L^2(0,T;L^2(\Omega^p))}\\
&\quad+||\partial_{tt}\boldsymbol{U}||^2_{L^2(0,T;H^1(\Omega^p))}+||\partial_{ttt}\boldsymbol{U}||^2_{L^2(0,T;L^2(\Omega^p))}\\
&\quad+||\partial_{ttt}\boldsymbol{\eta}||^2_{L^2(0,T;L^2(0,L))}+||\partial_{ttt}\boldsymbol{V}||^2_{L^2(0,T;L^2(\Omega^p))}\\
&\quad+||\partial_{tt}\boldsymbol{U}||^2_{l^\infty(0,T;L^2(\Omega^p))}+||\partial_{tt}\boldsymbol{\eta}||^2_{l^\infty(0,T;L^2(0,L))}+||\partial_{tt}\boldsymbol{V}||^2_{l^\infty(0,T;L^2(\Omega^p))}.
\end{aligned}$$

Proof. With the purpose of presenting the proof in a clear manner, we will separate the proof into four main steps.

Step 1: Application of the stability result (4.12) to the truncation error equation. Choose $\boldsymbol{\varphi}_h^f=\delta_f^{n+1}$, $\psi_h^f=\delta_{fp}^{n+1}$, $\boldsymbol{\varphi}_h^p=d_t\delta_u^{n+1}$, $\boldsymbol{\phi}_h^p=d_t\delta_v^{n+1}$, and $\psi_h^p=\delta_p^{n+1}$ in Eq. (5.7). Thanks to (5.5), the pressure terms simplify as follows

$$-b_f(\delta_{fp}^{n+1},\theta_f^{n+1})=b_f(\delta_{fp}^{n+1},S_h\boldsymbol{v}^{n+1})=0. \tag{5.8}$$

Then, multiplying Eq. (5.7) by Δt, summing over $0\leq n\leq N-1$, and using the stability estimate (4.12) for the truncation error, we get

$$\mathcal{E}_\delta^N+\frac{\rho_f\Delta t^2}{2}\sum_{n=0}^{N-1}||d_t\delta_f^{n+1}||^2_{L^2(\Omega^f)}+\frac{\rho_m r_m\Delta t^2}{2}\sum_{n=0}^{N-1}\left\|\frac{\delta_f^{n+1}\cdot\boldsymbol{\tau}-\delta_v^n\cdot\boldsymbol{\tau}}{\Delta t}\right\|^2_{L^2(\Gamma)}$$
$$+\gamma\Delta t\sum_{n=0}^{N-1}||D(\delta_f^{n+1})||^2_{L^2(\Omega^f)}+\frac{\rho_m r_m\Delta t^2}{2}\sum_{n=0}^{N-1}\left\|\frac{\delta_v^{n+1}\cdot\boldsymbol{\tau}-\delta_f^{n+1}\cdot\boldsymbol{\tau}}{\Delta t}\right\|^2_{L^2(\Gamma)}$$

$$
\begin{aligned}
&+\frac{\rho_m r_m \Delta t^2}{2}||d_t\delta_v^{n+1}\cdot\boldsymbol{n}||^2_{L^2(\Gamma)}+\frac{\rho_p\Delta t^2}{2}\sum_{n=0}^{N-1}||d_t\delta_v^{n+1}||^2_{L^2(\Omega^p)}+\frac{\Delta t^2}{2}\sum_{n=0}^{N-1}||d_t\delta_u^{n+1}||^2_E\\
&+\frac{\Delta t^2}{2}\sum_{n=0}^{N-1}||d_t\delta_u^{n+1}|_\Gamma||^2_M+\frac{\Delta t^2}{4}\sum_{n=0}^{N-1}||d_t\delta_p^{n+1}||^2_{L^2(\Omega^p)}+\Delta t\sum_{n=0}^{N-1}||\sqrt{\kappa}\nabla\delta_p^{n+1}||^2_{L^2(\Omega^p)}\\
\le\ &\mathcal{E}_\delta^0+\Delta t\sum_{n=0}^{N-1}(\mathcal{R}_f^{n+1}(\delta_f^{n+1})+\mathcal{R}_s^{n+1}(d_t\delta_u^{n+1})+\mathcal{R}_v^{n+1}(d_t\delta_v^{n+1})+\mathcal{R}_p^{n+1}(\delta_p^{n+1})+\mathcal{R}_{\mathrm{os1}}^{n+1}(\delta_f^{n+1})\\
&+\mathcal{R}_{\mathrm{os2}}^{n+1}(\delta_f^{n+1}-d_t\delta_u^{n+1}))-\rho_f\Delta t\sum_{n=0}^{N-1}\int_{\Omega^f}d_t\theta_f^{n+1}\cdot\delta_f^{n+1}d\boldsymbol{x}-\Delta t\sum_{n=0}^{N-1}a_f(\theta_f^{n+1},\delta_f^{n+1})\\
&+\Delta t\sum_{n=0}^{N-1}b_f(\theta_{fp}^{n+1},\delta_f^{n+1})+\rho_p\Delta t\sum_{n=0}^{N-1}\int_{\Omega^p}d_t\theta_u^{n+1}\cdot d_t\delta_v^{n+1}d\boldsymbol{x}\\
&-\rho_m r_m\sum_{n=0}^{N-1}\int_\Gamma(\theta_f^{n+1}\cdot\boldsymbol{\tau}-\theta_v^n\cdot\boldsymbol{\tau})(\delta_f^{n+1}\cdot\boldsymbol{\tau})dx-\rho_m r_m\sum_{n=0}^{N-1}\int_\Gamma(\theta_v^{n+1}\cdot\boldsymbol{\tau}-\theta_f^{n+1}\cdot\boldsymbol{\tau})(d_t\delta_u^{n+1}\cdot\boldsymbol{\tau})dx\\
&-\rho_p\Delta t\sum_{n=0}^{N-1}\int_{\Omega^p}\theta_v^{n+1}\cdot d_t\delta_v^{n+1}d\boldsymbol{x}+\rho_p\Delta t\sum_{n=0}^{N-1}\int_{\Omega^p}d_t\theta_v^{n+1}\cdot d_t\delta_u^{n+1}d\boldsymbol{x}-\Delta t\sum_{n=0}^{N-1}a_e(\theta_u^{n+1},d_t\delta_u^{n+1})\\
&-\Delta t\sum_{n=0}^{N-1}a_p(\theta_p^{n+1},\delta_p^{n+1})+\Delta t\sum_{n=0}^{N-1}b_{ep}(\theta_p^{n+1},d_t\delta_u^{n+1})-\Delta t\sum_{n=0}^{N-1}b_{ep}(\delta_p^{n+1},d_t\theta_u^{n+1})\\
&-\Delta t\sum_{n=0}^{N-1}a_m(\theta_u^{n+1}|_\Gamma,d_t\delta_u^{n+1}|_\Gamma)-\rho_m r_m\Delta t\sum_{n=0}^{N-1}\int_\Gamma(d_t\theta_v^{n+1}\cdot\boldsymbol{n})(d_t\delta_u^{n+1}\cdot\boldsymbol{n})dx\\
&+\Delta t\sum_{n=0}^{N-1}c_{ep}(\theta_p^{n+1},d_t\delta_u^{n+1})-\Delta t\sum_{n=0}^{N-1}c_{ep}(\delta_p^{n+1},d_t\theta_u^{n+1})+\Delta t\sum_{n=0}^{N-1}c_{fp}(\delta_p^{n+1},\theta_f^{n+1})\\
&-\Delta t\sum_{n=0}^{N-1}c_{fp}(\theta_p^n,\delta_f^{n+1}).
\end{aligned}
\tag{5.9}
$$

The right-hand side of (5.9) consists of consistency error terms $\mathcal{R}_f^{n+1},\mathcal{R}_s^{n+1},\mathcal{R}_v^{n+1},\mathcal{R}_p^{n+1}$, the operator splitting errors $\mathcal{R}_{\mathrm{os1}}^{n+1}$ and $\mathcal{R}_{\mathrm{os2}}^{n+1}$, and mixed truncation and interpolation error terms. We will proceed by bounding the consistency error terms.

Step 2: The consistency and splitting error estimate. In this step, we will use the following bound of the consistency error terms proved in Lemma 5 in Appendix:

$$
\begin{aligned}
&\Delta t\sum_{n=0}^{N-1}(\mathcal{R}_f^{n+1}(\delta_f^{n+1})+\mathcal{R}_s^{n+1}(d_t\delta_u^{n+1})+\mathcal{R}_v^{n+1}(d_t\delta_v^{n+1})\\
&\quad+\mathcal{R}_p^{n+1}(\delta_p^{n+1})+\mathcal{R}_{\mathrm{os1}}^{n+1}(\delta_f^{n+1})+\mathcal{R}_{\mathrm{os2}}^{n+1}(\delta_f^{n+1}-d_t\delta_u^{n+1}))\\
&\le C\Delta t^2(||\partial_{tt}\boldsymbol{v}||^2_{L^2(0,T;L^2(\Omega^f))}+||\partial_t p_p||^2_{L^2(0,T;H^1(\Omega^p))}+||\partial_{tt}p_p||^2_{L^2(0,T;L^2(\Omega^p))}
\end{aligned}
$$

$$+ ||\partial_{tt}\boldsymbol{U}||^2_{L^2(0,T;H^1(\Omega^p))} + ||\partial_{ttt}\boldsymbol{U}||^2_{L^2(0,T;L^2(\Omega^p))} + ||\partial_{ttt}\boldsymbol{\eta}||^2_{L^2(0,T;L^2(0,L))}$$
$$+ ||\partial_{ttt}\boldsymbol{V}||^2_{L^2(0,T;L^2(\Omega^p))} + ||\partial_{tt}\boldsymbol{U}||^2_{l^\infty(0,T;L^2(\Omega^p))} + ||\partial_{tt}\boldsymbol{\eta}||^2_{l^\infty(0,T;L^2(0,L))} + ||\partial_{tt}\boldsymbol{V}||^2_{l^\infty(0,T;L^2(\Omega^p))})$$
$$+ C\Delta t||\eta||^2_{l^2(0,T;H^2(0,L))} + C\Delta t^3||\partial_{tt}\boldsymbol{v}||^2_{L^2(0,T;L^2(\Gamma))} + \mathcal{A}(\delta_f,\delta_p,\delta_v,\delta_u),$$

where

$$\mathcal{A}(\delta_f,\delta_p,\delta_v,\delta_u) = \frac{\gamma\Delta t}{8}\sum_{n=0}^{N-1}||D(\delta_f^{n+1})||^2_{L^2(\Omega^f)} + \frac{\rho_m r_m}{4}\sum_{n=0}^{N-1}||\delta_f^{n+1}\cdot\boldsymbol{\tau} - \delta_v^{n+1}\cdot\boldsymbol{\tau}||^2_{L^2(\Gamma)}$$
$$+ \frac{\Delta t}{6}\sum_{n=0}^{N-1}||\sqrt{\kappa}\nabla\delta_p^{n+1}||^2_{L^2(\Omega^p)} + \epsilon(||\delta_v^N||^2_{L^2(\Omega^p)} + ||\delta_v^N||^2_{L^2(\Gamma)} + ||D(\delta_u^N)||^2_{L^2(\Omega^p)})$$
$$+ C\Delta t\sum_{n=1}^{N-1}(||\delta_v^n||^2_{L^2(\Omega^p)} + ||\delta_v^n||^2_{L^2(\Gamma)} + ||D(\delta_u^n)||^2_{L^2(\Omega^p)}).$$

Referring to the terms collected into the expression $\mathcal{A}(\delta_f,\delta_p,\delta_v,\delta_u)$, we observe that the discrete Gronwall Lemma is required to obtain an upper bound.

Step 3: The mixed truncation and interpolation error terms estimate. In this step, we estimate the remaining terms of (5.9), which are terms that contain both truncation and interpolation error.

Using Cauchy–Schwartz (A5), Young's (A3), Poincaré (A6), and Korn's (A8) inequalities, we have the following:

$$-\rho_f\Delta t\sum_{n=0}^{N-1}\int_{\Omega^f} d_t\theta_f^{n+1}\cdot\delta_f^{n+1}d\boldsymbol{x} \le C\Delta t\sum_{n=0}^{N-1}||\nabla d_t\theta_f^{n+1}||^2_{L^2(\Omega^f)} + \frac{\gamma\Delta t}{8}\sum_{n=0}^{N-1}||D(\delta_f^{n+1})||^2_{L^2(\Omega^f)}.$$

Furthermore, using Young's (A3), Korn's (A8), and trace (A7) inequalities, we can estimate

$$-\Delta t\sum_{n=0}^{N-1}(a_f(\theta_f^{n+1},\delta_f^{n+1}) + a_p(\theta_p^{n+1},\delta_p^{n+1}) - c_{fp}(\delta_p^{n+1},\theta_f^{n+1}) + c_{fp}(\theta_p^n,\delta_f^{n+1}))$$
$$\le C\Delta t\sum_{n=0}^{N-1}||D(\theta_f^{n+1})||^2_{L^2(\Omega^f)} + \frac{\gamma\Delta t}{8}\sum_{n=0}^{N-1}||D(\delta_f^{n+1})||^2_{L^2(\Omega^f)}$$
$$+ C\Delta t\sum_{n=0}^{N-1}||\nabla\theta_p^{n+1}||^2_{L^2(\Omega^p)} + \frac{\Delta t}{6}\sum_{n=0}^{N-1}||\sqrt{\kappa}\nabla\delta_p^{n+1}||^2_{L^2(\Omega^p)}.$$

Due to (2.20), we have

$$\theta_v^{n+1}\cdot\boldsymbol{\tau} - \theta_f^{n+1}\cdot\boldsymbol{\tau} = \boldsymbol{V}^{n+1}\cdot\boldsymbol{\tau} - I_h\boldsymbol{V}^{n+1}\cdot\boldsymbol{\tau} - \boldsymbol{v}^{n+1}\cdot\boldsymbol{\tau} + I_h\boldsymbol{v}^{n+1}\cdot\boldsymbol{\tau} = 0 \quad \text{on } \Gamma.$$

Hence,

$$-\rho_m r_m\sum_{n=0}^{N-1}\int_\Gamma(\theta_f^{n+1}\cdot\boldsymbol{\tau} - \theta_v^n\cdot\boldsymbol{\tau})(\delta_f^{n+1}\cdot\boldsymbol{\tau})dx - \rho_m r_m\sum_{n=0}^{N-1}\int_\Gamma(\theta_v^{n+1}\cdot\boldsymbol{\tau} - \theta_f^{n+1}\cdot\boldsymbol{\tau})(d_t\delta_u^{n+1}\cdot\boldsymbol{\tau})dx$$
$$= -\rho_m r_m\Delta t\sum_{n=0}^{N-1}\int_\Gamma(d_t\theta_v^{n+1}\cdot\boldsymbol{\tau})(\delta_f^{n+1}\cdot\boldsymbol{\tau})dx - \rho_m r_m\sum_{n=0}^{N-1}\int_\Gamma(\theta_v^{n+1}\cdot\boldsymbol{\tau} - \theta_f^{n+1}\cdot\boldsymbol{\tau})$$

$$\times (d_t\delta_u^{n+1}\cdot\boldsymbol{\tau}-\delta_f^{n+1}\cdot\boldsymbol{\tau})dx=-\rho_m r_m\Delta t\sum_{n=0}^{N-1}\int_\Gamma (d_t\theta_v^{n+1}\cdot\boldsymbol{\tau})(\delta_f^{n+1}\cdot\boldsymbol{\tau})dx \tag{5.10}$$

We bound the last term as follows

$$-\rho_m r_m\Delta t\sum_{n=0}^{N-1}\int_\Gamma (d_t\theta_v^{n+1}\cdot\boldsymbol{\tau})(\delta_f^{n+1}\cdot\boldsymbol{\tau})dx\le C\Delta t\sum_{n=0}^{N-1}||d_t\theta_v^{n+1}||^2_{L^2(\Gamma)}+\frac{\gamma\Delta t}{6}\sum_{n=0}^{N-1}||D(\delta_f^{n+1})||^2_{L^2(\Omega^f)}.$$

The next two terms can be controlled as follows

$$-\Delta t\sum_{n=0}^{N-1}(b_{ep}(\delta_p^{n+1},d_t\theta_u^{n+1})+c_{ep}(\delta_p^{n+1},d_t\theta_u^{n+1}))\le\frac{\Delta t}{8}\sum_{n=0}^{N-1}||\sqrt{\kappa}\nabla\delta_p^{n+1}||^2_{L^2(\Omega^p)}$$
$$+C\Delta t\sum_{n=0}^{N-1}||\nabla d_t\theta_u^{n+1}||^2_{L^2(\Omega^p)}.$$

We bound the pressure term as follows

$$\Delta t\sum_{n=0}^{N-1}b_f(\theta_{fp}^{n+1},\delta_f^{n+1})\le C\Delta t\sum_{n=0}^{N-1}||\theta_{fp}^{n+1}||^2_{L^2(\Omega^f)}+\frac{\gamma\Delta t}{8}\sum_{n=0}^{N-1}||D(\delta_f^{n+1})||^2_{L^2(\Omega^f)}.$$

To estimate the remaining terms, we use discrete integration by parts in time. Using Eq. (A2), we have

$$\Delta t\sum_{n=0}^{N-1}b_{ep}(\theta_p^{n+1},d_t\delta_u^{n+1})=\alpha\int_{\Omega^p}\theta_p^N\nabla\cdot\delta_u^N d\boldsymbol{x}-\alpha\Delta t\sum_{n=0}^{N-1}\int_{\Omega^p}d_t\theta_p^{n+1}\nabla\cdot\delta_u^n d\boldsymbol{x}$$
$$\le C_\epsilon||\theta_p^N||^2_{L^2(\Omega^p)}+\epsilon||D(\delta_u^N)||^2_{L^2(\Omega^p)}+C\Delta t\sum_{n=0}^{N-1}||d_t\theta_p^{n+1}||^2_{L^2(\Omega^p)}+C\Delta t\sum_{n=0}^{N-1}||D(\delta_u^n)||^2_{L^2(\Omega^p)},$$

and

$$\Delta t\sum_{n=0}^{N-1}c_{ep}(\theta_p^{n+1},d_t\delta_u^{n+1})=\alpha\int_\Gamma\theta_p^N\delta_u^N\cdot\boldsymbol{n}dx-\alpha\Delta t\sum_{n=0}^{N-1}\int_\Gamma d_t\theta_p^{n+1}\delta_u^n\cdot\boldsymbol{n}dx\le C_\epsilon||\nabla\theta_p^N||^2_{L^2(\Omega^p)}$$
$$+\epsilon||D(\delta_u^N)||^2_{L^2(\Omega^p)}+C\Delta t\sum_{n=0}^{N-1}||\nabla d_t\theta_p^{n+1}||^2_{L^2(\Omega^p)}+C\Delta t\sum_{n=0}^{N-1}||D(\delta_u^n)||^2_{L^2(\Omega^p)}.$$

Also,

$$\rho_p\Delta t\sum_{n=0}^{N-1}\int_{\Omega^p}d_t\theta_u^{n+1}\cdot d_t\delta_v^{n+1}d\boldsymbol{x}=\rho_p\int_{\Omega^p}d_t\theta_u^N\cdot\delta_v^N d\boldsymbol{x}-\rho_p\Delta t\sum_{n=1}^{N-1}\int_{\Omega^p}d_{tt}\theta_u^{n+1}\cdot\delta_v^n d\boldsymbol{x}$$
$$\le C_\epsilon||d_t\theta_u^N||^2_{L^2(\Omega^p)}+\epsilon||\delta_v^N||^2_{L^2(\Omega^p)}+C\Delta t\sum_{n=1}^{N-1}||d_{tt}\theta_u^{n+1}||^2_{L^2(\Omega^p)}+C\Delta t\sum_{n=1}^{N-1}||\delta_v^n||^2_{L^2(\Omega^p)},$$

and

$$-\rho_p \Delta t \sum_{n=0}^{N-1} \int_{\Omega^p} \theta_v^{n+1} \cdot d_t \delta_v^{n+1} d\boldsymbol{x} = -\rho_p \int_{\Omega^p} \theta_v^N \cdot \delta_u^N d\boldsymbol{x} + \rho_p \Delta t \sum_{n=1}^{N-1} \int_{\Omega^p} d_t \theta_v^{n+1} \cdot \delta_v^n d\boldsymbol{x}$$

$$\leq C_\epsilon ||\theta_v^N||^2_{L^2(\Omega^p)} + \epsilon ||D(\delta_u^N)||^2_{L^2(\Omega^p)} + C\Delta t \sum_{n=1}^{N-1} ||d_t \theta_v^{n+1}||^2_{L^2(\Omega^p)} + C\Delta t \sum_{n=1}^{N-1} ||D(\delta_u^n)||^2_{L^2(\Omega^p)}.$$

In a similar way,

$$\rho_p \Delta t \sum_{n=0}^{N-1} \int_{\Omega^p} d_t \theta_v^{n+1} \cdot d_t \delta_u^{n+1} d\boldsymbol{x} = \rho_p \int_{\Omega^p} d_t \theta_v^N \cdot \delta_u^N d\boldsymbol{x} - \rho_p \Delta t \sum_{n=1}^{N-1} \int_{\Omega^p} d_{tt} \theta_v^{n+1} \cdot \delta_u^n d\boldsymbol{x}$$

$$\leq C_\epsilon ||d_t \theta_v^N||^2_{L^2(\Omega^p)} + \epsilon ||D(\delta_u^N)||^2_{L^2(\Omega^p)} + C\Delta t \sum_{n=1}^{N-1} ||d_{tt} \theta_v^{n+1}||^2_{L^2(\Omega^p)} + C\Delta t \sum_{n=1}^{N-1} ||D(\delta_u^n)||^2_{L^2(\Omega^p)}.$$

and

$$-\rho_m r_m \Delta t \sum_{n=0}^{N-1} \int_\Gamma (d_t \theta_v^{n+1} \cdot \boldsymbol{n})(d_t \delta_u^{n+1} \cdot \boldsymbol{n}) dx = -\rho_m r_m \int_\Gamma (d_t \theta_v^N \cdot \boldsymbol{n})(\delta_u^N \cdot \boldsymbol{n}) dx$$

$$+ \rho_m r_m \Delta t \sum_{n=1}^{N-1} \int_\Gamma (d_{tt} \theta_v^{n+1} \cdot \boldsymbol{n})(\delta_u^n \cdot \boldsymbol{n}) dx \leq C_\epsilon ||d_t \theta_v^N||^2_{L^2(\Gamma)} + \epsilon ||\delta_u^N|_\Gamma||^2_M$$

$$+ C\Delta t \sum_{n=1}^{N-1} ||d_{tt} \theta_v^{n+1}||^2_{L^2(\Gamma)} + C\Delta t \sum_{n=1}^{N-1} ||\delta_u^n|_\Gamma||^2_M.$$

Furthermore,

$$-\Delta t \sum_{n=0}^{N-1} a_e(\theta_u^{n+1}, d_t \delta_u^{n+1}) = -a_e(\theta_u^N, \delta_u^N) + \Delta t \sum_{n=1}^{N-1} a_e(d_t \theta_u^{n+1}, \delta_u^n) \leq C_\epsilon ||D(\theta_u^N)||^2_{L^2(\Omega^p)}$$

$$+ \epsilon ||D(\delta_u^N)||^2_{L^2(\Omega^p)} + C\Delta t \sum_{n=1}^{N-1} ||D(d_t \theta_u^{n+1})||^2_{L^2(\Gamma)} + C\Delta t \sum_{n=1}^{N-1} ||D(\delta_u^n)||^2_{L^2(\Omega^p)}.$$

Lastly,

$$-\Delta t \sum_{n=0}^{N-1} a_m(\theta_u^{n+1}|_\Gamma, d_t \delta_u^{n+1}|_\Gamma) = -a_m(\theta_u^N|_\Gamma, \delta_u^N|_\Gamma) + \Delta t \sum_{n=1}^{N-1} a_m(d_t \theta_u^{n+1}|_\Gamma, \delta_u^n|_\Gamma)$$

$$\leq C_\epsilon ||\theta_u^N|_\Gamma||^2_M + \epsilon ||\delta_u^N|_\Gamma||^2_M + C\Delta t \sum_{n=1}^{N-1} ||d_t \theta_u^{n+1}|_\Gamma||^2_M + C\Delta t \sum_{n=1}^{N-1} ||\delta_u|_\Gamma||^2_M.$$

Using the estimates from Steps 1–3, we have

$$\mathcal{TE} \leq \mathcal{N}_\epsilon + \mathcal{G} + \mathcal{S} + \mathcal{T}, \tag{5.11}$$

where $\mathcal{TE}$ denotes the terms on the left-hand side of the stability estimate for the truncation error

$$\mathcal{TE} = \mathcal{E}_\delta^N + \frac{\rho_f \Delta t^2}{2} \sum_{n=0}^{N-1} ||d_t \delta_f^{n+1}||^2_{L^2(\Omega^f)} + \frac{\rho_m r_m \Delta t^2}{2} \sum_{n=0}^{N-1} \left\| \frac{\delta_f^{n+1} \cdot \boldsymbol{\tau} - \delta_v^n \cdot \boldsymbol{\tau}}{\Delta t} \right\|^2_{L^2(\Gamma)}$$

$$+\frac{\gamma}{2}\Delta t\sum_{n=0}^{N-1}||D(\delta_f^{n+1})||^2_{L^2(\Omega^f)}+\frac{\rho_m r_m\Delta t^2}{4}\sum_{n=0}^{N-1}\left\|\frac{\delta_v^{n+1}\cdot\boldsymbol{\tau}-\delta_f^{n+1}\cdot\boldsymbol{\tau}}{\Delta t}\right\|^2_{L^2(\Gamma)}$$
$$+\frac{\rho_p\Delta t^2}{2}\sum_{n=0}^{N-1}||d_t\delta_v^{n+1}||^2_{L^2(\Omega^p)}+\frac{\Delta t^2}{2}\sum_{n=0}^{N-1}||d_t\delta_u^{n+1}||^2_E+\frac{\Delta t^2}{2}\sum_{n=0}^{N-1}||d_t\delta_u^{n+1}|_\Gamma||^2_M$$
$$+\frac{\Delta t^2}{4}\sum_{n=0}^{N-1}||d_t\delta_p^{n+1}||^2_{L^2(\Omega^p)}+\frac{\Delta t}{2}\sum_{n=0}^{N-1}||\sqrt{\kappa}\nabla\delta_p^{n+1}||^2_{L^2(\Omega^p)},$$

$\mathcal{N}_\epsilon$ denotes the terms at time N, multiplied by ϵ, that can be incorporated in the left-hand side

$$\mathcal{N}_\epsilon=\epsilon(||D(\delta_u^N)||^2_{L^2(\Omega^p)}+||\delta_v^N||^2_{L^2(\Omega^p)}+||\delta_v^N||^2_{L^2(\Gamma)}+||\delta_u^N|_\Gamma||^2_M),$$

$\mathcal{G}$ denotes the terms for which we have to apply the discrete Gronwall lemma

$$\mathcal{G}=C\Delta t\sum_{n=0}^{N-1}(||D(\delta_u^n)||^2_{L^2(\Omega^p)}+||\delta_v^n||^2_{L^2(\Omega^p)}+||\delta_v^n||^2_{L^2(\Gamma)}+||\delta_u^n|_\Gamma||^2_M),$$

$\mathcal{S}$ denotes the approximation error terms

$$\begin{aligned}\mathcal{S}=C\Delta t\sum_{n=0}^{N-1}&(||D(\theta_f^{n+1})||^2_{L^2(\Omega^f)}+||\theta_{fp}^{n+1}||^2_{L^2(\Omega^f)}+||\nabla\theta_p^{n+1}||^2_{L^2(\Omega^p)}+||\nabla d_t\theta_f^{n+1}||^2_{L^2(\Omega^f)}\\&+||\nabla d_t\theta_u^{n+1}||^2_{L^2(\Omega^p)}+||d_t\theta_p^{n+1}||^2_{L^2(\Omega^p)}+||\nabla d_t\theta_p^{n+1}||^2_{L^2(\Omega^p)}+||d_{tt}\theta_u^{n+1}||^2_{L^2(\Omega^p)}\\&+||d_{tt}\theta_v^{n+1}||^2_{L^2(\Omega^p)}+||d_{tt}\theta_v^{n+1}||^2_{L^2(\Gamma)}+||d_t\theta_v^{n+1}||^2_{L^2(\Omega^p)}+||d_t\theta_v^{n+1}||^2_{L^2(\Gamma)}+||D(d_t\theta_u^{n+1})||^2_{L^2(\Omega^p)}\\&+||d_t\theta_u^{n+1}|_\Gamma||^2_M)+C\max_{0\le n\le N}(||\theta_p^n||^2_{L^2(\Omega^p)}+||\nabla\theta_p^n||^2_{L^2(\Omega^p)}+||\theta_v^n||^2_{L^2(\Omega^p)}+||D(\theta_u^n)||^2_{L^2(\Omega^p)}\\&+||\theta_u^n|_\Gamma||^2_M+||d_t\theta_u^n||^2_{L^2(\Omega^p)}+||d_t\theta_v^n||^2_{L^2(\Omega^p)}+||d_t\theta_v^n||^2_{L^2(\Gamma)}).\end{aligned}$$

Using Lemma 6, we bound the approximation error terms as follows

$$\begin{aligned}\mathcal{S}\le Ch^{2k}\Big(&||\boldsymbol{v}||^2_{l^2(0,T;H^{k+1}(\Omega^f))}+||p_p||^2_{l^2(0,T;H^{k+1}(\Omega^p))}+||\partial_t\boldsymbol{v}||^2_{L^2(0,T;H^{k+1}(\Omega^f))}+||\partial_t\boldsymbol{U}||^2_{L^2(0,T;H^{k+1}(\Omega^p))}\\&+||\partial_t p_p||^2_{L^2(0,T;H^{k+1}(\Omega^p))}+||\partial_t\boldsymbol{\eta}||^2_{L^2(0,T;H^{k+1}(0,L))}+||p_p||^2_{l^\infty(0,T;H^{k+1}(\Omega^p))}+||\boldsymbol{U}||^2_{l^\infty(0,T;H^{k+1}(\Omega^p))}\\&+||\boldsymbol{\eta}||^2_{l^\infty(0,T;H^{k+1}(0,L))}\Big)+Ch^{2s+2}||p_f||^2_{l^2(0,T;H^{s+1}(\Omega^f))}\\&+Ch^{2k+2}\Big(||\partial_t p_p||^2_{L^2(0,T;H^{k+1}(\Omega^p))}+||\partial_{tt}\boldsymbol{U}||^2_{L^2(0,T;H^{k+1}(\Omega^p))}+||\partial_{tt}\boldsymbol{V}||^2_{L^2(0,T;H^{k+1}(\Omega^p))}\\&+||\partial_{tt}\boldsymbol{\xi}\|^2_{L^2(0,T;H^{k+1}(0,L))}+||\partial_t\boldsymbol{V}||^2_{L^2(0,T;H^{k+1}(\Omega^p))}+||\partial_t\boldsymbol{\xi}||^2_{L^2(0,T;H^{k+1}(0,L))}+||p_p||^2_{l^\infty(0,T;H^{k+1}(\Omega^p))}\\&+||\boldsymbol{V}||^2_{l^\infty(0,T;H^{k+1}(\Omega^p)}+||\partial_t\boldsymbol{U}||^2_{l^\infty(0,T;H^{k+1}(\Omega^p))}+||\partial_t\boldsymbol{V}||^2_{l^\infty(0,T;H^{k+1}(\Omega^p))}+||\partial_t\boldsymbol{\xi}||^2_{l^\infty(0,T;H^{k+1}(0,L))}\Big)\\&+Ch^{2k+4}\Big(||\partial_{tt}\boldsymbol{U}||^2_{l^\infty(0,T;H^{k+1}(\Omega^p))}+||\partial_{tt}\boldsymbol{V}||^2_{l^\infty(0,T;H^{k+1}(\Omega^p))}+||\partial_{tt}\boldsymbol{\xi}||^2_{l^\infty(0,T;H^{k+1}(0,L))}\Big).\end{aligned}\tag{5.12}$$

In the statement of the theorem, terms multiplying h^{2k} are denoted by $\mathcal{B}_1(\boldsymbol{v},\boldsymbol{U},\boldsymbol{\eta},p_p)$, terms multiplying h^{2k+2} are denoted by $\mathcal{B}_2(\boldsymbol{U},\boldsymbol{V},\boldsymbol{\eta},\boldsymbol{\xi},p_p)$, and terms multiplying h^{2k+4} are denoted by $\mathcal{B}_3(\boldsymbol{U},\boldsymbol{V},\boldsymbol{\xi})$.

Lastly, $\mathcal{T}$ denotes the bound on the consistency and splitting error terms

$$\begin{aligned}\mathcal{T} =& C\Delta t^2(||\partial_{tt}\boldsymbol{v}||^2_{L^2(0,T;L^2(\Omega^f))}+||\partial_t p_p||^2_{L^2(0,T;H^1(\Omega^p))}+||\partial_{tt}p_p||^2_{L^2(0,T;L^2(\Omega^p))}+||\partial_{tt}\boldsymbol{U}||^2_{L^2(0,T;H^1(\Omega^p))}\\ &+||\partial_{ttt}\boldsymbol{U}||^2_{L^2(0,T;L^2(\Omega^p))}+||\partial_{ttt}\boldsymbol{\eta}||^2_{L^2(0,T;L^2(0,L))}+||\partial_{ttt}\boldsymbol{V}||^2_{L^2(0,T;L^2(\Omega^p))}+||\partial_{tt}\boldsymbol{U}||_{l^\infty(0,T;L^2(\Omega^p))}\\ &+||\partial_{tt}\boldsymbol{\eta}||_{l^\infty(0,T;L^2(0,L))}+||\partial_{tt}\boldsymbol{V}||_{l^\infty(0,T;L^2(\Omega^p))})+C\Delta t||\eta||^2_{l^2(0,T;H^2(0,L))}+C\Delta t^3||\partial_{tt}\boldsymbol{v}||^2_{L^2(0,T;L^2(\Gamma))}.\end{aligned}$$

The terms multiplying $C\Delta t^2$ in $\mathcal{T}$ give rise to terms denoted by $\mathcal{B}_4(\boldsymbol{v},\boldsymbol{U},\boldsymbol{V},\boldsymbol{\eta},\boldsymbol{\xi},p_p)$ in the statement of the theorem.

Finally, using estimates (5.12), approximation properties (A10)–(A15), triangle inequality, and the discrete Gronwall inequality, we prove the desired estimate, except for the pressure error in the fluid domain.

Step 4: Analysis of the fluid pressure error. To control this part of the error, we proceed as for the stability estimate. More precisely, we start by taking $\psi_h^f=0,\boldsymbol{\varphi}_h^p=0,\boldsymbol{\phi}_h^p=0$, and $\psi_h^p=0$ in (5) and rearranging it as follows

$$\begin{aligned}b_f(\delta_{fp}^{n+1},\boldsymbol{\varphi}_h^f)=&\rho_f\int_{\Omega^f}d_t e_f^{n+1}\cdot\boldsymbol{\varphi}_h^f d\boldsymbol{x}+a_f(e_f^{n+1},\boldsymbol{\varphi}_h^f)+\rho_m r_m\int_\Gamma\frac{e_f^{n+1}\cdot\boldsymbol{\tau}-e_v^n\cdot\boldsymbol{\tau}}{\Delta t}(\boldsymbol{\varphi}_h^f\cdot\boldsymbol{\tau})dx\\ &+c_{fp}(e_p^n,\boldsymbol{\varphi}_h^f)-b_f(\theta_{fp}^{n+1},\boldsymbol{\varphi}_h^f)-\mathcal{R}_f^{n+1}(\boldsymbol{\varphi}_h^f)-\mathcal{R}_{\mathrm{os1}}^{n+1}(\boldsymbol{\varphi}_h^f)-\mathcal{R}_{\mathrm{os2}}^{n+1}(\boldsymbol{\varphi}_h^f).\end{aligned}\tag{5.13}$$

For simplicity of notation, let us group the terms on the right-hand side of the previous equation,

$$\begin{aligned}\mathcal{T}(\boldsymbol{\varphi}_h^f):=&\rho_f\int_{\Omega^f}d_t e_f^{n+1}\cdot\boldsymbol{\varphi}_h^f d\boldsymbol{x}+a_f(e_f^{n+1},\boldsymbol{\varphi}_h^f)\\ &+\rho_m r_m\int_\Gamma\frac{e_f^{n+1}\cdot\boldsymbol{\tau}-e_v^n\cdot\boldsymbol{\tau}}{\Delta t}(\boldsymbol{\varphi}_h^f\cdot\boldsymbol{\tau})dx+c_{fp}(e_p^n,\boldsymbol{\varphi}_h^f)+b_f(\theta_{fp}^{n+1},\boldsymbol{\varphi}_h^f).\end{aligned}$$

Owing to the inf-sup condition (4.15) between spaces V_h^f and Q_h^f there exists a positive constant β_f independent of the mesh characteristic size such that,

$$\beta_f||\delta_{fp}^{n+1}||_{L^2(\Omega^f)}\le\sup_{\boldsymbol{\varphi}_h^f\in V_h^f}\frac{\mathcal{T}(\boldsymbol{\varphi}_h^f)-\mathcal{R}_f^{n+1}(\boldsymbol{\varphi}_h^f)-\mathcal{R}_{\mathrm{os1}}^{n+1}(\varphi_h^f)-\mathcal{R}_{\mathrm{os2}}^{n+1}(\varphi_h^f)}{||\boldsymbol{\varphi}_h^f||_{H^1(\Omega^f)}}.\tag{5.14}$$

Moving along the lines of the stability estimate, the following upper bounds for the right hand side of (5.14) hold true, with a generic constant C which depends on the trace (A7), Korn (A8), and Poincaré (A6) inequalities, as well as on the parameters of the problem,

$$\begin{aligned}\sup_{\boldsymbol{\varphi}_h^f\in V_h^f}\frac{\mathcal{T}(\boldsymbol{\varphi}_h^f)}{||\boldsymbol{\varphi}_h^f||_{H^1(\Omega^f)}}\le C\Bigg(&||e_f^{n+1}||_{H^1(\Omega^f)}+||\delta_p^n||_{H^1(\Omega^p)}+||\theta_p^n||_{H^1(\Omega^p)}+||\theta_{fp}^{n+1}||_{L^2(\Omega^f)}\\ &+||d_t e_f^{n+1}||_{L^2(\Omega^f)}+\left\|\frac{\delta_f^{n+1}\cdot\boldsymbol{\tau}-\delta_v^n\cdot\boldsymbol{\tau}}{\Delta t}\right\|_{L^2(\Gamma)}+||d_t\theta_f^{n+1}\cdot\boldsymbol{\tau}||_{L^2(\Gamma)}\Bigg).\end{aligned}$$

Using the bounds detailed in Lemma 5 of Appendix, we get

$$\sup_{\boldsymbol{\varphi}_h^f \in V_h^f} \frac{\mathcal{R}_f^{n+1}(\boldsymbol{\varphi}_h^f) - \mathcal{R}_{\text{os1}}^{n+1}(\boldsymbol{\varphi}_h^f) - \mathcal{R}_{\text{os2}}^{n+1}(\boldsymbol{\varphi}_h^f \cdot \boldsymbol{\tau})}{||\boldsymbol{\varphi}_h^f||_{H^1(\Omega^f)}} \leq C\Bigg(||d_t \boldsymbol{v}^{n+1} - \partial_t \boldsymbol{v}^{n+1}||_{L^2(\Omega^f)}$$
$$+ ||\nabla(p_p^{n+1} - p_p^n)||_{L^2(\Omega^p)} + \left\| \boldsymbol{\tau} \cdot \boldsymbol{\sigma}^f \boldsymbol{n} + \rho_m r_m \frac{\boldsymbol{v}^{n+1} \cdot \boldsymbol{\tau} - \boldsymbol{V}^n \cdot \boldsymbol{\tau}}{\Delta t} \right\|_{L^2(\Gamma)} \Bigg).$$

Finally, we replace the previous estimates into (5.14), square all terms, sum up with respect to n and multiply by Δt^2. There exists a positive constant c small enough such that

$$c\Delta t^2 \sum_{n=0}^{N-1} ||\delta_{fp}^{n+1}||_{L^2(\Omega^f)}^2 \leq \Delta t^2 \sum_{n=0}^{N-1} \Bigg(||d_t e_f^{n+1}||_{L^2(\Omega^f)}^2 + \left\| \frac{\delta_f^{n+1} \cdot \boldsymbol{\tau} - \delta_v^n \cdot \boldsymbol{\tau}}{\Delta t} \right\|_{L^2(\Gamma)}^2 + ||d_t \theta_v^{n+1}||_{L^2(\Gamma)}^2$$
$$+ ||e_f^{n+1}||_{H^1(\Omega^f)}^2 + ||\delta_p^n||_{H^1(\Omega^p)}^2 + ||\theta_p^n||_{H^1(\Omega^p)}^2 + ||\theta_{fp}^{n+1}||_{L^2(\Omega^f)}^2 + ||d_t \boldsymbol{v}^{n+1} - \partial_t \boldsymbol{v}^{n+1}||_{L^2(\Omega^f)}^2$$
$$+ ||\nabla(p_p^{n+1} - p_p^n)||_{L^2(\Omega^p)}^2 + \left\| \boldsymbol{\tau} \cdot \boldsymbol{\sigma}^f \boldsymbol{n} + \rho_m r_m \frac{\boldsymbol{v}^{n+1} \cdot \boldsymbol{\tau} - \boldsymbol{V}^n \cdot \boldsymbol{\tau}}{\Delta t} \right\|_{L^2(\Gamma)}^2 \Bigg).$$

To conclude, combining the triangle inequality with the approximation properties of the discrete pressure space and bounding the right-hand side using Lemma 4 and Eq. (5.11), we obtain

$$\Delta t ||p_f - p_{f,h}||_{l^2(0,T;L^2(\Omega^f))}^2 \leq C\Bigg(h^{2k} \mathcal{B}_1(\boldsymbol{v}, \boldsymbol{U}, \boldsymbol{\eta}, p_p) + h^{2k+2} \mathcal{B}_2(\boldsymbol{v}, \boldsymbol{U}, \boldsymbol{V}, \boldsymbol{\eta}, \boldsymbol{\xi}, p_p)$$
$$+ h^{2s+2} ||p_f||_{l^2(0,T;H^{s+1}(\Omega^f))}^2 + h^{2k+4} \mathcal{B}_3(\boldsymbol{U}, \boldsymbol{V}, \boldsymbol{\xi}) + \Delta t ||\eta||_{l^2(0,T;H^2(0,L))}^2$$
$$+ \Delta t^2 \mathcal{B}_4(\boldsymbol{v}, \boldsymbol{U}, \boldsymbol{V}, \boldsymbol{\eta}, \boldsymbol{\xi}, p_p) + \Delta t^3 ||\partial_{tt} \boldsymbol{v}||_{L^2(0,T;L^2(\Gamma))}^2 \Bigg).$$

■

VI. NUMERICAL RESULTS

The focus of this section is on verification of the results presented in this work and exploration of poroelastic effects in the model. We test the scheme on a classical benchmark problem used for convergence studies of FSI problems [13, 45, 50, 75, 76]. In Example 1, we present the convergence of our scheme in space and time. Furthermore, we validate the necessity of the stability condition (4.11).

In Example 2, we analyze the role of poroelastic effects in blood flow. In particular, we compare our results to the ones obtained using a purely elastic model. We distinguish a high permeability and a high storativity case, and present a comparison between the two cases and the purely elastic model.

In both examples, we use the full Navier–Stokes equations for fluid flow given on a moving domain. The fluid domain and ALE velocity $\boldsymbol{w}^n$ are computed as follows

$$\mathcal{A}_{t^n}(\hat{\boldsymbol{x}}) = \hat{\boldsymbol{x}} + \text{Ext}(\hat{\boldsymbol{\eta}}^n), \quad \Omega^f(t^n) = \mathcal{A}_{t^n}(\hat{\Omega}^f), \quad \boldsymbol{w}^n = d_t \boldsymbol{x}^n,$$

where $\hat{\boldsymbol{x}} \in \hat{\Omega}, \boldsymbol{x}^n \in \Omega(t^n)$, and $\boldsymbol{x}^{n-1} \in \Omega(t^{n-1})$.

TABLE I. Geometry, fluid, and structure parameters that are used in Example 1.

Parameters	Values	Parameters	Values
Radius R (cm)	0.5	Length L (cm)	6
Membrane thickness r_m (cm)	0.02	Poroelastic wall thickness r_p (cm)	0.1
Membrane density ρ_m (g/cm^3)	1.1	Poroelastic wall density ρ_p (g/cm^3)	1.1
Fluid density ρ_f (g/cm^3)	1	Dyn. viscosity μ (g/cm s)	0.035
Lamé coeff. μ_m (dyne/cm^2)	1.07×10^6	Lamé coeff. λ_m (dyne/cm^2)	4.28×10^6
Lamé coeff. μ_p (dyne/cm^2)	1.07×10^6	Lamé coeff. λ_p (dyne/cm^2)	4.28×10^6
Hydraulic conductivity κ (cm^3 s/g)	5×10^{-9}	Mass storativity coeff. s_0 (cm^2/dyne)	5×10^{-6}
Biot–Willis constant α	1	Spring coeff. β (dyne/cm^4)	5×10^7

A. Example 1

We consider the classical test problem used in several works [13, 45, 50, 76] as a benchmark problem for testing the results of FSI algorithms for blood flow. In our case, the flow is driven by the time-dependent pressure data:

$$p_{\text{in}}(t) = \begin{cases} \frac{p_{\max}}{2}\left(1 - \cos\left(\frac{2\pi t}{T_{\max}}\right)\right) & \text{if } t \le T_{\max} \\ 0 & \text{if } t > T_{\max}, \end{cases} \tag{6.1}$$

where $p_{\max} = 1.3334\,\text{dyne/cm}^2$ and $T_{\max} = 0.003\,\text{s}$. For the elastic skeleton, we consider the following equation of linear elasticity:

$$\rho_p \frac{D^2\boldsymbol{U}}{Dt^2} + \beta \boldsymbol{U} - \nabla \cdot \boldsymbol{\sigma}^p = 0.$$

The additional term $\beta\boldsymbol{U}$ comes from the axially symmetric formulation, accounting for the recoil due to the circumferential strain. Namely, it acts like a spring term, keeping the top and bottom structure displacements connected in 2D, see, for example, [49, 75, 77]. The values of the parameters used in this example are given in Table I.

Parameters given in Table I are within the range of physiological values for blood flow. The problem was solved over the time interval [0,0.006] s.

To verify the convergence estimates from Theorem 2, let the errors between the computed and the reference solution be defined as $e_f = \boldsymbol{v} - \boldsymbol{v}_{\text{ref}}, e_{fp} = p_f - p_{f,\text{ref}}, e_v = \boldsymbol{V} - \boldsymbol{V}_{\text{ref}}, e_p = p_p - p_{p,\text{ref}}$, and $e_u = \boldsymbol{U} - \boldsymbol{U}_{\text{ref}}$. We start by computing the rates of convergence in time. To do so, fix $\Delta x = 0.016$ and define the reference solution to be the one obtained with $\Delta t = 5 \times 10^{-7}$. Table II shows the error between the reference solution and solutions obtained with $\Delta t = 10^{-6}, 5 \times 10^{-6}, 10^{-5}$, and 3×10^{-5} for the fluid velocity $\boldsymbol{v}$, fluid pressure p_f, pressure in the pores p_p, displacement $\boldsymbol{U}$ and its velocity $\boldsymbol{V}$, respectively.

To study the convergence in space, we take $\Delta t = 5 \times 10^{-6}$ and define the reference solution to be the one obtained with $\Delta x = r_p/14 = 0.007$. Table III shows errors between the reference solution and the solutions obtain using $\Delta x = 0.01, 0.0125, 0.0167$, and 0.025.

As we can see, we observe the first-order convergence in space. Even thought our error estimates predict half-order convergence in time, our numerical results indicate the first order. This may be due to the fact that the second-order derivative of the structure is rather small.

To verify the necessity of the time-step condition (4.11), we compute the total energy E^N of the system using different time steps. The time at which E^N is computed is either the time when E^N becomes greater than 10^{250}, or the final time $t^N = 6$ ms. Figure 2 shows the relation of the

TABLE II. Convergence in time.

Δt	$\|\|e_f\|\|_{l^\infty(L^2)}$	Rate	$\|\|e_f\|\|_{l^2(H^1)}$	Rate	$\|\|e_{fp}\|\|_{l^2(L^2)}$	Rate	$\|\|e_v\|\|_{l^\infty(L^2)}$	Rate	$\|\|e_p\|\|_{l^\infty(L^2)}$	Rate	$\|\|e_p\|\|_{l^2(H^1)}$	Rate	$\|\|e_u\|\|_{l^\infty(H^1)}$	Rate
3×10^{-5}	$7.6e-1$	–	$8.8e-2$	–	$8.9e-1$	–	$3.0e-2$	–	$6.3e-1$	–	$4.1e-1$	–	$7.7e-5$	–
10^{-5}	$2.7e-1$	0.93	$3.1e-2$	0.95	$3.4e-1$	0.88	$1.0e-2$	0.84	$2.2e-1$	0.95	$1.5e-1$	0.92	$3.0e-5$	0.85
5×10^{-6}	$1.3e-1$	1.04	$1.5e-2$	1.03	$1.6e-1$	1.05	$6.0e-3$	0.97	$1.1e-1$	1.04	$7.4e-2$	1.02	$1.5e-5$	0.97
10^{-6}	$1.5e-2$	1.36	$1.8e-3$	1.32	$1.8e-2$	1.36	$6.9e-4$	1.36	$1.2e-2$	1.35	$8.5e-3$	1.34	$1.8e-6$	1.32

TABLE III. Convergence in space.

Δx	$\|\|e_f\|\|_{l^\infty(L^2)}$	Rate	$\|\|e_f\|\|_{l^2(H^1)}$	Rate	$\|\|e_{fp}\|\|_{l^2(L^2)}$	Rate	$\|\|e_v\|\|_{l^\infty(L^2)}$	Rate	$\|\|e_p\|\|_{l^\infty(L^2)}$	Rate	$\|\|e_p\|\|_{l^2(H^1)}$	Rate	$\|\|e_u\|\|_{l^\infty(H^1)}$	Rate
$r_p/4$	$2.4e-1$	–	$6.8e-1$	–	$3.1e-1$	–	$2.5e-2$	–	$1.2e+0$	–	$4.0e-1$	–	$3.1e-1$	–
$r_p/5$	$1.9e-1$	1.01	$6.2e-1$	0.43	$2.6e-1$	0.83	$1.8e-2$	1.46	$0.9e-1$	0.92	$3.6e-1$	0.47	$2.6e-1$	0.84
$r_p/6$	$1.5e-1$	1.55	$5.3e-1$	0.87	$2.1e-1$	1.12	$1.4e-2$	1.37	$0.8e-1$	1.10	$3.2e-1$	0.73	$2.1e-1$	1.08
$r_p/7$	$1.2e-1$	1.37	$4.5e-1$	1.06	$1.7e-1$	1.32	$1.0e-2$	1.6	$0.6e-1$	1.34	$2.7e-1$	1.01	$1.8e-1$	1.08

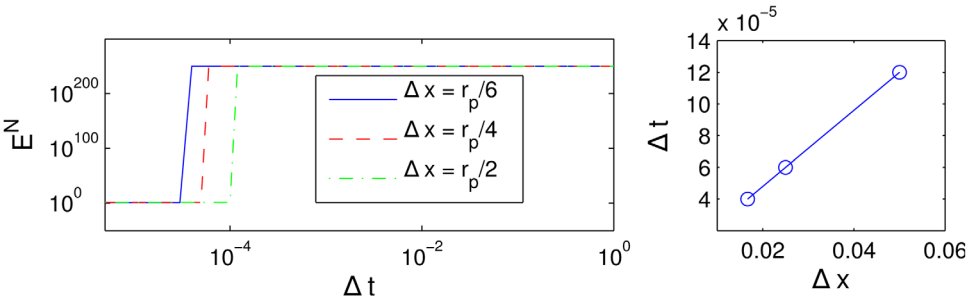

FIG. 2. Verification of the time-step condition (4.11). Left: Relation between the total energy of the system and the time step. Right: Relation between Δx and the critical Δt. [Color figure can be viewed in the online issue, which is available at wileyonlinelibrary.com.]

energy of the system and the time step (left), and the relation between Δx and the critical Δt (right). Indeed, we observe a linear relation between Δx and the critical value of Δt, with the proportionality constant 2.4e − 3. This is less restrictive than the prediction (4.11) from the theory, where the proportionality constant for the parameters in Table I can be estimated as 3.5e − 7, indicating that the scheme enjoys better stability properties than prescribed by (4.11).

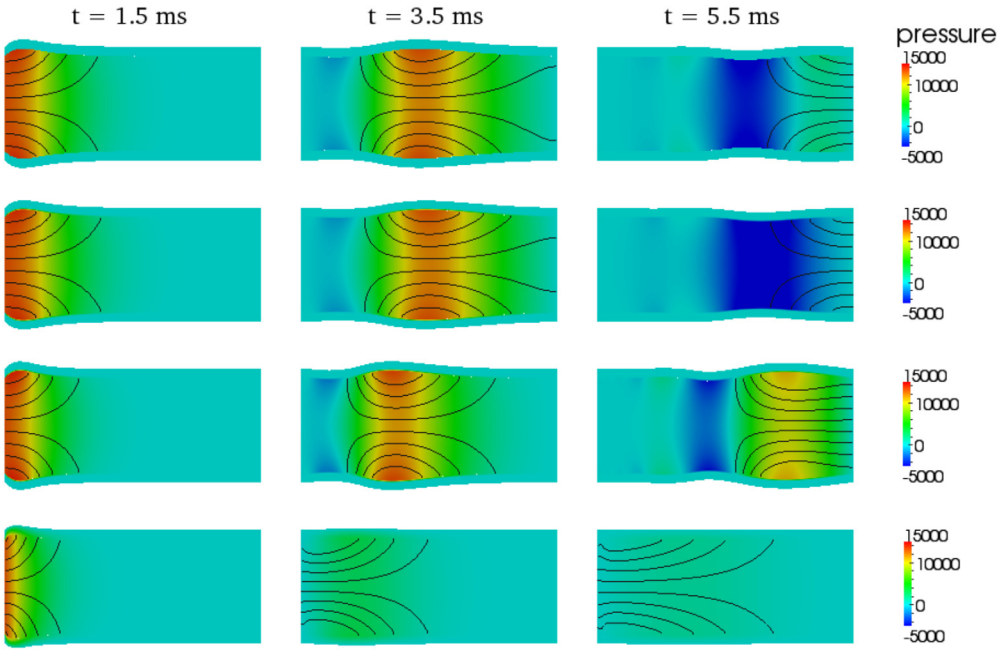

FIG. 3. Pressure in the lumen, velocity streamlines, and pressure in the wall at times $t = 1.5$ ms, $t = 3.5$ ms and $t = 5.5$ ms. The outer layer of the arterial wall is model using a elastic model (top), poroelastic model with $s_0 = 5 \times 10^{-6}$, $\kappa = 5 \times 10^{-9}$ (middle top), poroelastic model with $s_0 = 2 \times 10^{-5}$, $\kappa = 5 \times 10^{-9}$ (middle bottom), and poroelastic model with $s_0 = 5 \times 10^{-6}$, $\kappa = 10^{-4}$ (bottom). [Color figure can be viewed in the online issue, which is available at wileyonlinelibrary.com.]

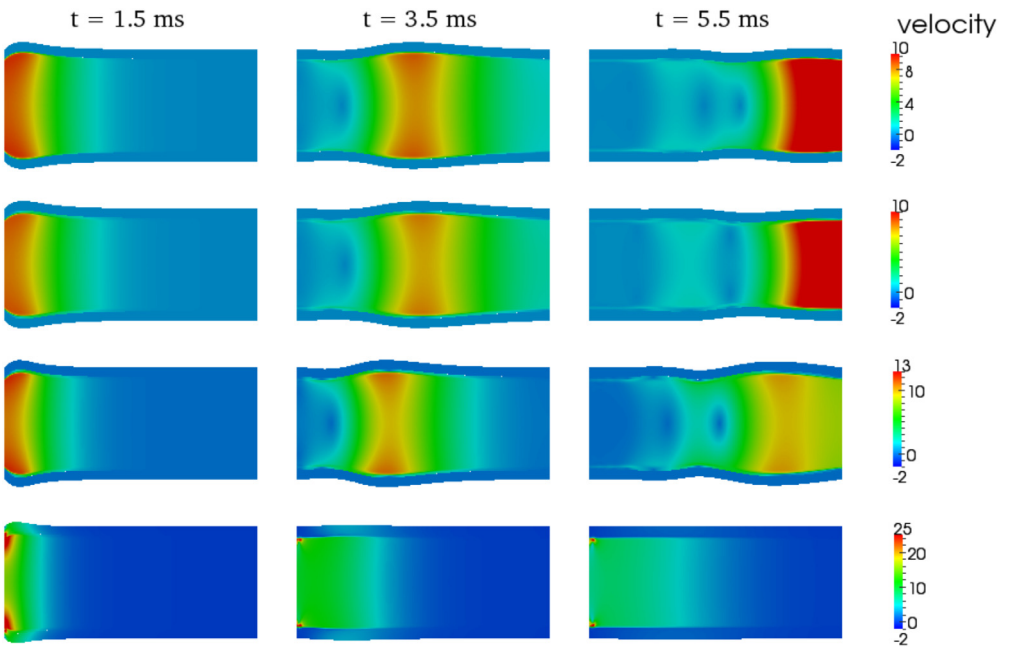

FIG. 4. Velocity magnitude at times $t = 1.5$ ms, $t = 3.5$ ms and $t = 5.5$ ms. The outer layer of the arterial wall is model using a elastic model (top), poroelastic model with $s_0 = 5 \times 10^{-6}$, $\kappa = 5 \times 10^{-9}$ (middle top), poroelastic model with $s_0 = 2 \times 10^{-5}$, $\kappa = 5 \times 10^{-9}$ (middle bottom), and poroelastic model with $s_0 = 5 \times 10^{-6}$, $\kappa = 10^{-4}$ (bottom). [Color figure can be viewed in the online issue, which is available at wileyonlinelibrary.com.]

B. Example 2

In this example, we compare our numerical results to the ones obtained using a purely elastic model for the outer layer of the arterial wall. More precisely, while the fluid and the membrane are modeled as before, we assume there is no fluid contained within the wall, and we model the thick wall using 2D linear elasticity

$$\rho_p \frac{D^2 \boldsymbol{U}}{Dt^2} + \beta \boldsymbol{U} - \nabla \cdot \boldsymbol{\sigma}^E = 0; \quad \text{in } \Omega^p(t) \text{ for } t \in (0, T).$$

The coupling conditions in this case are given as follows:

$$\boldsymbol{v} = \boldsymbol{\xi}, \boldsymbol{\eta} = \boldsymbol{U} \quad \text{on } \Gamma(t), \tag{6.2}$$

$$\boldsymbol{\sigma}^f \boldsymbol{n} - \sigma^E \boldsymbol{n} + J^{-1} \boldsymbol{f} = 0 \quad \text{on } \Gamma(t). \tag{6.3}$$

The problem is solved using an operator-splitting approach performed in the same spirit as in this manuscript. The unconditional stability is due to the Robin boundary conditions that involve membrane inertia, appearing in both fluid, and thick structure subproblems. For more details see [78].

For the purpose of understanding the poroelastic effects to the structure displacement, we distinguish two cases: the high storativity case $s_0 \gg \kappa$, and the high permeability case $\kappa \gg s_0$. We give a comparison of the results obtained using the elastic model for the outer wall, and poroelastic model

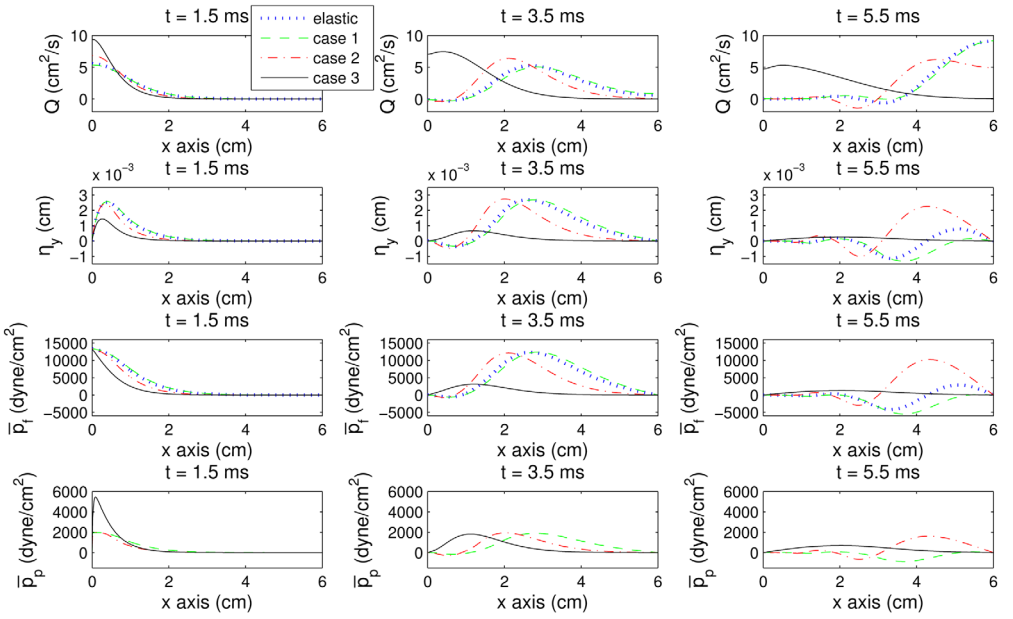

FIG. 5. From top to bottom: Flow rate, radial displacement of the membrane, mean pressure in the lumen, and mean pressure in the pores. Results were obtained using the elastic model (dotted line), and poroelastic model with the following parameters: case 1 ($s_0 = 5 \times 10^{-6}$, $\kappa = 5 \times 10^{-9}$; dashed line), case 2 ($s_0 = 2 \times 10^{-5}$, $\kappa = 5 \times 10^{-9}$; dash dot line), and case 3 ($s_0 = 5 \times 10^{-6}$, $\kappa = 1 \times 10^{-4}$; solid line). [Color figure can be viewed in the online issue, which is available at wileyonlinelibrary.com.]

using two different values for s_0, and two different values for κ. The first test case for the poroelastic wall will correspond to the parameters s_0 and κ from Example 1 ($s_0 = 5 \times 10^{-6}, \kappa = 5 \times 10^{-9}$), the second test case will correspond to the increased value of s_0 ($s_0 = 2 \times 10^{-5}, \kappa = 5 \times 10^{-9}$), and the third example to the increased value of κ ($s_0 = 5 \times 10^{-6}, \kappa = 10^{-4}$). Figure 3 shows the pressure pulse (colormap) and velocity streamlines obtained with the two models. The velocity magnitude is shown in Fig. 4.

To quantify the differences, we compute average quantities on each vertical line S_i^r of the computational mesh Ω^r, corresponding to the position $x_i = i \cdot \Delta x$, where $\Delta x = 0.016$ and $r \in \{f, m\}$. The quantities of interest are membrane displacement, the mean pressure, and the flow rate in the lumen:

$$\bar{p}_f(x_i) = \frac{1}{S_i^f} \int_{S_i^f} p_{f,h} ds, \quad \bar{p}_p(x_i) = \frac{1}{S_i^p} \int_{S_i^p} p_{p,h} ds, \quad Q(x_i) = \int_{S_i^f} \boldsymbol{v}_h \cdot \boldsymbol{e}_x ds.$$

Figure 5 shows a comparison between the flow rate in the lumen, membrane displacement, and the mean pressure in the lumen and in the wall, obtained using a poroelastic model and an elastic model. In the high permeability regime, the structure displacement is the smallest, while in this case, we observe the largest mean pressure in the wall. In the high storativity regime, we observe a delay in the pressure wave propagation speed, and qualitatively different displacement.

VII. CONCLUSION

The focus of this article is on modeling and implementation of a fluid-poroelastic structure interaction problem. In particular, we study the interaction between the fluid a multilayered wall, where the wall consists of a thin membrane, and a thick poroelastic medium. We proposed an explicit numerical algorithm based on the Lie operator splitting scheme. An alternative discrete problem formulation based on Nitsche's method for the enforcement of the interface conditions is under study [79]. This new method can accommodate a mixed formulation for the Darcy's equations.

We prove the conditional stability of the algorithm, and derive error estimates. Stability and convergence results are validated by the numerical simulations. The drawback of the scheme is that it requires pressure formulation for the Darcy equation. Concerning the application of the scheme to blood flow in arteries, we test numerically the porous effects in the wall, comparing results obtained with different coefficients to the ones obtained using a purely elastic model. We observe different behavior depending on the storativity or permeability dominant regime.

APPENDIX AUXILIARY RESULTS

We collect in this section some auxiliary results and proofs that complement the stability and convergence analysis of the proposed scheme. They are either a consequence of the standard theory of the finite element method or they follow from basic results of approximation theory. For the reader's convenience, we report them separately from the main body of the manuscript.

For any real numbers a, b, the following algebraic identities are satisfied:

$$(a-b)a = \frac{1}{2}a^2 - \frac{1}{2}b^2 + \frac{1}{2}(a-b)^2, \tag{A1}$$

$$\Delta t \sum_{n=0}^{N-1} a^{n+1} d_t b^{n+1} = a^N b^N - \Delta t \sum_{n=0}^{N-1} d_t a^{n+1} b^n - a^0 b^0, \tag{A2}$$

and for non-negative real numbers a, b, and $\epsilon > 0$

$$ab \leq \frac{a^2}{2\epsilon} + \frac{\epsilon b^2}{2}. \tag{A3}$$

Lemma 2. *Given the functional spaces $V_h^f \subset V^f, Q_h^f \subset Q^f, V_h^p \subset V^p$, and $Q_h^p \subset Q^p$, the following inequalities hold true:*

- *local trace-inverse inequality:*

$$h||\psi_h||^2_{L^2(\Gamma)} \leq C_{TI}||\psi_h||^2_{L^2(\Omega^p)}, \quad \forall \psi_h \in Q_h^p; \tag{A4}$$

- *Cauchy-Schwarz inequality:*

$$\left| \int_{\Omega^{f/p}} \boldsymbol{v} \cdot \boldsymbol{u} d\boldsymbol{x} \right| \leq ||\boldsymbol{v}||_{L^2(\Omega^{f/p})}||\boldsymbol{u}||_{L^2(\Omega^{f/p})} \quad \forall \boldsymbol{v}, \boldsymbol{u} \in V^{f/p}; \tag{A5}$$

- *Poincaré inequality:*

$$||\boldsymbol{v}||_{L^2(\Omega^{f/p})} \leq C_{PF}||\nabla \boldsymbol{v}||_{L^2(\Omega^{f/p})} \quad \forall \boldsymbol{v} \in V^{f/p}; \tag{A6}$$

- *trace inequality:*

$$||\boldsymbol{v}||_{L^2(\Gamma)} \leq C_T ||\boldsymbol{v}||^{1/2}_{L^2(\Omega^{f/p})} ||\nabla \boldsymbol{v}||^{1/2}_{L^2(\Omega^{f/p})} \quad \forall \boldsymbol{v} \in V^{f/p}; \tag{A7}$$

- *Korn inequality:*

$$||\nabla \boldsymbol{v}||_{L^2(\Omega^{f/p})} \leq C_K ||D(\boldsymbol{v})||_{L^2(\Omega^{f/p})} \quad \forall \boldsymbol{v} \in V^{f/p}. \tag{A8}$$

Here, constants C_{PF}, C_T and C_K depend on the domain Ω, and constant C_{TI} depends on the angles in the finite element mesh.

Our analysis holds provided that the following regularity assumptions are satisfied by the exact solution of the problem.

Assumption 1. *Let X be a Banach space, and $(0,T) \subset \mathbb{R}$ a time interval. We define the L^2-space of functions $u : (0,T) \to X$ by*

$$L^2(0,T;X) = \left\{ u | u \text{ is measurable and } \int_0^T ||u||_X^2 dt < \infty \right\},$$

and L^∞-space by

$$L^\infty(0,T;X) = \left\{ u | u \text{ is measurable and } ||u||_X \text{ is essentially bounded} \right\}.$$

Then, the Sobolev space $W^{k,2}(0,T;X) = H^k(0,T;X)$ is defined to be the set of all functions $u \in L^2(0,T;X)$ whose distributional time derivative $D_t^\alpha u$ belongs to $L^2(0,T;X)$, for every α with $|\alpha| \leq k$. We assume that the weak solution of (2.28), complemented by the prescribed interface, boundary and initial conditions, is such that

$$\begin{aligned}
&\boldsymbol{v} \in H^1(0,T;H^{k+1}(\Omega^f)) \cap H^2(0,T;L^2(\Omega^f)),\\
&p_f \in L^2(0,T;H^{s+1}(\Omega^f)),\\
&\boldsymbol{\eta} \in L^\infty(0,T;H^{k+1}(0,L)) \cap H^1(0,T;H^{k+1}(0,L)) \cap H^3(0,T;L^2(0,L)),\\
&\boldsymbol{\xi} \in H^2(0,T;H^{k+1}(0,L)) \cap H^3(0,T;L^2(0,L)),\\
&\partial_t \boldsymbol{\xi} \in L^\infty(0,T;H^{k+1}(0,L)),\\
&\partial_{tt} \boldsymbol{\xi} \in L^\infty(0,T;H^{k+1}(0,L)),\\
&\boldsymbol{U} \in L^\infty(0,T;H^{k+1}(\Omega^p)) \cap H^2(0,T;H^{k+1}(\Omega^p)) \cap H^3(0,T;L^2(\Omega^p)),\\
&\boldsymbol{V} \in L^\infty(0,T;H^{k+1}(\Omega^p)) \cap H^3(0,T;L^2(\Omega^p)),\\
&\partial_t \boldsymbol{V} \in L^\infty(0,T;H^{k+1}(\Omega^p)),\\
&\partial_{tt} \boldsymbol{V} \in L^\infty(0,T;H^{k+1}(\Omega^p)),\\
&p_p \in L^\infty(0,T;H^{k+1}(\Omega^p)) \cap H^1(0,T;H^{k+1}(\Omega^p)) \cap H^2(0,T;L^2(\Omega^p)).
\end{aligned} \tag{A9}$$

Then, our finite element spaces satisfy the approximation properties reported below.

Lemma 3. *Let P_h be the Lagrangian interpolation operator onto V_h^p, $I_h = P_h|_\Gamma$ be the Lagrangian interpolation operator onto V_h^m, S_h be a Stokes-like projection operator defined in*

(5.5) , and let $\Pi_h^{f/p}$ be the L^2-orthogonal projections onto $Q_h^{f/p}$ defined in (5.1) . Using piecewise polynomials of degree k and s, we have:

$$||\boldsymbol{v} - S_h\boldsymbol{v}||_{H^1(\Omega^f)} \leq Ch^k||\boldsymbol{v}||_{H^{k+1}(\Omega^f)}, \tag{A10}$$

$$||p_f - \Pi_h^f p_f||_{L^2(\Omega^f)} \leq Ch^{s+1}||p_f||_{H^{s+1}(\Omega^f)}, \tag{A11}$$

$$||\boldsymbol{U} - P_h\boldsymbol{U}||_{L^2(\Omega^p)} \leq Ch^{k+1}||\boldsymbol{U}||_{H^{k+1}(\Omega^p)}, \tag{A12}$$

$$||\boldsymbol{U} - P_h\boldsymbol{U}||_{H^1(\Omega^p)} \leq Ch^{k}||\boldsymbol{U}||_{H^{k+1}(\Omega^p)}, \tag{A13}$$

$$||p_p - \Pi_h^p p_p||_{L^2(\Omega^p)} \leq Ch^{k+1}||p_p||_{H^{k+1}(\Omega^p)}, \tag{A14}$$

$$||p_p - \Pi_h^p p_p||_{H^1(\Omega^p)} \leq Ch^{k}||p_p||_{H^{k+1}(\Omega^p)}. \tag{A15}$$

Furthermore, since $I_h = P_h|_\Gamma$ is a Lagrangian interpolant, we have:

$$||\boldsymbol{U} - P_h\boldsymbol{U}||_{L^2(\Gamma)} = ||\boldsymbol{\eta} - I_h\boldsymbol{\eta}||_{L^2(\Gamma)} \leq Ch^{k+1}||\boldsymbol{\eta}||_{H^{k+1}(\Gamma)}, \tag{A16}$$

$$||\boldsymbol{U} - P_h\boldsymbol{U}||_{H^1(\Gamma)} = ||\boldsymbol{\eta} - I_h\boldsymbol{\eta}||_{H^1(\Gamma)} \leq Ch^{k}||\boldsymbol{\eta}||_{H^{k+1}(\Gamma)}, \tag{A17}$$

$$||\boldsymbol{V} - P_h\boldsymbol{V}||_{L^2(\Gamma)} = ||\boldsymbol{\xi} - I_h\boldsymbol{\xi}||_{L^2(\Gamma)} \leq Ch^{k+1}||\boldsymbol{\xi}||_{H^{k+1}(\Gamma)}. \tag{A18}$$

Proof. The proof of (A10) can be found in [15], Theorem B.5. For the proof of the other inequalities, see [74]. ∎

Lemma 4 (Consistency and splitting errors)**.** *The following inequalities hold:*

$$\Delta t\sum_{n=0}^{N-1}||d_t\boldsymbol{\varphi}^{n+1} - \partial_t\boldsymbol{\varphi}^{n+1}||^2_{L^2(\Omega)} \leq C\Delta t^2||\partial_{tt}\boldsymbol{\varphi}||^2_{L^2(0,T;L^2(\Omega))},$$

$$\Delta t\sum_{n=1}^{N-1}||d_{tt}\boldsymbol{\varphi}^{n+1} - \partial_t(d_t\boldsymbol{\varphi}^{n+1})||^2_{L^2(\Omega)} \leq C\Delta t^2||\partial_{ttt}\boldsymbol{\varphi}||^2_{L^2(0,T;L^2(\Omega))},$$

$$\Delta t^2\sum_{n=0}^{N-1}||\boldsymbol{\tau}\cdot\boldsymbol{\sigma}^f\boldsymbol{n} + \rho_m r_m\frac{\boldsymbol{v}^{n+1}\cdot\boldsymbol{\tau} - \boldsymbol{V}^n\cdot\boldsymbol{\tau}}{\Delta t}||^2_{L^2(\Gamma)} \leq C\Delta t||\eta||^2_{l^2(0,T;H^2(0,L))}$$
$$+ C\Delta t^3||\partial_{tt}\boldsymbol{v}\cdot\boldsymbol{\tau}||^2_{L^2(0,T;L^2(\Gamma))}$$

$$\Delta t\sum_{n=0}^{N-1}||\nabla(\boldsymbol{\varphi}^{n+1} - \boldsymbol{\varphi}^n)||^2_{L^2(\Omega)} \leq C\Delta t^2||\partial_t\boldsymbol{\varphi}||^2_{L^2(0,T;H^1(\Omega))},$$

$$\Delta t\sum_{n=0}^{N-1}||\nabla(d_t\boldsymbol{\varphi}^{n+1} - \partial_t\boldsymbol{\varphi}^{n+1})||^2_{L^2(\Omega)} \leq C\Delta t^2||\partial_{tt}\boldsymbol{\varphi}||^2_{L^2(0,T;H^1(\Omega))},$$

$$||d_t\boldsymbol{\varphi}^N - \partial_t\boldsymbol{\varphi}^N||^2_{L^2(\Omega)} \leq \Delta t^2\max_{0\leq n\leq N}||\partial_{tt}\boldsymbol{\varphi}^n||^2_{L^2(\Omega)} = \Delta t^2||\partial_{tt}\boldsymbol{\varphi}||^2_{l^\infty(0,T;L^2(\Omega))},$$

Proof. We will prove the first three inequalities. The proofs for other inequalities are similar. Using Cauchy–Schwartz inequality, we have

$$\Delta t\sum_{n=0}^{N-1}||d_t\boldsymbol{\varphi}^{n+1} - \partial_t\boldsymbol{\varphi}^{n+1}||^2_{L^2(\Omega)} = \Delta t\sum_{n=0}^{N-1}\int_\Omega\left|\frac{1}{\Delta t}\int_{t^n}^{t^{n+1}}(t-t^n)\partial_{tt}\boldsymbol{\varphi}(t)dt\right|^2 dx$$

$$\leq \frac{1}{\Delta t}\int_\Omega \sum_{n=0}^{N-1}\left(\int_{t^n}^{t^{n+1}} |t-t^n|^2 dt \int_{t^n}^{t^{n+1}} |\partial_{tt}\boldsymbol{\varphi}|^2 dt\right) dx \leq C\Delta t^2 \int_\Omega \int_0^T |\partial_{tt}\boldsymbol{\varphi}|^2 dt dx$$

$$\leq C\Delta t^2 ||\boldsymbol{\varphi}||^2_{L^2(0,T;L^2(\Omega))}.$$

To prove the next two inequalities, we integrate by parts twice, and use Cauchy–Schwartz inequality:

$$\Delta t \sum_{n=1}^{N-1} ||d_{tt}\boldsymbol{\varphi}^{n+1} - \partial_t(d_t\boldsymbol{\varphi}^{n+1})||^2_{L^2(\Omega)}$$

$$= \Delta t \sum_{n=0}^{N-1} \left|\left|\frac{1}{\Delta t^2}\left(\int_{t^n}^{t^{n+1}} (t-t^n)\partial_{tt}\boldsymbol{\varphi} dt + \int_{t^n}^{t^{n-1}} (t-t^{n-1})\partial_{tt}\boldsymbol{\varphi} dt\right)\right|\right|^2_{L^2(\Omega)}$$

$$= \frac{1}{\Delta t^3}\sum_{n=0}^{N-1} \left|\left|\left(\frac{\Delta t^2}{2}\int_{t^n}^{t^{n+1}} \partial_{ttt}\boldsymbol{\varphi} dt - \int_{t^n}^{t^{n+1}} \frac{(t-t^n)^2}{2}\partial_{ttt}\boldsymbol{\varphi} dt - \int_{t^n}^{t^{n-1}} \frac{(t-t^{n-1})^2}{2}\partial_{ttt}\boldsymbol{\varphi} dt\right)\right|\right|^2_{L^2(\Omega)}$$

$$\leq \frac{1}{\Delta t^3}\int_\Omega \sum_{n=0}^{N-1}\left(\frac{\Delta t^4}{4}\left|\int_{t^n}^{t^{n+1}} \partial_{ttt}\boldsymbol{\varphi} dt\right|^2 + \left|\int_{t^n}^{t^{n+1}} \frac{(t-t^n)^2}{2}\partial_{ttt}\boldsymbol{\varphi} dt\right|^2\right.$$

$$\left. + \left|\int_{t^n}^{t^{n-1}} \frac{(t-t^{n-1})^2}{2}\partial_{ttt}\boldsymbol{\varphi} dt\right|^2\right) dx$$

$$\leq \frac{1}{\Delta t^3}\int_\Omega \sum_{n=0}^{N-1}\left(\frac{\Delta t^5}{4}\int_{t^n}^{t^{n+1}} |\partial_{ttt}\boldsymbol{\varphi}|^2 dt + \frac{\Delta t^5}{10}\int_{t^n}^{t^{n+1}} |\partial_{ttt}\boldsymbol{\varphi}|^2 dt + \frac{\Delta t^5}{10}\int_{t^n}^{t^{n-1}} |\partial_{ttt}\boldsymbol{\varphi}|^2 dt\right) dx$$

$$\leq C\Delta t^2 ||\partial_{ttt}\boldsymbol{\varphi}||^2_{L^2(0,T;L^2(\Omega))}$$

To prove the third inequality, note that $\boldsymbol{V}^n \cdot \boldsymbol{\tau} = \boldsymbol{v}^n \cdot \boldsymbol{\tau}$ on Γ, since $\boldsymbol{V}^n$ and $\boldsymbol{v}^n$ are solutions to the continuous problem. Thus, since the exact solution satisfies Eq. (2.22), we have

$$\Delta t^2 \sum_{n=0}^{N-1} \left|\left|\boldsymbol{\tau}\cdot\boldsymbol{\sigma}^f\boldsymbol{n} + \rho_m r_m \frac{\boldsymbol{v}^{n+1}\cdot\boldsymbol{\tau} - \boldsymbol{v}^n\cdot\boldsymbol{\tau}}{\Delta t}\right|\right|^2_{L^2(\Gamma)} = \Delta t^2 \sum_{n=0}^{N-1} ||\boldsymbol{\tau}\cdot\boldsymbol{\sigma}^f\boldsymbol{n} + \rho_m r_m d_t\boldsymbol{v}^{n+1}\cdot\boldsymbol{\tau}||^2_{L^2(\Gamma)}$$

$$= \Delta t^2 \sum_{n=0}^{N-1} ||\boldsymbol{\tau}\cdot\mathcal{L}\boldsymbol{\eta} + \boldsymbol{\tau}\cdot\boldsymbol{\sigma}^p\boldsymbol{n} + \rho_m r_m(d_t\boldsymbol{v}^{n+1}\cdot\boldsymbol{\tau} - \partial_t\boldsymbol{v}^{n+1}\cdot\boldsymbol{\tau})||^2_{L^2(\Gamma)}$$

$$\leq C\Delta t^2 \sum_{n=0}^{N-1} ||\eta^{n+1}||^2_{H^2(0,L)} + C\Delta t^2 \sum_{n=0}^{N-1} ||d_t\boldsymbol{v}^{n+1}\cdot\boldsymbol{\tau} - \partial_t\boldsymbol{v}^{n+1}\cdot\boldsymbol{\tau}||^2_{L^2(\Gamma)}$$

$$\leq C\Delta t||\eta||^2_{l^2(0,T;H^2(0,L))} + C\Delta t^3||\partial_{tt}\boldsymbol{v}\cdot\boldsymbol{\tau}||^2_{L^2(0,T;L^2(\Gamma))}.$$

■

Lemma 5. *The following estimate holds:*

$$\Delta t\sum_{n=0}^{N-1}(\mathcal{R}_f^{n+1}(\delta_f^{n+1}) + \mathcal{R}_s^{n+1}(d_t\delta_u^{n+1}) + \mathcal{R}_v^{n+1}(d_t\delta_v^{n+1}) + \mathcal{R}_p^{n+1}(\delta_p^{n+1}) + \mathcal{R}_{os1}^{n+1}(\delta_f^{n+1}) + \mathcal{R}_{os2}^{n+1}(\delta_f^{n+1} - d_t\delta_u^{n+1}))$$

$$\leq C\Delta t^2\big(||\partial_{tt}\boldsymbol{v}||^2_{L^2(0,T;L^2(\Omega^f))}+||\partial_t p_p||^2_{L^2(0,T;H^1(\Omega^p))}+||\partial_{tt} p_p||^2_{L^2(0,T;L^2(\Omega^p))}+||\partial_{tt}\boldsymbol{U}||^2_{L^2(0,T;H^1(\Omega^p))}$$
$$+||\partial_{ttt}\boldsymbol{U}||^2_{L^2(0,T;L^2(\Omega^p))}+||\partial_{ttt}\boldsymbol{\eta}||^2_{L^2(0,T;L^2(0,L))}+||\partial_{ttt}\boldsymbol{V}||^2_{L^2(0,T;L^2(\Omega^p))}$$
$$+||\partial_{tt}\boldsymbol{U}||^2_{l^\infty(0,T;L^2(\Omega^p))}+||\partial_{tt}\boldsymbol{\eta}||^2_{l^\infty(0,T;L^2(0,L))}+||\partial_{tt}\boldsymbol{V}||^2_{l^\infty(0,T;L^2(\Omega^p))}\big)$$
$$+C\Delta t||\eta||^2_{l^2(0,T;H^2(0,L))}+C\Delta t^3||\partial_{tt}\boldsymbol{v}||^2_{L^2(0,T;L^2(\Gamma))}+\mathcal{A}(\delta_f,\delta_p,\delta_v,\delta_u),$$

where

$$\mathcal{A}(\delta_f,\delta_p,\delta_v,\delta_u)=\frac{\gamma\Delta t}{8}\sum_{n=0}^{N-1}||D(\delta_f^{n+1})||^2_{L^2(\Omega^f)}+\frac{\rho_m r_m}{4}\sum_{n=0}^{N-1}||\delta_f^{n+1}\cdot\boldsymbol{\tau}-\delta_v^{n+1}\cdot\boldsymbol{\tau}||^2_{L^2(\Gamma)}$$
$$+\frac{\Delta t}{6}\sum_{n=0}^{N-1}||\sqrt{\kappa}\nabla\delta_p^{n+1}||^2_{L^2(\Omega^p)}+\epsilon\big(||\delta_v^N||^2_{L^2(\Omega^p)}+||\delta_v^N||^2_{L^2(\Gamma)}+||D(\delta_u^N)||^2_{L^2(\Omega^p)}\big)$$
$$+C\Delta t\sum_{n=1}^{N-1}\big(||\delta_v^n||^2_{L^2(\Omega^p)}+||\delta_v^n||^2_{L^2(\Gamma)}+||D(\delta_u^n)||^2_{L^2(\Omega^p)}\big).$$

Proof. Using the formula for integration by parts in time (A2), the consistency errors are bounded as follows:

$$\Delta t\sum_{n=0}^{N-1}\mathcal{R}_f^{n+1}(\delta_f^{n+1})\leq C\Delta t\sum_{n=0}^{N-1}||d_t\boldsymbol{v}^{n+1}-\partial_t\boldsymbol{v}^{n+1}||^2_{L^2(\Omega^f)}+\frac{\gamma\Delta t}{16}\sum_{n=0}^{N-1}||D(\delta_f^{n+1})||^2_{L^2(\Omega^f)},$$

$$\Delta t\sum_{n=0}^{N-1}\mathcal{R}_p^{n+1}(\delta_p^{n+1})\leq C\Delta t\sum_{n=0}^{N-1}||d_t p_p^{n+1}-\partial_t p_p^{n+1}||^2_{L^2(\Omega^p)}+\frac{\Delta t}{6}\sum_{n=0}^{N-1}||\sqrt{\kappa}\nabla\delta_p^{n+1}||^2_{L^2(\Omega^p)}$$
$$+C\Delta t\sum_{n=0}^{N-1}||\nabla(d_t\boldsymbol{U}^{n+1}-\partial_t\boldsymbol{U}^{n+1})||^2_{L^2(\Omega^p)},$$

$$\Delta t\sum_{n=0}^{N-1}\mathcal{R}_v^{n+1}(d_t\delta_v^{n+1})=-\rho_p\int_{\Omega^p}(d_t\boldsymbol{U}^N-\partial_t\boldsymbol{U}^N)\cdot\delta_v^N d\boldsymbol{x}-\rho_m r_m\int_\Gamma(d_t\boldsymbol{U}^N-\partial_t\boldsymbol{U}^N)\cdot\delta_v^N dx$$
$$+\rho_p\Delta t\sum_{n=1}^{N-1}\int_{\Omega^p}(d_{tt}\boldsymbol{U}^{n+1}-\partial_t(d_t\boldsymbol{U}^{n+1}))\cdot\delta_v^n d\boldsymbol{x}+\rho_m r_m\Delta t\sum_{n=1}^{N-1}\int_\Gamma(d_{tt}\boldsymbol{U}^{n+1}-\partial_t(d_t\boldsymbol{U}^{n+1}))\cdot\delta_v^n dx$$
$$\leq C_\epsilon||d_t\boldsymbol{U}^N-\partial_t\boldsymbol{U}^N||^2_{L^2(\Omega^p)}+C\Delta t\sum_{n=1}^{N-1}||d_{tt}\boldsymbol{U}^{n+1}-\partial_t(d_t\boldsymbol{U}^{n+1})||^2_{L^2(\Omega^p)}$$
$$+C_\epsilon||d_t\boldsymbol{U}^N-\partial_t\boldsymbol{U}^N||^2_{L^2(\Gamma)}+C\Delta t\sum_{n=1}^{N-1}||d_{tt}\boldsymbol{U}^{n+1}-\partial_t(d_t\boldsymbol{U}^{n+1})||^2_{L^2(\Gamma)}+\epsilon||\delta_v^N||^2_{L^2(\Omega^p)}$$
$$+\epsilon||\delta_v^N||^2_{L^2(\Gamma)}+C\Delta t\sum_{n=1}^{N-1}||\delta_v^n||^2_{L^2(\Omega^p)}+C\Delta t\sum_{n=1}^{N-1}||\delta_v|_\Gamma^n||^2_{L^2(\Gamma)}.$$

$$\Delta t\sum_{n=0}^{N-1}\mathcal{R}_s^{n+1}(d_t\delta_u^{n+1})=\rho_p\int_{\Omega^p}(d_t\boldsymbol{V}^N-\partial_t\boldsymbol{V}^N)\cdot\delta_u^N d\boldsymbol{x}$$

$$
\begin{aligned}
&- \rho_p \Delta t \sum_{n=1}^{N-1} \int_{\Omega^p} (d_{tt} \boldsymbol{V}^{n+1} - \partial_t (d_t \boldsymbol{V}^{n+1})) \cdot \delta_u^n d\boldsymbol{x} \leq C_\epsilon ||d_t \boldsymbol{V}^N - \partial_t \boldsymbol{V}^N||^2_{L^2(\Omega^p)} \\
&+ C \Delta t \sum_{n=1}^{N-1} ||d_{tt} \boldsymbol{V}^{n+1} - \partial_t (d_t \boldsymbol{V}^{n+1})||^2_{L^2(\Omega^p)} + \epsilon ||D(\delta_u^N)||^2_{L^2(\Omega^p)} \\
&+ C \Delta t \sum_{n=1}^{N-1} ||D(\delta_u^n)||^2_{L^2(\Omega^p)} \Delta t \sum_{n=0}^{N-1} \mathcal{R}_{os1}^{n+1}(\delta_f^{n+1}) \leq C \Delta t \sum_{n=0}^{N-1} ||\nabla (p_p^{n+1} - p_p^n)||^2_{L^2(\Omega^p)} \\
&+ \frac{\gamma \Delta t}{16} \sum_{n=0}^{N-1} ||D(\delta_f^{n+1})||^2_{L^2(\Omega^f)}, \Delta t \sum_{n=0}^{N-1} \mathcal{R}^{os}(\delta_f^{n+1} - d_t \delta_u^{n+1}) = \Delta t \sum_{n=0}^{N-1} \int_\Gamma \\
&\times \left(\boldsymbol{\tau} \cdot \boldsymbol{\sigma}^f \boldsymbol{n} + \rho_m r_m \frac{\boldsymbol{v}^{n+1} \cdot \boldsymbol{\tau} - \boldsymbol{V}^n \cdot \boldsymbol{\tau}}{\Delta t} \right) (\delta_f^{n+1} \cdot \boldsymbol{\tau} - \delta_v^{n+1} \cdot \boldsymbol{\tau}) dx \\
&\leq \frac{\Delta t^2}{\rho_m r_m} \sum_{n=0}^{N-1} \left|\left| \boldsymbol{\tau} \cdot \boldsymbol{\sigma}^f \boldsymbol{n} + \rho_m r_m \frac{\boldsymbol{v}^{n+1} \cdot \boldsymbol{\tau} - \boldsymbol{V}^n \cdot \boldsymbol{\tau}}{\Delta t} \right|\right|^2_{L^2(\Gamma)} + \frac{\rho_m r_m}{4} \sum_{n=0}^{N-1} ||\delta_f^{n+1} \cdot \boldsymbol{\tau} - \delta_v^{n+1} \cdot \boldsymbol{\tau}||^2_{L^2(\Gamma)}.
\end{aligned}
$$

The final consistency error estimate follows by applying Lemma 4. ∎

Lemma 6. (Interpolation errors)**.** *The following inequalities hold:*

$$
\begin{aligned}
&\Delta t \sum_{n=0}^{N-1} ||d_t \theta_p^{n+1}||^2_{L^2(\Omega^p)} \leq ||\partial_t \theta_p^n||^2_{L^2(0,T;L^2(\Omega^p))} \leq h^{2k+2} ||\partial_t p_p||^2_{L^2(0,T;H^{k+1}(\Omega^p))}, \\
&\Delta t \sum_{n=0}^{N-1} ||\nabla d_t \theta_f^{n+1}||^2_{L^2(\Omega^f)} \leq ||\partial_t \theta_f||^2_{L^2(0,T;H^1(\Omega^f))} \leq h^{2k} ||\partial_t \boldsymbol{v}||^2_{L^2(0,T;H^{k+1}(\Omega^f))}, \\
&\Delta t \sum_{n=0}^{N-1} ||d_{tt} \theta_s^{n+1}||^2_{L^2(\Omega^p)} \leq ||\partial_{tt} \theta_s||^2_{L^2(0,T;L^2(\Omega^p))} \leq h^{2k+2} ||\partial_{tt} \boldsymbol{U}||^2_{L^2(0,T;H^{k+1}(\Omega^p))}, \\
&\Delta t \sum_{n=0}^{N-1} ||d_t \theta_v^{n+1}||^2_{L^2(\Gamma)} \leq ||\partial_t \theta_v||^2_{L^2(0,T;L^2(\Gamma))} \leq h^{2k+2} ||\partial_t \boldsymbol{\xi}||^2_{L^2(0,T;H^{k+1}(0,L)}, \\
&\Delta t \sum_{n=0}^{N-1} ||d_t \theta_s|_\Gamma^{n+1}||^2_M \leq ||\partial_t \theta_s|_\Gamma||^2_{L^2(0,T;H^1(0,L))} \leq h^{2k} ||\partial_t \boldsymbol{\eta}||^2_{L^2(0,T;H^{k+1}(0,L))}, \\
&\Delta t \sum_{n=0}^{N-1} \left(||D(\theta_f^{n+1})||^2_{L^2(\Omega^f)} + ||\nabla \theta_p^{n+1}||^2_{L^2(\Omega^p)} + ||\nabla \theta_p^n||^2_{L^2(\Omega^p)} \right) \\
&\quad \leq \Delta t \sum_{n=0}^{N} h^{2k} \left(||\boldsymbol{v}^n||^2_{H^{k+1}(\Omega^f)} + ||p_p^n||^2_{H^{k+1}(\Omega^p)} \right) \\
&\quad \leq h^{2k} \left(||\boldsymbol{v}||^2_{l^2(0,T;H^{k+1}(\Omega^f))} + ||p_p||^2_{l^2(0,T;H^{k+1}(\Omega^p))} \right). \\
&\max_{0 \leq n \leq N} ||d_t \theta_v^n||^2_{L^2(\Omega^p)} \leq C \left(h^{2k+2} ||\partial_t \boldsymbol{V}||^2_{l^\infty(0,T;H^{k+1}(\Omega^p))} + h^{2k+4} ||\partial_{tt} \boldsymbol{V}||^2_{l^\infty(0,T;H^{k+1}(\Omega^p))} \right),
\end{aligned}
$$

Proof. We only give the proof for the last inequality in Lemma 6. Other inequalities can be easily shown using manipulations similar to the ones in Lemma 5, and approximation properties (A10)–(A15).

From Taylor expansion, we have

$$d_t\theta_v^n = \partial_t\theta_v^n + \frac{\Delta t}{2}\partial_{tt}\theta_v(z), \quad z \in [t^n, t^{n+1}].$$

Using the equality above, we get the following

$$\begin{aligned}
\max_{0\le n\le N} ||d_t\theta_v^n||^2_{L^2(\Omega^p)} &= \max_{0\le n\le N} \left\| \partial_t\theta_v^n + \frac{\Delta t}{2}\partial_{tt}\theta_v(z) \right\|^2_{L^2(\Omega^p)} \\
&\le C\left(h^{2k+2}||\partial_t \boldsymbol{V}||^2_{l^\infty(0,T;H^{k+1}(\Omega^p))} + \Delta t^2 h^{2k+2}||\partial_{tt}\boldsymbol{V}||^2_{l^\infty(0,T;H^{k+1}(\Omega^p))}\right) \\
&\le C\left(h^{2k+2}||\partial_t \boldsymbol{V}||^2_{l^\infty(0,T;H^{k+1}(\Omega^p))} + h^{2k+4}||\partial_{tt}\boldsymbol{V}||^2_{l^\infty(0,T;H^{k+1}(\Omega^p))}\right).
\end{aligned}$$

The last inequality is obtained using the CFL condition (4.11). ∎

References

1. Y. Cao, M. Gunzburger, X. Hu, F. Hua, X. Wang, and W. Zhao, Finite element approximations for Stokes-Darcy flow with Beavers-Joseph interface conditions, SIAM J Numer Anal 47 (2010), 4239–4256.
2. M. Discacciati, E. Miglio, and A. Quarteroni, Mathematical and numerical models for coupling surface and groundwater flows, Appl Numer Math 43 (2002), 57–74.
3. M. Discacciati, A. Quarteroni, and A. Valli, Robin-Robin domain decomposition methods for the Stokes-Darcy coupling, SIAM J Numer Anal 45 (2007), 1246–1268.
4. V. Girault and B. Rivière, DG approximation of coupled Navier-Stokes and Darcy equations by Beaver-Joseph-Saffman interface condition, SIAM J Numer Anal 47 (2009), 2052–2089.
5. W. Layton, F. Schieweck, and I. Yotov, Coupling fluid flow with porous media flow, SIAM J Numer Anal 40 (2002), 2195–2218.
6. W. Layton, H. Tran, and X. Xiong, Long time stability of four methods for splitting the evolutionary Stokes–Darcy problem into Stokes and Darcy subproblems, J Comput Appl Math 236 (2012), 3198–3217.
7. M. Mu and J. Xu, A two-grid method of a mixed Stokes-Darcy model for coupling fluid flow with porous media flow, SIAM J Numer Anal 45 (2007), 1801–1813.
8. M. Mu and X. Zhu, Decoupled schemes for a non-stationary mixed Stokes-Darcy model, Math Comput 79 (2010), 707–731.
9. B. Rivière and I. Yotov, Locally conservative coupling of Stokes and Darcy flows, SIAM J Numer Anal 42 (2005), 1959–1977.
10. P. Song, C. Wang, and I. Yotov, Domain decomposition for Stokes-Darcy flows with curved interfaces, Proc Comput Sci 18 (2013), 1077–1086.
11. S. Badia, F. Nobile, and C. Vergara, Robin-Robin preconditioned Krylov methods for fluid-structure interaction problems, Comput Methods Appl Mech Eng 198 (2009), 2768–2784.
12. S. Badia, A. Quaini, and A. Quarteroni, Coupling Biot and Navier–Stokes equations for modelling fluid–poroelastic media interaction, J Comput Phys 228 (2009), 7986–8014.

13. M. Bukač, S. Čanić, R. Glowinski, J. Tambača, and A. Quaini, Fluid-structure interaction in blood flow capturing non-zero longitudinal structure displacement, J Comput Phys 235 (2012), 515–541.

14. M. A. Fernández and M. Landajuela, A fully decoupled scheme for the interaction of a thin-walled structure with an incompressible fluid, C R Math 351 (2013), 161–164.

15. M. A. Fernández, Incremental displacement-correction schemes for incompressible fluid-structure interaction: stability and convergence analysis, Numer Math 123 (2012), 210–65.

16. P. Hansbo, Nitsche's method for interface problems in computational mechanics, GAMM Mitt 28 (2005), 183–206.

17. M. Lukáčová-Medvid'ová, G. Rusnáková, and A. Hundertmark-Zaušková, Kinematic splitting algorithm for fluid-structure interaction in hemodynamics, Comput Methods Appl Mech Eng 265 (2013), 83–106.

18. B. Muha and S. Čanić, Existence of a solution to a fluid-multi-layered-structure interaction problem, J Differential Equations 256 (2014), 658–706.

19. F. Nobile and C. Vergara, An effective fluid-structure interaction formulation for vascular dynamics by generalized Robin conditions, SIAM J Sci Comput 30 (2008), 731–763.

20. A. Quaini and A. Quarteroni, A semi-implicit approach for fluid-structure interaction based on an algebraic fractional step method, Math Models Methods Appl Sci 17 (2007), 957–985.

21. P. Causin, J. F. Gerbeau, and F. Nobile, Added-mass effect in the design of partitioned algorithms for fluid-structure problems, Comput Methods Appl Mech Eng 194 (2005), 4506–4527.

22. R. L. Armentano, J. G. Barra, J. Levenson, A. Simon, and R. H. Pichel, Arterial wall mechanics in conscious dogs: Assessment of viscous, inertial, and elastic moduli to characterize aortic wall behavior, Circ Res 76 (1995), 468–478.

23. R. D. Bauer, R. Busse, A. Schabert, Y. Summa, and E. Wetterer, Separate determination of the pulsatile elastic and viscous forces developed in the arterial wall *in vivo*, Pflügers Arch 380 (1976), 221–226.

24. S. Canic, J. Tambaca, G. Guidoboni, A. Mikelic, C.J. Hartley, and D. Rosenstrauch, Modeling viscoelastic behavior of arterial walls and their interaction with pulsatile blood flow, SIAM J Appl Math 67 (2006), 164–193.

25. Y. C. Fung, Biomechanics: its foundation and objectives, Y. C. Fung, N. Perrone, and M. Anliker, editors, Prentice-Hall, Englewood Cliff, NJ, 1972.

26. J. D. Humphrey et al., Mechanics of the arterial wall: review and directions, Crit Rev Biomed Eng 23 (1995), 1.

27. A. Robertson, M. Hill, and D. Li, Structurally motivated damage models for arterial walls, Theory and application, Modeling of physiological flows, Springer Milan, 2012, pp. 143–185.

28. R. Vito and S. Dixon, Blood vessel constitutive models-1995–2002, Annu Rev Biomed Eng 5 (2003), 413–439.

29. J. Zhou and Y. C. Fung, The degree of nonlinearity and anisotropy of blood vessel elasticity, Proc Natl Acad Sci USA 94 (1997), 14255–14260.

30. M. Prosi, P. Zunino, K. Perktold, and A. Quarteroni, Mathematical and numerical models for transfer of low-density lipoproteins through the arterial walls: a new methodology for the model set up with applications to the study of disturbed lumenal flow, J Biomech 38 (2005), 903–917.

31. M. Lesinigo, Lumped mathematical models for intracranial dynamics, Ph.D. thesis, EPFL, Switzerland, 2013.

32. G. A. Holzapfel and R. W. Ogden, Constitutive modelling of passive myocardium: a structurally based framework for material characterization, Philos Trans R Soc A Math Phys Eng Sci 367 (2009), 3445–3475.

33. G. A. Holzapfel, G. Sommer, and P. Regitnig, Anisotropic mechanical properties of tissue components in human atherosclerotic plaques, Trans ASME K J Biomech Eng 126 (2004), 657–665.

34. S. M. K. Rausch, C. Martin, P. B. Bornemann, S. Uhlig, and W. A. Wall, Material model of lung parenchyma based on living precision-cut lung slice testing, J Mech Behav Biomed Mater 4 (2011), 583–592.

35. D. Tang, C. Yang, T. Geva, G. Gaudette, and P. Del Nido, Multi-physics MRI-based two-layer fluid–structure interaction anisotropic models of human right and left ventricles with different patch materials: cardiac function assessment and mechanical stress analysis, Comput Struct 89 (2011), 1059–1068.

36. J.-M. Kim, S.-H. Chang, and C.-B. Yun, Fluid-structure-soil interaction analysis of cylindrical liquid storage tanks subjected to horizontal earthquake loading, Struct Eng Mech 13 (2002), 615–638.

37. N. D. Botkin, K.-H. Hoffmann, O. A. Pykhteev, and V. L. Turova, Dispersion relations for acoustic waves in heterogeneous multi-layered structures contacting with fluids, J Franklin Inst 344 (2007), 520–534.

38. S. Chung and K. Vafai, Effect of the fluid–structure interactions on low-density lipoprotein transport within a multi-layered arterial wall, J Biomech 45 (2012), 371–381.

39. K. Lee, G. M. Saidel, and M. S. Penn, Permeability change of arterial endothelium is an age-dependent function of lesion size in apolipoprotein e-null mice, Am J Physiol Heart Circ Physiol 295 (2008), H2273–H2279.

40. M. Bukač, I. Yotov, R. Zakerzadeh, and P. Zunino, Effects of poroelasticity on fluid - structure interaction in arteries: a computational sensitivity studyModeling the heart and the circulatory system, in Springer Series in Modeling, Simulation and Applications (MS&A), Vol. 13, to appear.

41. N. Koshiba, J. Ando, X. Chen, and T. Hisada, Multiphysics simulation of blood flow and LDL transport in a porohyperelastic arterial wall model, J Biomech Eng 129 (2007), 374–385.

42. M. A. Murad, J. N. Guerreiro, and A. F. D. Loula, Micromechanical computational modeling of secondary consolidation and hereditary creep in soils, Comput Methods Appl Mech Eng 190 (2001), 1985–2016.

43. R. Showalter, Poroelastic filtration coupled to Stokes flow, Lect Notes Pure Appl Math 242 (2010), 229–241.

44. B. Tully and Y. Ventikos, Coupling poroelasticity and CFD for cerebrospinal fluid hydrodynamics, IEEE Trans Biomed Eng 56 (2009), 1644–1651.

45. S. Badia, F. Nobile, and C. Vergara, Fluid-structure partitioned procedures based on Robin transmission conditions, J Comput Phys 227 (2008), 7027–7051.

46. C. Förster, W. Wall, and E. Ramm, Artificial added mass instabilities in sequential staggered coupling of nonlinear structures and incompressible viscous flows, Comput Methods Appl Mech Eng 196 (2007), 1278–1293.

47. M. Astorino, F. Chouly, and M. A. Fernández, An added-mass free semi-implicit coupling scheme for fluid-structure interaction, C R Math 347 (2009), 99–104.

48. M. Astorino, F. Chouly, and M. A. Fernández Varela, Robin based semi-implicit coupling in fluid-structure interaction: stability analysis and numerics. SIAM J Sci Comput 31 (2009), 4041–4065.

49. S. Badia, A. Quaini, and A. Quarteroni, Splitting methods based on algebraic factorization for fluid-structure interaction, SIAM J Sci Comput 30 (2008), 1778–1805.

50. E. Burman and M. A. Fernández, Stabilization of explicit coupling in fluid-structure interaction involving fluid incompressibility, Comput Methods Appl Mech Eng 198 (2009), 766–784.

51. S. Deparis, M. Discacciati, G. Fourestey, and A. Quarteroni, Fluid-structure algorithms based on Steklov-Poincaré operators, Comput Methods Appl Mech Eng 195 (2006), 5797–5812.

52. S. Deparis, M. Fernandez, and L. Formaggia, Acceleration of a fixed point algorithm for a fluid-structure interaction using transpiration condition, Math Model Numer Anal 37 (2003), 601–616.

53. M. A. Fernández, Incremental displacement-correction schemes for the explicit coupling of a thin structure with an incompressible fluid, C R Math 349 (2011), 473–477.

54. M. A. Fernández, J. F. Gerbeau, and C. Grandmont, A projection algorithm for fluid-structure interaction problems with strong added-mass effect, C R Math 342 (2006), 279–284.

55. M. A. Fernández and J. Mullaert, Displacement-velocity correction schemes for incompressible fluid-structure interaction, C R Math Acad Sci Paris 349 (2011), 1011–1015.

56. G. Guidoboni, R. Glowinski, N. Cavallini, and S. Čanić, Stable loosely-coupled-type algorithm for fluid-structure interaction in blood flow, J Comput Phys 228 (2009), 6916–6937.

57. C. M. Murea and S. Sy, A fast method for solving fluid-structure interaction problems numerically, Int J Numer Methods Fluids 60 (2009), 1149–1172.

58. L. Gerardo-Giorda, F. Nobile, and C. Vergara, Analysis and optimization of Robin-Robin partitioned procedures in fluid-structure interaction problems, SIAM J Numer Anal 48 (2010), 2091–2116.

59. E. Burman and M. A. Fernández, An unfitted Nitsche method for incompressible fluid-structure interaction using overlapping meshes, Comput Methods Appl Mech Eng, DOI: 10.1016/j.cma.2014.07.007, (2014).

60. R. Glowinski, Finite element methods for incompressible viscous flow, P. G. Ciarlet and J.-L. Lions, editors, Handbook of numerical analysis, Vol. 9, North-Holland, Amsterdam, The Netherlands, 2003.

61. B. Muha and S. Čanić, Existence of a weak solution to a nonlinear fluid–structure interaction problem modeling the flow of an incompressible, viscous fluid in a cylinder with deformable walls, Arch Ration Mech Anal 207 (2013), 919–968.

62. A. Hundertmark-Zaušková, M. Lukáčová-Medvid'ová, and G. Rusnáková, Fluid-structure interaction for shear-dependent non-Newtonian fluids, Topics in mathematical modeling and analysis, Volume 7 of Jindrich Necas Center for Mathematical Modeling Lecture Notes, Matfyzpress, Prague, 2012, pp. 109–158.

63. L. Shan, H. Zheng, and W. Layton, A decoupling method with different subdomain time steps for the nonstationary Stokes–Darcy model, Numer Methods Partial Differential Equations 29 (2013), 549–583.

64. L. A. Miller and C. S. Peskin, A computational fluid dynamics of 'clap and fling' in the smallest insects, J Exp Biol 208 (2005), 195–212.

65. F. Nobile, Numerical approximation of fluidstructure interaction problems with application to haemodynamics, Ph.D. thesis, EPFL, Switzerland, 2001.

66. I. E. Vignon-Clementel, C. Alberto Figueroa, K. E. Jansen, and C. A. Taylor, Outflow boundary conditions for three-dimensional finite element modeling of blood flow and pressure in arteries, Comput Methods Appl Mech Eng 195 (2006), 3776–3796.

67. F. Nobile, M. Pozzoli, and C. Vergara, Time accurate partitioned algorithms for the solution of fluid-structure interaction problems in haemodynamics, Comput Fluids 86 (2013), 470–482.

68. P. Moireau, N. Xiao, M. Astorino, A. Figueroa, D. Chapelle, C. Taylor, and J.-F. Gerbeau, External tissue support and fluid–structure simulation in blood flows, Biomech Model Mechanobiol 11 (2012), 1–18.

69. P. Crosetto, S. Deparis, G. Fourestey, and A. Quarteroni, Parallel algorithms for fluid-structure interaction problems in haemodynamics, SIAM J Sci Comput 33 (2011), 1598–1622.

70. E. Detournay and A. H. D. Cheng, Fundamentals of poroelasticity, Chapter 5 in Comprehensive rock engineering: principles, practice and projects, Vol. II, C. Fairhurst, editor, Analysis and design method, Pergamon Press, 1993, pp. 113–171.

71. J. Donea, Arbitrary Lagrangian-Eulerian finite element methods, Computational methods for transient analysis, North-Holland, Amsterdam, The Netherlands, 1983.

72. T. J. R. Hughes, W. K. Liu, and T. K. Zimmermann, Lagrangian-Eulerian finite element formulation for incompressible viscous flows, Comput Methods Appl Mech Eng 29 (1981), 329–349.

73. A. Mikelić and M. Wheeler, Convergence of iterative coupling for coupled flow and geomechanics, Comput Geosci 17 (2013), 1–7.

74. P. Ciarlet, The finite element method for elliptic problems, Vol. 4, North Holland, 1978.

75. A. T. Barker and X. C. Cai, Scalable parallel methods for monolithic coupling in fluid-structure interaction with application to blood flow modeling, J Comput Phys 229 (2010), 642–659.

76. L. Formaggia, J.F. Gerbeau, F. Nobile, and A. Quarteroni, On the coupling of 3D and 1D Navier–Stokes equations for flow problems in compliant vessels, Comput Methods Appl Mech Eng 191 (2001), 561–582.

77. X. Ma, G. C. Lee, and S. G. Wu, Numerical simulation for the propagation of nonlinear pulsatile waves in arteries, J Biomech Eng 114 (1992), 490.

78. M. Bukač, S. Čanić, and B. Muha, A partitioned scheme for fluid-composite structure interaction problems, Submitted, arXiv:1402.0110, J Comp Phys, doi: 10.1016/j.jcp.2014.10.045 (2014).

79. M. Bukač, I. Yotov, R. Zakerzadeh, and P. Zunino, Partitioning strategies for the interaction of a fluid with a poroelastic material based on a Nitsche's coupling approach, Submitted.